A how-to guide through the physicochemical and biological methods for the development of polymeric drug delivery systems: Antimalarial vectors as study case

M.C. Casanova, P. Vanelle, N. Azas, Julie Broggi Broggi

Next Materials 6 (2025) 100394

Contents lists available at ScienceDirect

Next Materials

journal homepage: www.sciencedirect.com/journal/next-materials

Review article

A how-to guide through the physicochemical and biological methods for the development of polymeric drug delivery systems: Antimalarial vectors as study case

M.C. Casanova [a,b], P. Vanelle [a], N. Azas [b,*], J. Broggi [a,*]

[a] Aix Marseille Univ, CNRS, Institut de Chimie Radicalaire ICR UMR 7273, Faculté de Pharmacie, Marseille, France
[b] Aix Marseille Univ, IHU Méditerranée Infection, UMR VITROME, Marseille, France

ARTICLE INFO

Keywords:
Drug delivery systems
polymeric nanocarriers
polymer-drug conjugates
micelles
dendrimers
antimalarial-drug vectorization

ABSTRACT

Macromolecular drug delivery systems are engineered nanotechnologies used for the targeted delivery and controlled release of therapeutic agents to a specific biologic target, a rapidly growing need in the age of tailor-made therapeutic treatments. The rise of drug delivery systems stems from their ability to solve the pharmacological issues that often impede the drug development process. The aim of this review is to provide a detailed how-to guide through the early stages of the discovery of new drug-loaded nanocarriers. From their synthesis to their biological evaluations, their development requires multidisciplinary knowledge of chemistry, physics, and biology and involves mastering leading-edge technological equipment. The essential steps and techniques are thus described and discussed in the context of the preparation, physicochemical characterization, and biological study of polymeric drug delivery systems. This guide is intended as a comprehensive and didactic resource to assist (bio)chemists, (bio)physicists, and biologists, as well as beginners, in their work and discussions on polymeric nanocarriers. Although this review addresses general themes applicable to all polymeric nanocarriers, the implementation of these different physicochemical and biological strategies is highlighted through the concrete case of antimalarial-drug vectorization.

Abbreviations: AFM, Atomic Force Microscopy; AM, Arthemeter; AN, Artesunate; AR, Aspect ratio; ART, Artemisinine; BAC, 2,2-Bisacrylamidoacetic acid; BHEED, Bishydroxy-ethyl ethylene diamine; Boc, Tert-butyloxycarbonyl; BP, Bisacryloyl piperazine; $CC_{50:,}$, Cytotoxic concentration that reduced the cell *via*bility by 50%; CLSM, Confocal Laser Scanning Microscopy; CMC, Critic Micellar Concentration; CQ, Chloroquine; CTA, Chain Transfer Agent; CuAAc, Copper-Catalyzed Azide-Alkyne Cycloaddition; *Đ*, Dispersity; DACH-Pt, 1,2-diaminocyclohexane platinum; DAPI, 4′,6-diamidino-2-phenylindole; DCC, *N,N'*-Dicyclohexylcarbodiimide; DDS, Drug Delivery System; DEP, 3-Diethylamino-1-propylamine; DHP, Dendronized Hyperbranched Polymers; DL, Drug Loading; DLS, Dynamic Light Scattering; DMAP, Dimethyl aminopyridine; DMF, Dimethylformamide; DMSO, Dimethylsulfoxide; DNA, Deoxyribonucleic acid; DOSY, Diffusion-ordered spectroscopy; DSC, Differential Scanning Calorimetry; DTT, Dithiothreitol reducing agent; DTX, Docetaxel; EDA, Ethylenediamine; EDX, Energy Dispersive X-ray; EE, Encapsulation Efficiency; F127, Pluronic® poloxamer; FACS, Fluorescence-activated cell sorting; FITC, Fluorescein isothiocyanate; FLISA, Fluorescence-Linked Immunosorbent Assay; FT-IR, Fourier Transform Infrared Spectroscopy; G6PD, Glucose-6-phosphate deshydrogenase; Gal, Galactose; GMPA, Glycyloxymethyl propionic acid; HDLDBC, Hybrid Dendritic-Linear-Dendritic Block Co-polymers; HEP, Heparin; HPLC, High Performance Liquid Chromatography; $IC_{50,}$, Inhibitory concentration that reduced the parasite growth by 50%; LCSM, Laser Confocal Scanning Microscopy; LUM, Lumefantrine; 2-MePip, 2-Methylpiperazine; M_n, Number Average Molecular Weight; MPA, Hydroxymethyl propionic acid; MPEG, polyethylene-glycol monomethyl ether; MTT, 3-[4,5-dimethylthiazol-2-yl]-2,5-diphenyltetrazolium bromide; M_w, Weight Average Molecular Weight; Nd, not determined; NHS, N-Hydroxysuccinimide; NMR, Nuclear Magnetic Resonance; NPPs, New Permeability Pathways; NVP, *N*-Vinylpyrrolidone; PAAs, Polyamido-amines; PBS, Phosphate Buffer Solution; PCL, Polycaprolactone; PDC, Polymer-Drug Conjugates; PDI, Polydispersity Index; PEG, Polyethylene-glycol; PEO, Polyethylene-oxide; PLys, Poly-L-Lysine; PMOXA, Poly2-methyl-2-oxazoline; PPCL, Polyα-pyridylthio cysteamine caprolactone; PPI, Polypropylene-imine; PPO, Polypropylene-oxide; PQ, Primaquine; PRBCs, Parasited Red Blood Cells; PVL, Polyα-allylvalerolactone; PVM, parasitophorous vacuole membrane; PVP, poly N-vinylpyrrolidone; PYR, Pyrimethamine; QN, Quinacrine; RAFT, Reversible Addition-Fragmentation Transfer; RBCs, Red Blood Cells; Rho, Rhodamine; ROP, Ring-Opening Polymerization; SEC, Size Exclusion Chromatography also called Gel permeation chromatography GPC; SEM, Scanning Electron Microscopy; SHMT, Serine Hydroxymethyltransferase; TBTA, , Trisbenzyltriazolylmethylamine); TEM, Transmission Electronic Microscopy; VE, Vinyl ether; WHO, World Health Organization; ZP, Zeta Potential.

* Corrresponding authors.
E-mail addresses: nadine.azas@univ-amu.fr (N. Azas), julie.broggi@univ-amu.fr (J. Broggi).

https://doi.org/10.1016/j.nxmate.2024.100394
Received 15 May 2024; Received in revised form 25 September 2024; Accepted 30 September 2024
Available online 16 October 2024

1. Introduction

Macromolecular drug delivery systems (DDS) are engineered nanotechnologies used for the targeted delivery and controlled release of therapeutic agents to a specific biologic target [1–4]. For the past decades, several drug delivery strategies have stood out from classical therapeutic routes, successfully culminating in marketed products [5–8]. The rise of drug delivery systems stems from their ability to solve the pharmacological issues that often impede the drug development process. Both promising drug candidates or marketed drugs have side effects, arising from their interactions with off-target tissues, and these are obstacles to the design of optimal disease treatments. Incorporation of these drugs into macromolecular DDS can improve their pharmacokinetic properties such as bioavailability, efficiency, targeting, solubility, lifetime, while reducing their side effects, degradation, and toxicity. These nanocarriers are made of different materials, such as natural [9–12] and synthetic polymers [13–16], lipids [17–19] or metallic nanoparticles [20–23]. The variety of available building blocks gives access to biocompatible and biodegradable vectors [24,25] that can adopt different macromolecular shapes with characteristic physicochemical and pharmacokinetic properties. Notably, their large surface allows the anchorage of multiple specific targeting ligands, enabling active vectorization of the drug up to the biological target. Ultimately, once at its destination, the drug delivery system is designed to release the drug through the application of external or endogen stimuli [26–29].

These benefits unsurprisingly attract the interest of numerous therapeutic domains [30–35]. The design of drug delivery vectors offering high recognition of its biological target is rapidly becoming a priority in the age of tailor-made and individualized therapeutic treatments. Many reviews deal with the successful applications of these drug delivery systems to a specific disease, from the perspective of their biological characteristics and activities. Significant attention is also paid to new concepts and disruptive examples of nanovectors, with a focus on their salient physicochemical and biological features. Nevertheless, the field of research on drug delivery systems remains challenging and under-exploited, due to technological barriers. One difficulty might be the high level of interdisciplinarity of these therapeutic strategies. These rely on the one hand, on organic, material, and analytical chemists, biochemists, physicists for the preparation and characterization of drug-loaded macromolecular vectors, and on the other hand, on biologists, biophysicists, pharmacokineticists, pharmacists, medical and clinical doctors for their biological and medical analysis. From their synthesis to their biological evaluations, the development of new DDS thus requires multidisciplinary knowledge in chemistry, physics, and biology. Full physicochemical and biological characterizations also involve the mastering of leading-edge technological equipment. Coordination of these different trades, each with their own language and specific technical vocabulary, can also be tricky for the progress in projects, especially for new incomers in the field. Yet, no reviews so far reflected this amount and variety of theoretical and technical work behind the design and evaluation of nanovectors.

Hence, the aim of this review is to provide a general practical guide gathering all the essential steps in the preparation, characterization, and evaluation of a drug delivery system. This guide is intended as a comprehensive and didactic resource to assist (bio)chemists, (bio) physicists, and biologists, as well as beginners, in their work and discussions on polymeric drug-delivery systems. Our review will thus include different synthetic strategies for the preparation of polymeric systems such as polymer-drug conjugates, micelles, or dendrimers. As well, methods of drug-incorporation into the vector will be presented. Then, physicochemical characterization techniques will be described, and discussed, including essential techniques for the determination of important parameters such as the size, shape, homogeneity, and surface morphology of nanoparticles. Finally, the review will also introduce the biological assays, indispensable for their biological evaluation and the study of their mechanism of action. This focus on the early stages of the discovery of new drug-loaded nanocarriers will therefore not include pharmacokinetic, *in vivo* nor clinical evaluations. The technical problems inherent to industrial developments will not be addressed either (storage stability, galenic formulation, etc).

Because of the variety of macromolecular vectors under investigation, we chose to focus on polymeric drug-delivery systems. Therefore, this review will not include works on liposome [17], metal-containing nanoparticles [21], carbon nanotubes [36], protein-polymer conjugates [37] or other hybrids systems. As well, it would not have been possible to deal with biological studies from the perspective of all diseases targeted by DDS strategies. For instance, antitumoral-drug nanovectors for the oncology field have already been largely reviewed and will not be covered here [38–40]. Hence, although this review addresses general themes applicable to all polymeric DDS, we chose to describe them in regard of the concrete case study of the antimalarial-drug vectorization. Over the past decades, an increasing number of DDS have been developed for infectious diseases [41–44]. It is therefore quite natural that these findings also aroused the interest of researchers committed in the fight against malaria. Recent reviews gather the biological features of these new antimalarial DDS [45–50]. To trace the background on the vectorization of antiplasmodial drugs, this practical guide will therefore start by giving to the non-specialized readers, some basic information on malaria.

2. Why vectorize antimalarial drugs?

2.1. Background: malarial infections

With 249 million cases reported in 2022 for 85 malaria endemic countries (including 608.000 deaths), the World Health Organization (WHO) classified malaria among the infectious diseases of poverty and as a real public health emergency. [51] Most of the infections (82%) and deaths (95%) were in the WHO African Region, followed by the WHO South-East Asia Region (10% of cases and 2% of deaths) (Fig. 1). One of the major causative agents in Africa appears to be the *Plasmodium falciparum* species accounting for more than 80% of estimated cases. Moreover, children under 5 years of age are the most vulnerable to malaria (76% of global deaths). [52] Although the number of cases is not significantly increasing, the rate incidence appears to be more or less stationary these last years. Since October 2020, WHO recommends the recent RTS, S/AS01 (Mosquirix™) and R21/Matrix-M (R21) malaria vaccines for the prevention of *P. falciparum* malaria in children living in regions with moderate to high transmission. Nevertheless, malaria eradication is still out of range and the search for innovative treatment strategies remains necessary.

The lifecycle of the *Plasmodium falciparum* strain is very complex and includes different cycles and stages of the parasite's development (Fig. 2). [54] It is made of two cycles that take place in two different hosts: the sexual cycle in the mosquito and the asexual cycle in the human. During the sexual cycle, the mosquito produces parasites called sporozoites that are injected into the human during a bite from an infected female mosquito (Anopheles) (**1**). These sporozoites invade the hepatic cells (liver or "pre-erythrocytic" stages (**2**)) and asexually multiply there until cell lysis, to liberate a thousand of free merozoites in the human blood. This step **2** is not symptomatic for the host. In turn, the free merozoites invade the human red blood cells (RBCs). This is the symptomatic erythrocytic stage (**3**) which causes symptoms such as fever, chills, anemia, muscular pains, and headaches. During this step, different forms of the parasite are found according to its development stage: rings, trophozoites and schizonts. These latter can evolve into either new merozoites (after cell lysis) or, less frequently, mature gametocytes (male and female). The extraction of these gametocytes during the blood meal of another mosquito allows the repetition of a new sexual cycle (**4**) that will then infect another human (**1**).

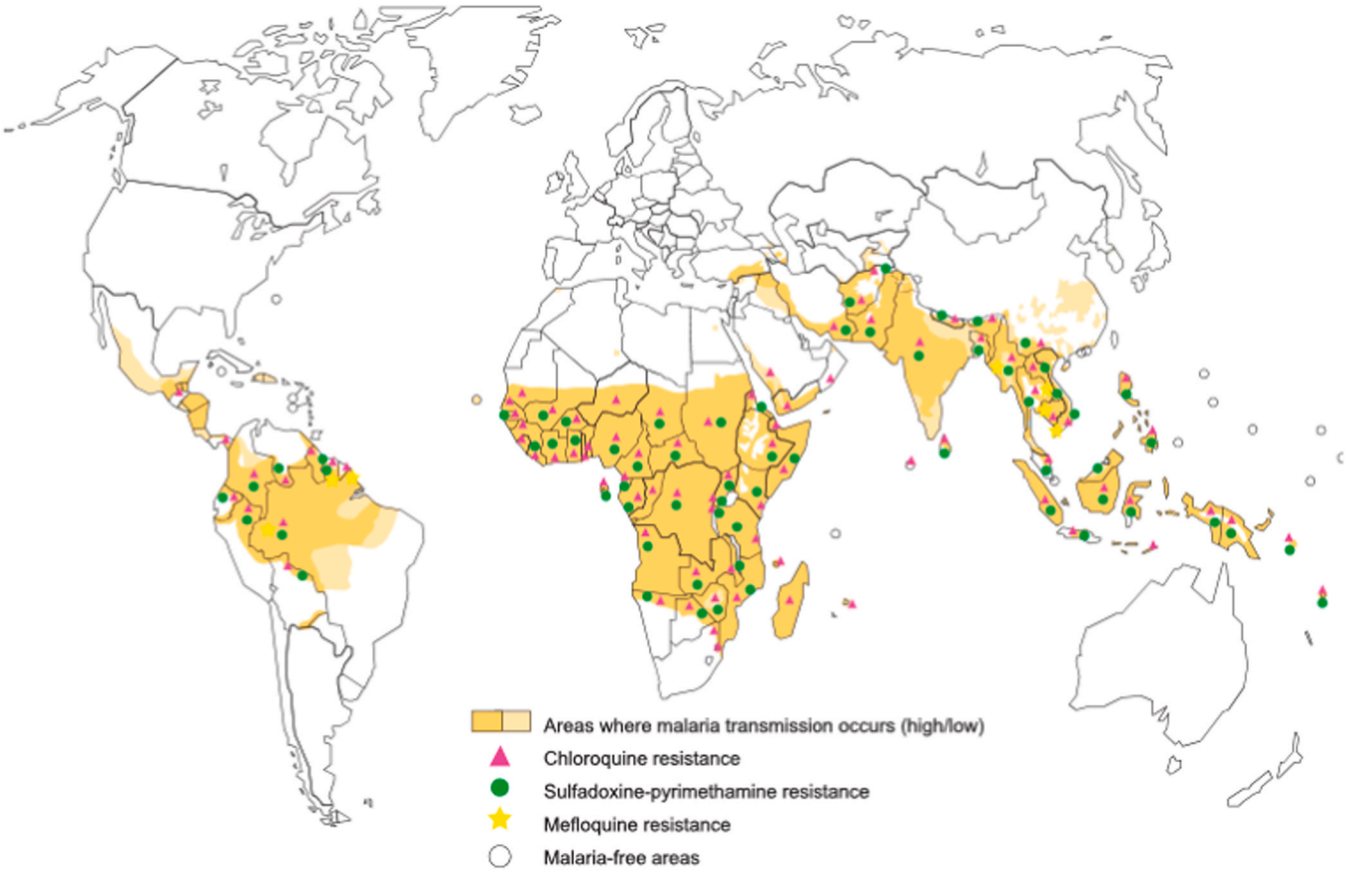

Fig. 1. Geographical distribution of drug-resistant *P. falciparum,* according to WHO. Reproduced from World malaria report, 2005 [53].

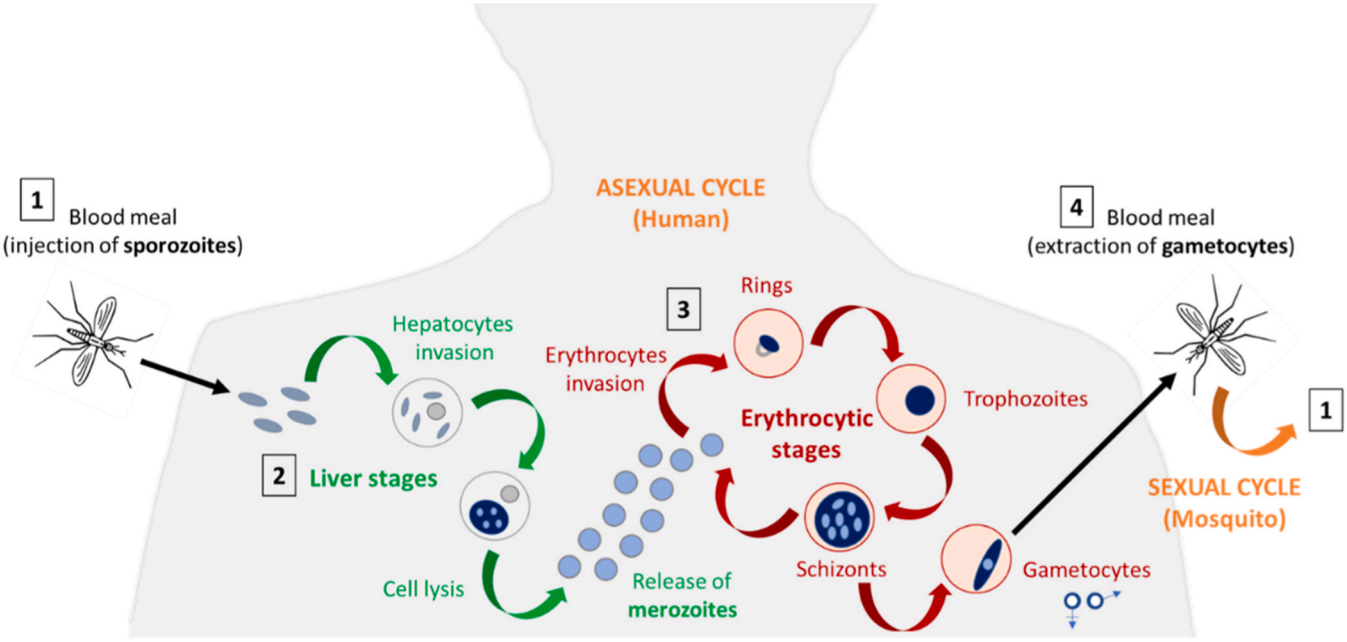

Fig. 2. Representation of the *P. falciparum* lifecycle in the human body.

2.2. Antimalarial drugs that can benefit from a vectorization strategy

Nowadays, the cures from malaria infections are dramatically impeded by the appearance of resistance mechanisms against antimalarial treatments, leading to an increase in reported cases world-wide (Fig. 1). In this regard, WHO currently encourages combination therapies where at least two drugs with different properties are used together to prevent or delay drug resistance. [55] In this context, the vectorization of antimalarial drugs takes its whole meaning. Targeted delivery of one or two drugs incorporated within a nanocarrier can help circumvent

the resistance mechanisms of the parasite and improve the synergic effect of combotherapies. A large variety of antimalarial drugs have hence been subjected to drug delivery system studies (Fig. 3).

Four families of antimalarial drugs have been commonly associated with DDS: Aminoquinoline (Primaquine (PQ), Chloroquine (CQ), Quinacrine (QN)); Aryl amino alcohol (Lumefantrine (LUM)); Antifolate (Pyrimethamine (PYR) and Serine hydroxymethyltransferase (SHMT inhibitor 1); and Artemisinin (Artemisinin (ART), Artemether (AM), Artesunate (AN)). The structural diversity of these drugs is explained by the complexity of the *P. falciparum* lifecycle, which can be targeted at different stages of the parasite development. Thus, these drug families have different mechanisms of action.

In the aminoquinoline family, quinacrine (QN) was once the primary drug on the market for the prevention and the treatment of malaria infections, especially during World War II. Nevertheless, it is now rarely used as an antimalarial. Chloroquine (CQ, 4-aminoquinoline derivative), a synthetic derivative of quinoline, was also widely used as a primary approach to eradicate malaria during the 1940s. The overuse of CQ around the world (especially in Asia and Africa) contributed to the rapid emergence and spread of resistance within ten years of its introduction. In the 1950s, several adverse toxicities were reported including cardiotoxicity, neurotoxicity, hepatotoxicity or even reprotoxicity. Despite thoughtful studies that explored the different mechanisms of action of CQ, its exact role is still not clear. [56–58] CQ could prevent the heme detoxification step in trophozoites: To survive, the parasite needs to crystallize the toxic free heme (an iron-containing porphyrin precursor to hemoglobin) into a nontoxic insoluble crystalline hemozoin form. By inhibiting this hemozoin crystallization, the chloroquine kills the parasite through heme accumulation. [59] 4-Aminoquinolines are also weak bases which accumulate in the digestive vacuole of the parasite and decrease its acidity. These derivatives could also be implicated in mechanisms of influx/efflux. CQ is still used to treat uncomplicated malaria cases. and remains effective for malaria prevention in areas where the parasite is sensitive to chloroquine. It is also the first-line chemoprophylaxis infection drug for chloroquine-sensitive *P. falciparum*, *P. vivax*, *P. ovale*, *P. malariae,* and *P. knowlesi* strains. With the emergence of resistance issues, a structurally related drug, amodiaquine, is often prescribed as an alternative. Primaquine (8-aminoquinoline derivative) displays activity against the intrahepatic forms (hypnozoites) of *P.vivax* and *P.ovale* malaria strains and thereby prevents the development of the erythrocytic forms (gametocytes), the main cause of malaria relapses. [60,61] PQ is generally administered in combination with blood schizonticide derivatives (artemisinin derivatives or CQ). However, PQ was revealed to be dangerous for patients with glucose-6-phosphate dehydrogenase deficiency.[48]

Antifolate drugs, like pyrimethamine (PYR) or the SHMT inhibitor,

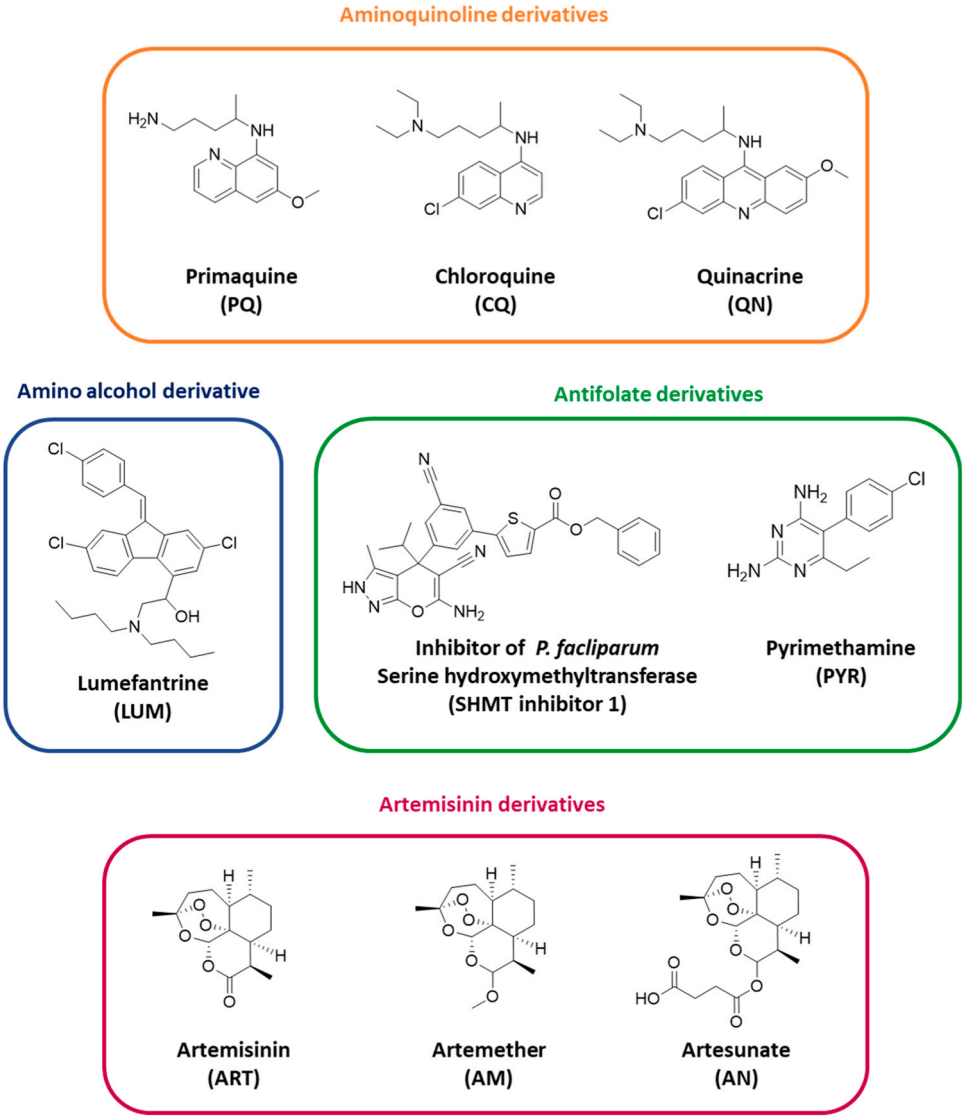

Fig. 3. Antimalarial drugs vectorized by drug delivery systems.

inhibit the dihydrofolate reductase of *Plasmodium* and thereby block the biosynthesis of purine and pyrimidine bases, which are essential for the DNA synthesis and cell multiplication of the parasite. [62] PYR also possesses a schizonticidal activity. They are often used in combination with Artesunate (AN) to treat acute and uncomplicated malaria cases.

Finally, artemisinin-combination therapies (ACTs) appear to constitute the current WHO-recommended treatment for uncomplicated and CQ-resistant malaria infections. As pointed out above, artemisinin drugs are commonly associated with the other antimalarial families to reduce resistance. [63] Artemisinin derivatives act fast on the early and late stages of human malaria. These compounds contain endoperoxide bridges which are essential for antimalarial activity. The general mechanism relies on the heme-catalyzed cleavage of the endoperoxide bond to produce cytotoxic radical species. The released free radical intermediates then kill the parasite by alkylating and poisoning one or more essential malaria proteins. [64,65]

Aryl-amino alcohol derivatives like the widely used Lumefantrine (LUM) also inhibit the intraparasitic polymerization of free heme into hemozoin. LUM is usually co-administered with artemether (in a combination called Coartem® or Riamet®) to treat uncomplicated *P. falciparum* or CQ-resistant P. *vivax* malaria (first commercialized by Novartis, 2009). [66] Combination of LUM and artemether (AM) blocks the synthesis of intraparasitic nucleic acids and proteins which are essential for the parasite growth. This combination offers rapid, high efficacy and is relatively well tolerated. Both drugs also have schizonticidal activities (and gametocidal for AM) and LUM is known to prolong the action of AM. [67,68] However, recent reports described a decreasing efficacy of this combotherapy. [69]

The multiplication of drawbacks encountered with these antimalarial drugs and the emergence of resistance issues prompted researchers to study polymeric drug delivery systems (DDS) as a new therapeutic strategy for their vectorization.

2.3. What is the contribution of nanopolymeric drug delivery systems to malaria treatments?

In the past few years, several studies on nanovector systems for antimalarial drugs have emerged. The stated aim of these anti-malarial vectorization strategies is basically the same as for most vectorized drugs: to overcome the common disadvantages of antimalarial drugs. Such disadvantages include low blood circulation time, low solubility, repeated drug administration, quick metabolization, adverse toxicities and of course, resistance. Nanocarriers can for instance improve the bioavailability of antiplasmodial drugs, which is highly dependent on the method of administration. Drugs used to treat severe malaria are injected through a parenteral or intramuscular route, while drugs used for the uncomplicated forms of the infection are delivered orally. Bioavailability is also dependant on drug solubility, rate of physiological degradations, and other physicochemical factors that impact the pharmacokinetic profile of the drugs. Drugs with poor oral bioavailability often require high and/or repeated doses that can result, over time, in toxic side effects and the appearance of resistance. Macromolecular DDS generally have a longer lifetime in the blood thanks to their large size and thus improve the circulation time of the drug in the blood. [50,70] They also allow the encapsulation of large amounts of drugs while protecting them against degradation. In the case of malaria, nanocarriers can also have an impact on the erythrocytic stages, helping drugs to penetrate the parasite-infected red blood cells (pRBCs) to target the erythrocytic forms. Passive absorption of a free drug into these erythrocytes is often problematic as the latter does not have an endocytic system to favour the penetration. The high lipophilicity of drugs, necessary to penetrate pRBCs, also results in a poor pharmacokinetic profile and leads to drug-accumulation in non-targeted tissues or interactions with plasma proteins.

These issues of bioavailability and penetrability of antimalarial drugs could be solved by the use of nanocarriers. Indeed, new permeability pathways (NPPs), absent from healthy RBCs, have been observed in pRBCs (Scheme 1). NPPs are transmembrane channels present in the plasma membrane of pRBCs and are essential for parasite nutrition and waste excretion. [71] These channels have been estimated to range between 50 and 80 nm in diameter [72] and to be permeable to biomacromolecules. [73] Hence, these NPPs represent an interesting specific access route for both the passive and the active entry of drug-delivery systems. [74] Incorporation of antimalarial drugs within a nanocarrier of the appropriate size can thus promote selective penetration into pRBCs while maintaining the integrity of healthy RBCs.

As in other therapeutic fields, DDS targeting malaria infections can take different forms, such as liposomes, hydrogels, micelles, dendrimers, or even inorganic particles. [45–50] This review focuses on polymeric DDS like polymer-drug conjugates, micelles, or dendrimers. Section 2 describes the different strategies employed to synthesize these nanocarriers as well as the methods used to anchor or encapsulate the drug.

3. Design and synthesis of polymeric DDS

Whether for polymer-drug conjugates, micellar or dendrimeric systems, the polymer matrix is generally synthesized before the incorporation or conjugation of the drug. Depending on the nanocarrier system, distinctive methods are used to synthesize the polymeric backbone of the vector. All the physicochemical and biological aspects of these DDS will be discussed and described in Sections 3 and 4.

3.1. Polymer-drug conjugates (PDC)

Polymer-drug conjugates, also called polymeric prodrugs, generally consist of a polymeric backbone made of two or three covalently-linked distinct units of polymers (also called blocks), (Fig. 4). [75] According to the first model proposed by Helmut Ringsdorf in 1975, [76] several items can then be connected to this backbone, including different types of drugs, solubilizing agents, or even specific targeting agents. Compared to systems where the drug is encapsulated, direct drug conjugation to the PDC significantly enhances the drug loading efficiency.

3.1.1. General strategies for the synthesis of PDC

The drug and these items are usually covalently anchored to the polymeric backbone *via* a linker that will later allow drug release under certain conditions (pH, enzymes, etc.). [77,78] Obviously, the choice of the linker has a strong impact on both drug loading and release mechanism. [79] The linker can be a distinct molecular moiety or a simple functional group existing on the polymer. The anchorage of the drug and the polymer through the linker usually takes advantage of the presence of amine, alcohol, ester, or carboxylic acid groups to form amide, ether or ester bonds (Fig. 4). The most widespread methods to anchor the drug on the polymer thus involve condensation reactions, like esterification between a drug moiety (-COOH or OH) and the polymer backbone, or addition reactions of amino-drug derivatives on the polymer chain.

Three general strategies can be used for PDC synthesis (Scheme 2): a) the drug is incorporated into a previously synthesized polymer (*via* a linker); b) the drug is first linked to some monomer units which are then polymerized with other monomer units; and c) more rarely, a modified drug is activated and used as initiator of the polymerization of the monomer units. While it can be difficult to evaluate the efficiency of the conjugation rate and/or the position of the drug units on the polymer backbone with strategies a) and b), method c) allows accurate control of drug loading and directly positions the modified drug at the end of the newly formed polymer chain. However, the method c) is not suitable for a large variety of drugs and sometimes requires tedious modification of the drug. Moreover, it only introduces one molecule of drug per PDC.

Regarding the constitution of the backbone, a polymer with only one kind of monomer unit is called a homopolymer, whereas polymers with more than one type of monomers are called co-polymer s (Scheme 3).

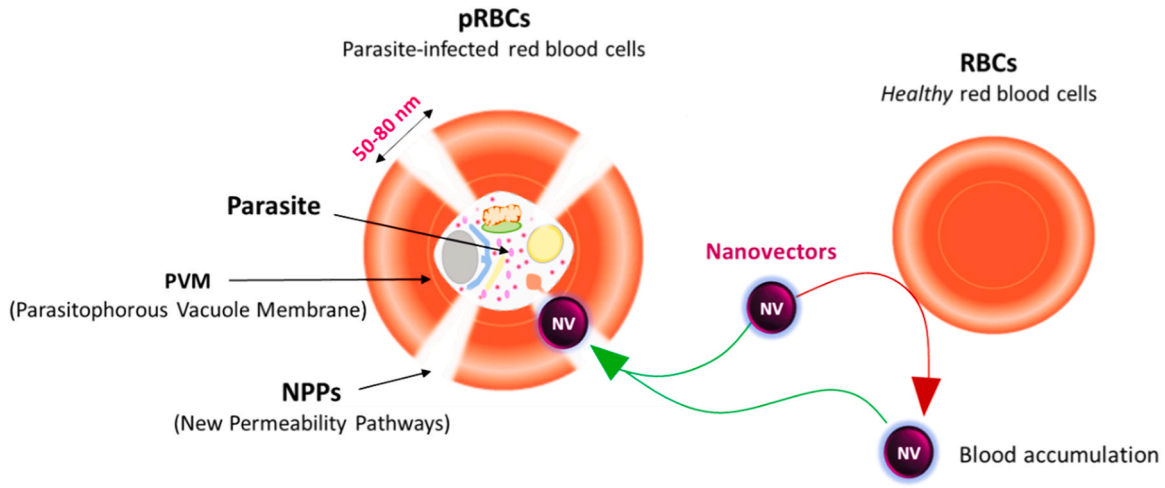

Scheme 1. Selectivity of macromolecular DDS for parasite-infected red blood cells (pRBCs).

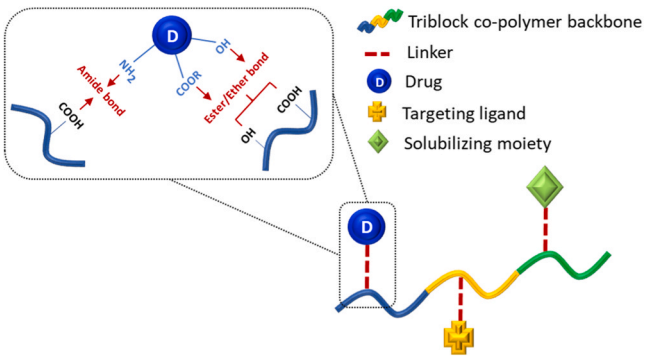

Fig. 4. Representation of the Ringsdorf model for PDC.

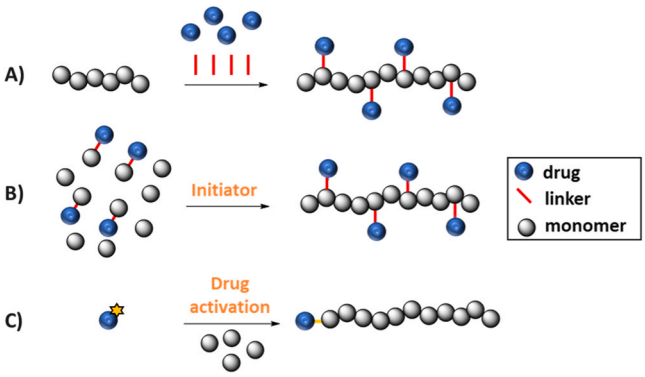

Scheme 2. General strategies for the synthesis of polymer-drug conjugates.

Co-polymers can be made of random or distinct blocks (often diblocks and triblocks), which significantly increases the range and diversity of their chemical properties. Block co-polymers can be synthesized combining different living or controlled polymerization mechanisms such as radical, cationic, anionic, ring-opening polymerizations or polyaddition reactions. [80] However, because of reactivities specific to each monomer, not all combinations of co-polymers can occur. Generally, four strategies of co-polymerization can be used to combine these different propagating modes: A) Sequential monomer polymerizations, B) Site transformation, C) Sequential block-polymer couplings, and D) Dual initiation method.

In method A, an initiator (green triangle) is used to trigger the polymerization of a first monomer 1 (grey). Depending on the mode of propagation of the polymerization, a specific reactive center (*) is present at the chain-end of the growing polymer (e.g.: an anion in the case of anionic polymerization). As long as this chain-end remains reactive, different monomers can be sequentially added to pursue the polymerization with a new block. In Scheme 3A, after the polymerization of monomer 1, the reactive center initiates the polymerization, through the same mechanism of propagation, of a second sequentially added monomer 2 (purple) to form the diblock co-polymer. Quenching of the reactive center prevents further elongation of the polymer chain.

In the site transformation process (B), the polymerization of the first block is initiated as in method A. The propagation of this first block is then stopped transforming the propagating reactive centre (*) into a new kind of initiator (red triangle) which stays hung to the polymer chain-end. This second initiator triggers the polymerization of a second monomer (purple) to form the diblock co-polymer. Polymerization of the second block by means of this homopolymeric initiator allows the copolymerization of monomers that polymerize through different mechanisms (e.g. living cationic polymerization followed by radical or anionic polymerizations).

A diblock co-polymer can also be formed *via* coupling of preformed homopolymers (C). The two beforehand prepared homopolymers contain complementary functional groups at their chain-ends that react together to form the block copolymer (e.g. through alkyne-azide cycloaddition reaction).

In the dual initiation method (D), a dual-initiator featuring two distinct activating groups (green and red) is used to initiate two kinds of polymerization mechanisms. The polymerizations triggered by each activating group can be performed sequentially, in any order, or simultaneously in some cases. This strategy generates diblock co-polymers connected through the dual initiator.

Ring-opening polymerization (ROP) [81] is the most commonly used method for the synthesis of biocompatible polymers like poly-D, L-lactide (PLA), poly-ethylene glycol (PEG), poly-caprolactone (PCL) or co-polymers like poly-D,L-lactide-*co*-glycolic acid (PLGA). [82] It also allows the formation of biodegradable ester or amide polymeric backbone. ROP consists in the chain-growth polymerization of cyclic monomers during which the chain opens the ring of the monomer to form a longer polymer chain. The main driving force for ROP is the release of the bond-angle ring strain which varies with the type and size of the cyclic structure. It essentially works with cyclic monomers containing alkane, alkene, and/or heteroatoms (nitrogen, oxygen, sulfur, and silicon) moieties in the ring. Ring-opening polymerization relies on different mechanisms depending on which initiator and catalytic system are used; it works through anionic (nucleophilic initiator), as well as

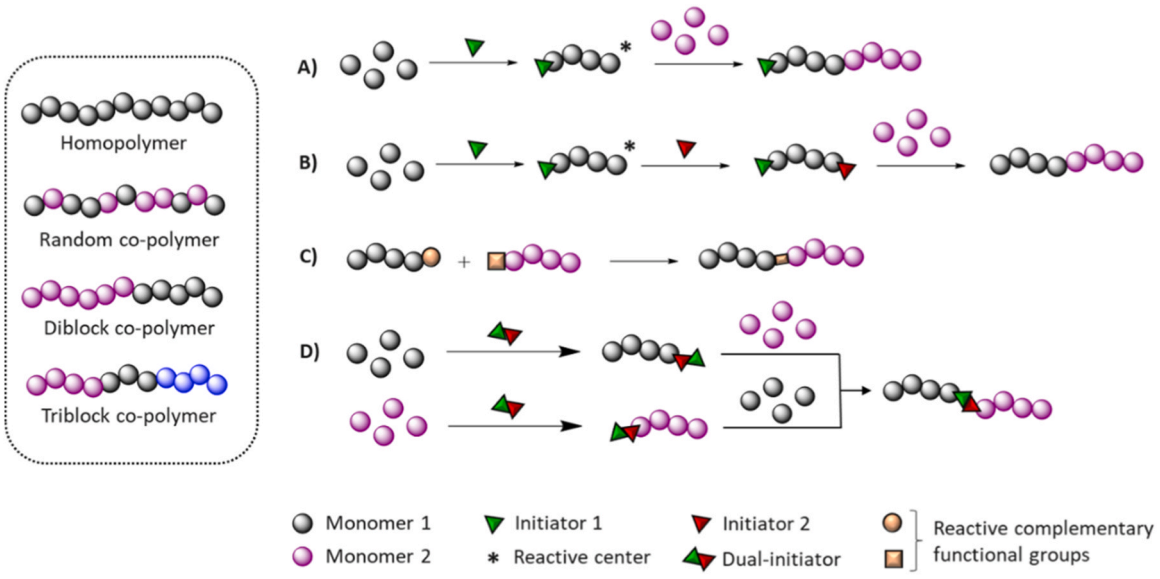

Scheme 3. General strategies for the synthesis of co-polymers.

through cationic (Bronsted acid or metal cations) or radical polymerizations (radical initiator) (Scheme 4).

In anionic ring-opening polymerization, the addition of the nucleophilic initiator on the carbonyl group of the monomer (such as ε-caprolactone) promotes the ring opening of the acyl-oxygen bond (**A**). The new negatively charged terminal alcoholate group of the opened monomer **B** initiates the propagation of the polymerization reaction by addition on the carbonyl group of another monomer. Anionic ROP is sensitive to water (anion quenching) and can be subjected to undesirable intramolecular reactions resulting in cyclic polymers, with lower molecular weights.

In cationic ROP, the monomer becomes positively-charged (**C-D**) after reaction between the carbonyl group and an electrophilic initiator. Nucleophilic substitution on the cationic monomer **D** by a new monomer

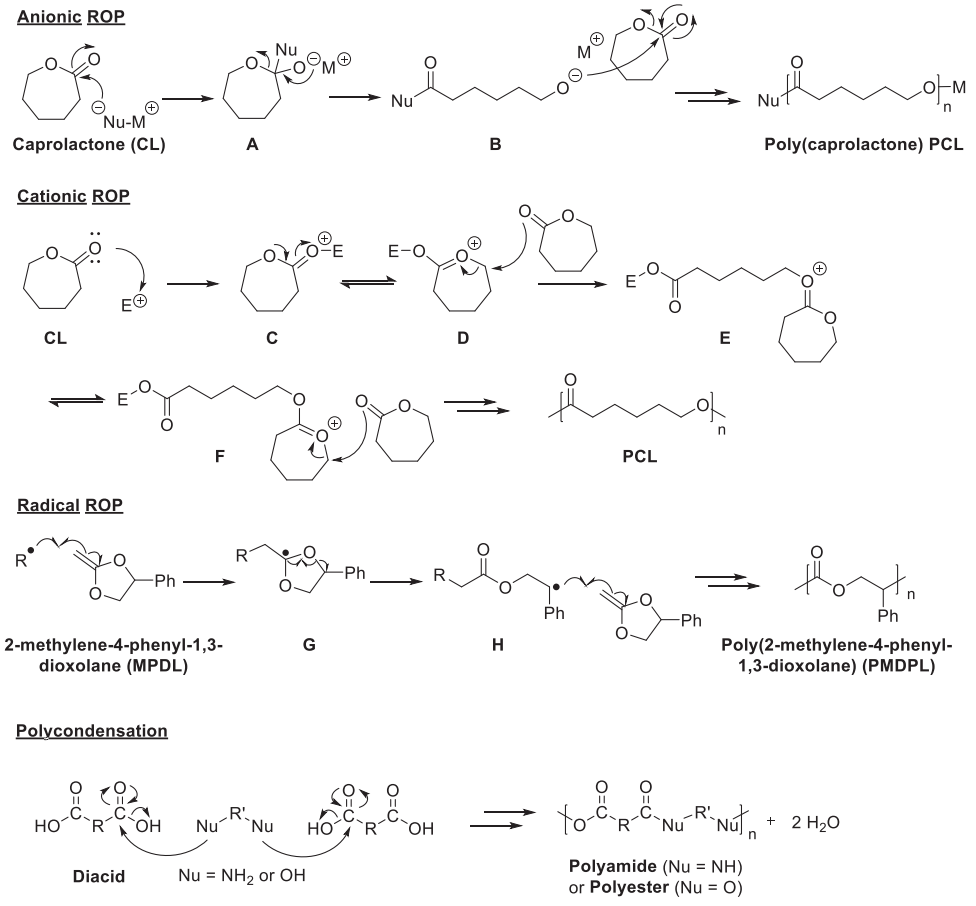

Scheme 4. Typical mechanisms of ring-opening polymerizations (ROP) and polycondensations.

molecule, leads to its ring opening. The terminal positively charged monomer C propagates the reaction upon addition of new monomers. Cationic ROP is difficult to control, often leading to high molecular weight polymers.

In radical ROP, the monomer must possess a radical accepting group (such as a C═C bond) and a highly distorted ring structure. The ring-opening reaction should be combined with an isomerization process to afford a thermodynamically stable functional group. For instance, the ring-opening mechanism of the cyclic ketene acetal monomer occurs by the formation of an acyclic ester bond (which is thermodynamically more stable) and by the stabilization of the resulting radical by the phenyl group. Radical ROP is limited by the choice of monomer and by its sensitivity to air.

Alternatively to ROP, polycondensations are also a common strategy to prepare biocompatible polyester and polyamide backbones (Scheme 4). Polycondensations consist in the step-growth polymerization of bi-functional (or even multifunctional) monomers that react to form first dimers, then trimers, longer oligomers and eventually long chain polymers.[80] In the depicted example, the two nucleophilic atoms (N or O) of a dinucleophile (diamine or dialcohol) can each add on the carboxylic acid of a diacid to form an amide or ester group, respectively, and concomitantly loss a molecule of water. The resulting diacid dimer in turn reacts with two dinucleophiles, and so on until the polyamide or polyester chain is formed.

3.1.2. *Immune system-evasive stealth nanocarriers*

Macromolecular vectors, whatever the therapeutic application, have the disadvantage of rapidly being recognized by the immune system (Scheme 5). [83] This rapid immune detection is favoured by the formation of a fast and dynamic coating of endogenous biomolecules around the surface of a nanoparticle upon exposure to biological environments. [84,85] This so-called protein corona forms spontaneously around colloidal nanomaterials and is usually composed of layers of proteins (albumin, apolipoproteins, immunoglobulins, complements C3-C4, etc.). [86] Corona protein-coating of the nanoparticle depends on many physicochemical factors including the size, shape, surface functionality, surface charge and solubility of the vector, as well as its binding affinities with proteins and the exposure time. It also depends on the type of media, nanoparticle to protein ratio, and the presence of ions and other molecular species that can interfere in this nanoparticle-protein interaction. This underestimated effect is responsible of a high failure rate in translating *in vitro* results to *in vivo* applications. Among this aggregation of plasma proteins, the phenomenon of opsonization is considered as the main immune-response clearance method for the removal of large undesirable materials from the blood. The opsonization corresponds to the attachment of opsonins to the proteins adsorbed on the surface of the nanoparticle or directly to its free surface, triggering their uptake by macrophages, and consequently their phagocytosis. Once phagocytosis occurs, the opsonin-covered nanoparticle is engulfed and/or eventually eliminated from the bloodstream.

Several research have been led on DDS to interrupt this opsonization mechanism and avoid immune-cell recognition. PEGylation of the nanoparticle is the most common strategy, preventing its non-specific adsorption and increasing its blood circulation half-life. [87,88] Indeed, the presence of a biocompatible hydrophilic polyethylene glycol (PEG) moiety on the surface of the nanoparticles reduces interactions with plasma proteins thanks to steric and electronic hindrance. PEGylated nanoparticles are thus considered as stealth systems. PEG is the most common polymer used to conceal DDS, but recently alternative hydrophilic polymers have been used, such as poly (2-methyl-2-oxazoline) (PMOXA). Despite to its many qualities, PEG can cause an immune response after repeated injections and has a limited long-term stability, particularly *in vivo*. PMOXA is free from cytotoxicities, hemocompatible and easily internalized by the cells. *In vitro* studies also revealed that PMOXA was not sensitive to hemolytic or enzymatic degradation under physiological conditions, but rather to oxidative degradation. [89]

Poly(ethylene glycol) blocks of different sizes (average molecular weight $M_n \approx 200$ to $> 20\,000$ g.mol^{-1}) are commercially available with different functional groups at their chain-end (OH, OR, NH_2, COOH, N_3, …). The PEG block is thus generally introduced at last on the co-polymer backbone, by nucleophilic substitution or addition reactions. This method is applicable to the PEGylation of polymer-drug conjugates, as well as the PEGylation of micelle and dendrimer's surfaces.

Alternatively, several researchers were recently interested in taking advantage of the protein corona effect as an indirect surface shield coating to protect the nanoparticles in the body. [90] An artificial corona coating composed of specifically selected proteins, pre-adsorbed on the nanoparticle surface prior to introduction into the bloodstream, could prevent nonspecific protein aggregation and thus phagocytosis. Moreover, this artificial protein corona could participate to the targeted

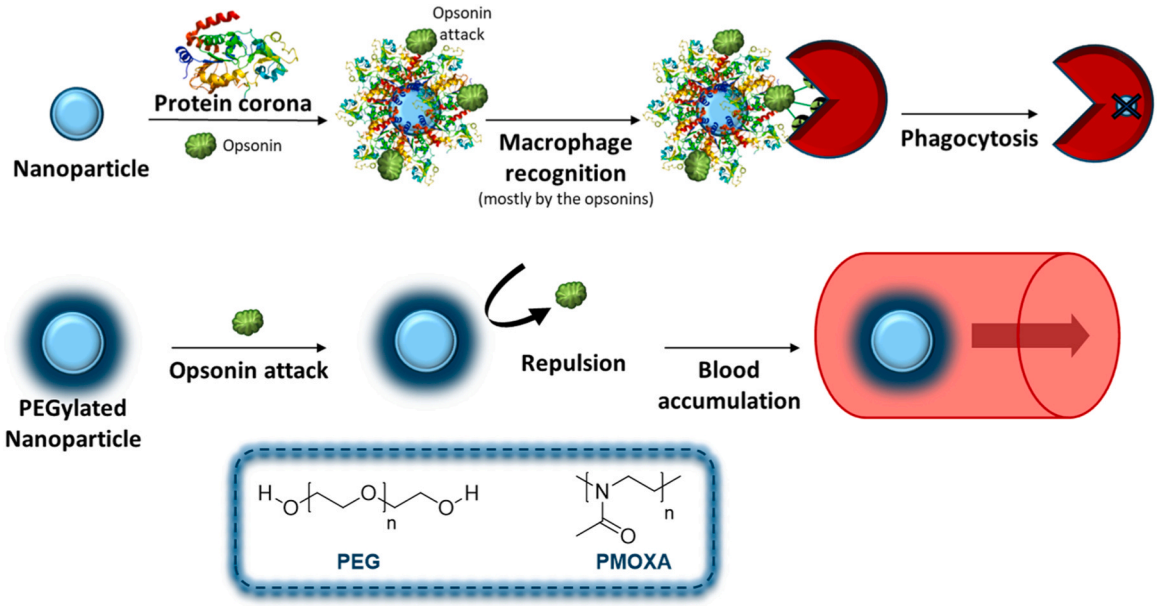

Scheme 5. Protein aggregation on nanoparticles.

delivery of the nanoparticle to the intended biological target. Another approach, less specific but simpler and more economical, consist in the functionalisation of the nanoparticle surface with selected ligands favouring the *in vivo* recognition and binding of specific endogenous proteins. Zhan and co. for instance, exploited the binding affinity of a short nontoxic peptide, derived from $A\beta_{1-42}$, with apolipoproteins to achieve brain-targeted delivery of a nanoparticle. [91] Although the corona effect remains poorly understood, this corona-mediated targeting strategy is expected to generate more interest in the following years for the functionalization of particle surfaces targeting challenging diseases.

3.1.3. Examples of PDC used in antimalarial therapy

These different synthetic strategies have been applied to the preparation of polymer-drug conjugates with antimalarial activities. Table 1 summarizes several examples of these PDC and gives an overview of their main physico-chemical and biological properties.

For instance, the water-soluble random triblock poly(aspartamide) co-polymer **4** was prepared for the vectorization of pyrimethamine (PYR) (Scheme 6), [92] following a step-growth polymerization strategy. The polycondensation of D,L-aspartic acid into poly(succinimide) backbone **1** was triggered by phosphoric acid at high temperatures, followed by sequential and random additions of amino-substituted derivatives to some succinimide units of this polymer (post-modification of the polymer chain). The hydrophilic 3-diethylamino-1-propylamine (DEP) was first added to ensure the solubility of the poly(aspartamide) (**2**). Then, the pyrimethamine drug (PYR) and a second antipyretic drug, the 4-aminosalicylic acid, were randomly conjugated to other succinimide units to finally generate the PYR-substituted poly(aspartamide) **4**. Amino acid-based polymers associated to antimalarial drugs can have an essential antiplasmodial action. Poly(aspartamide) conjugates inhibit the dihydrofolate reductase (DHFR), an enzyme involved in the NADPH-dependent reduction of dihydrofolate to tetrahydrofolate. This reduction reaction, essential for the *de novo* synthesis of purines and amino acids, is crucial for the rapid growth of the parasite. The 4-aminosalicylic acid may act as a good potentiating agent when used in combination with PYR, as it may interfere with folate metabolism by inhibiting the transport of *p*-aminobenzoic acid used by parasites for folate synthesis. [93] Using the same strategy, the authors also prepared poly(aspartamide) polymers conjugated to different ratios of other antimalarial drugs, including primaquine, 4-aminoquinoline or platinum-base complexes.[92,94] The energy-dispersive X-ray method (EDX) (section 3.2.4.) was used to confirm the elemental composition of each poly(aspartamide) conjugates. The particle sizes of all these conjugates ranged between 106 and 356 nm. Conjugate **4** was 254 nm in size with an almost neutral global electrical charge (zeta potential of + 1.62 mV, Table 1, entry 1). The drug loading of PYR and 4-aminosalicylic acid in conjugate **4** were 8 and 9% respectively. The drug release studies showed that the release of PYR was slow and sustained at pH 7.4 when compared to pH 5.4. Finally, conjugate **4** was found to be the most active poly(aspartamide) co-polymer conjugate against the asexual stage of the parasite, with an IC_{50} of 332 nM.

In the same vein, the group of Fernàndez-Busquets reported the synthesis of poly-amidoamine (PAAs) conjugates containing chloroquine (CQ) and primaquine (PQ) under their salt forms (Table 1, entry 2). [95,96] The random diblock co-polymer **5** or homopolymers **6** and **7** were first prepared upon Michael-type polyadditions of bis-amino-derivatives on bis-acrylamides (Scheme 7). Finally, CQ (or PQ) was incorporated into the PAA polymers by drop-wise addition of a basic solution of the drug (pH 12) to a solution of PAAs (isoelectric pH) until neutral pH was reached. While the article is not explicit on this point, it can reasonably be assumed that the drug deprotonates the OH or COOH group of PAAs **5-7** to form the ion pair. PAAs are water-soluble synthetic polymers designed to be biocompatible and biodegradable into oligomeric residues. PAAs also share some features with peptides and proteins, facilitating their penetration into pRBCs (pRBCs are permeable to high molecular mass and polyelectrolytic solutes). These CQ- and PQ-PAAs were referred as polymer-drug conjugates, although here the drug and the polymer were connected through an ionic bond rather than a covalent bond. Indeed, they formed an ion pair where the drug was incorporated as a cation while the pre-formed polymer was the anion.

Table 1
Polymer-drug conjugates with antimalarial activities.

Entry	1	2	3
PDC	**PYR-poly(aspartamide) (4)**	**CQ/PQ-PAAs (5−7)**	**AN-poly(heparin) (8)**
Vectorized drug(s)	Pyrimethamine (PYR)	Chloroquine (CQ) or Primaquine (PQ)	Artesunate (AN)
Biological target	*Plasmodium falciparum*	*Plasmodium falciparum*	*Plasmodium falciparum*
Polymer synthesis	Polyadditions of amino-derivatives on poly(succinimide) units	Michael Polyadditions	Incorporation of AN on a pre-formed heparin polymer (esterification)
Critical micellar concentration (CMC)	nd	nd	20 μg/mL
Zeta potential (ZP)	+1.62 mV	nd	-11.2 mV
Sizes (analysis method)	234 nm (DLS)	20–40 nm (TEM)	112 nm (DLS) 50–100 nm (TEM)
Drug loading (DL) or Weight/weight ratio (W/W)%	DL = 8% (PYR) DL= 9% (4-aminosalicylic acid)	W/W = 14–33% wt% (CQ) W/W = 15–29% wt% (PQ)	DL= 29 wt%
Conditions of drug release	Slow release at pH 7.4 (72 h) Fast release at pH 5.4	65–80% (CQ) 85–100 (PQ) at pH 7.4 (24 h)	pH 7.4: 34% (72 h) pH 5: 93% (72 h)
Antimalarial activities (IC_{50})	332 nM (free PYR: nd)	**6**: 19–109 nM (CQ) 4–18 μM (PQ) **7**: 15–73 nM (CQ) 2.5–13 μM (PQ) (free CQ: 16–99 nM) (free PQ: 4–12 μM)	10 nM (free AN: 6.3 nM)
Observations	Conjugates containing both 4-aminosalicylic acid and PYR were the most active against the asexual stage of the parasite.	Impact of basicity and hydrophobicity of the polymer backbone in drug release. High polymer lenghts allowed better IC_{50} values. Hemolytic activity observed for **7**.	The heparin polymer improved the pharmacokinetic properties of the PDC and blocked essential heparan sulfate parasite receptors.
References	92	95–96	98

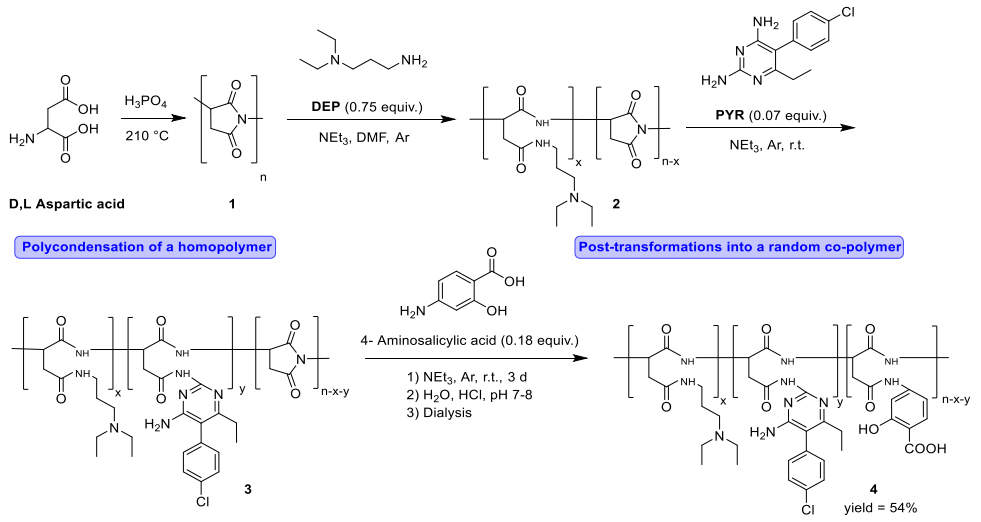

Scheme 6. Synthesis of antimalarial PYR-poly(aspartamide) conjugates **4** by random additions of amino-derivatives.

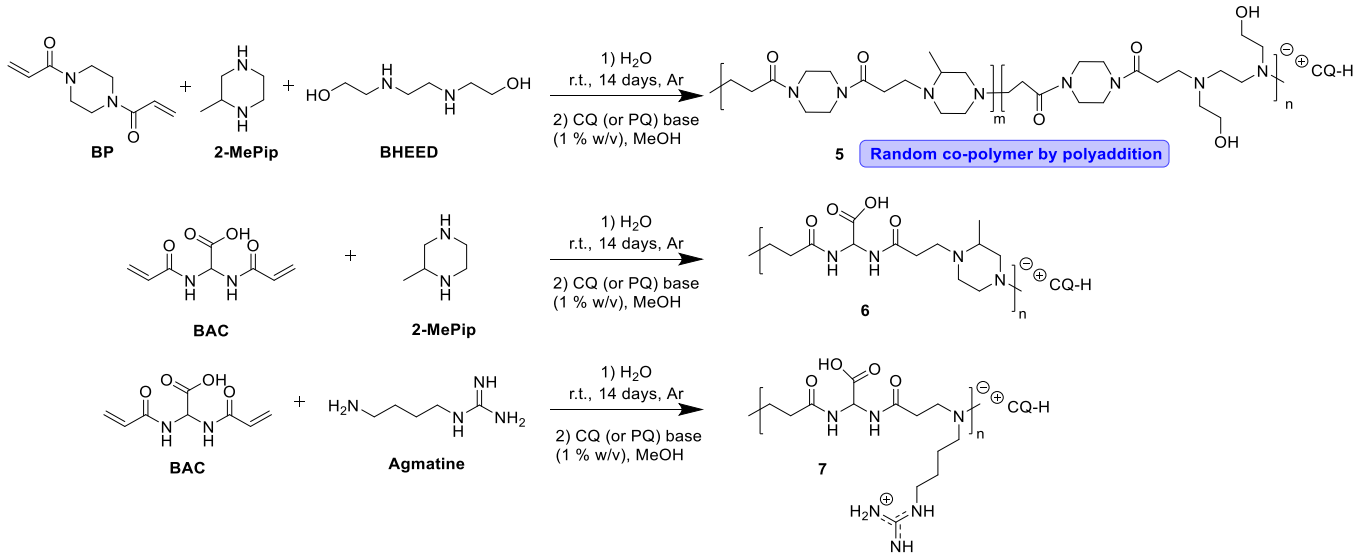

Scheme 7. Synthesis of PAA polymers 5, 6 and 7 by polyadditions reactions.

Globular-shape drug-polymer salts were obtained with sizes ranging from 20 to 40 nm with good w/w ratio ranging between 14 and 36 wt% (Table 1, entry 2). The PAAs-conjugates showed *in vitro* activities ranging from 15 to 109 nM (PAAs-CQ series) and from 2.5 to 18 μM (PAAs-PQ series). The highest *in vitro* values were obtained for the trophozoite stages. The *in vitro* antimalarial activities of the conjugated-drugs were not significantly increased compared to their free forms (except for the conjugate **7-PQ** displaying an IC_{50} reduced by about 35%, but which possessed hemolytic activity). However, the experimental *in vivo* results demonstrated that PAA-conjugates **6-CQ** and **7-CQ** were more effective than the free drug.

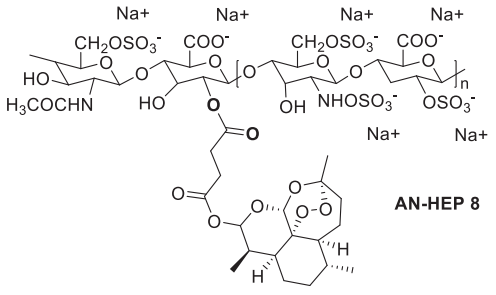

Fig. 5. Artesunate-poly(heparin) conjugate AN-HEP **8**.

In term of polymeric structures, polysaccharides are also widely applied as nanocarrier as they can extend the retention time in the bloodstream and provide good biodegradability. [97] The poly(heparin) backbone of the artesunate-poly(heparin) conjugate **8** also proved therapeutically interesting as it recognizes the heparan sulfate receptors present on the cellular surface of the parasite (Fig. 5). [98] Heparin disrupted both *in vitro* and *in vivo* interaction between the protein-1 of the *P. falciparum* erythrocyte membrane (PfEMP1) [99] and the host cell surface receptors, preventing the infection of the RBC. AN-HEP **8** displayed a hydrodynamic diameter of 112 nm and a negative global electrical charge (ZP = −11.2 mV, Table 1 entry 3). No hemolysis effect of AN-HEP **8** was noted, which offers the possibility of a safe use for intravenous injection.

3.2. Polymeric micelles

Micelles are ideal vectors for the delivery of therapeutic agents with low solubility in water. [100–102] Thanks to their small sizes and

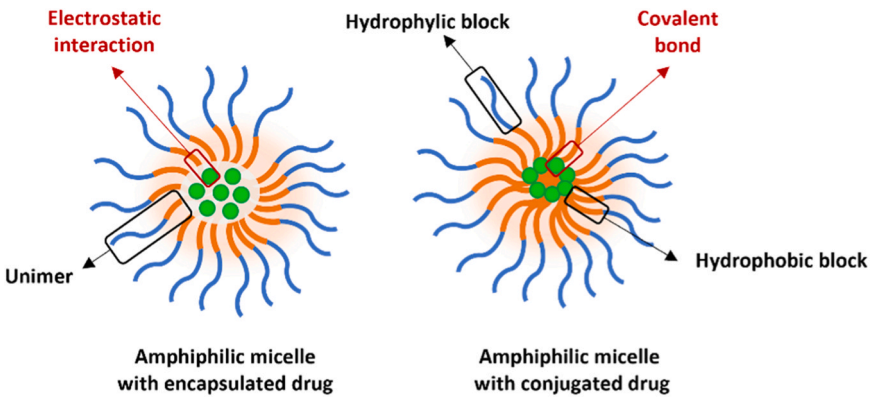

Scheme 8. Micellar DDS structures.

hydrophilic surfaces, micelles are poorly recognized by the immune system, which prolongs their plasma half-life. [103] Micelle vectors can also be functionalized by additional ligands or antibodies anchored to their surface, including targeting and stimuli responsive systems. [104, 105]

Micelles generally consist of the supramolecular assembly of co-polymer chains (unimers) composed of different blocks (Scheme 8). The polymer block of the center core of the micelle is usually hydrophobic. It serves as a reservoir in which non soluble bioactive entities can be incorporated. While the polymer block at the surface of the micelle is more hydrophilic and favours the assembly of micelles. [106] Hence, the essential characteristics for the hydrophilic block are good aqueous solubility, biocompatibility, capacity to form hydrogen bonds and create steric stabilization. The vectorized drug can be either conjugated or encapsulated in the micelle and is generally located in its inner core.

The strategy used to prepare drug-conjugated micelles consists in the synthesis of polymer-drug conjugates (PDC) followed by the assembly of these PDC unimers through a micellization process. Synthetic methods to prepare PDCs have already been described in the previous section 2.1.1. Hence, this section will focus on the micellization processes that allow the preparation of micellar particles and on the methods of drug encapsulation.

3.2.1. General strategies for the synthesis of micelles

In the case of drug-encapsulated systems, the polymer matrix of the micelle is generally synthesized before drug incorporation. The polymerization reactions used to prepare the co-polymer chains (unimers) are the same as for the synthesis of PDC-copolymer backbones (Scheme 3). Hence, the polymeric matrix of micellar DDS is usually made through polyaddition reactions or ring-opening polymerizations (ROP). [107] Other mechanisms such as ring-opening metathesis polymerization (ROMP) [108] and reversible addition-fragmentation transfer polymerization (RAFT) can also be employed.[107]

Micellization is then the process by which unimers assemble into nanoscopic supramolecular structures known as micelles, when they reach a threshold concentration in solution called the critical micelle concentration (CMC) (Scheme 9). Unimers are amphiphilic block co-polymers, also called surfactants. These unimers are composed of at least two polymeric segments of different nature, with one relatively non-polar or hydrophobic (e.g.: PCL block) and the other relatively polar or hydrophilic (e.g.: PEG block). These different solubility properties are responsible for the micellization process. Micellization is the result of attractive-repulsive interactions allowing formation of the micelles from the unimers. The attractive interaction between unimer segments allows the association of the polymer chain while the repulsive interaction prevents unlimited micelle growth to a distinct macroscopic phase. When the micellization process occurs in an aqueous media, the hydrophobic parts associate to form the micellar core, while the hydrophilic parts form the micellar shell and are positioned between the hydrophobic core and the aqueous bulk phase. In order to favor the formation of spherical micelles, the hydrophobic blocks must be shorter than or of similar length to the outer hydrophilic blocks.

The micellization process and the critical micelle concentration are entropically driven by the hydrophobic blocks. Indeed, the hydrophobic effect is associated to an increase in entropy (ΔS) due to the increased disorder caused by water molecules to reduce their exposure to the hydrophobic segments of the unimers. The water molecules are expelled from the central core of the micelle to the bulk aqueous phase. Increased hydrophobicity and size of the hydrophobic blocks lead to the formation of micelles at low CMC values, while the opposite is observed when the size of the hydrophilic block increases. The lower the CMC value, the

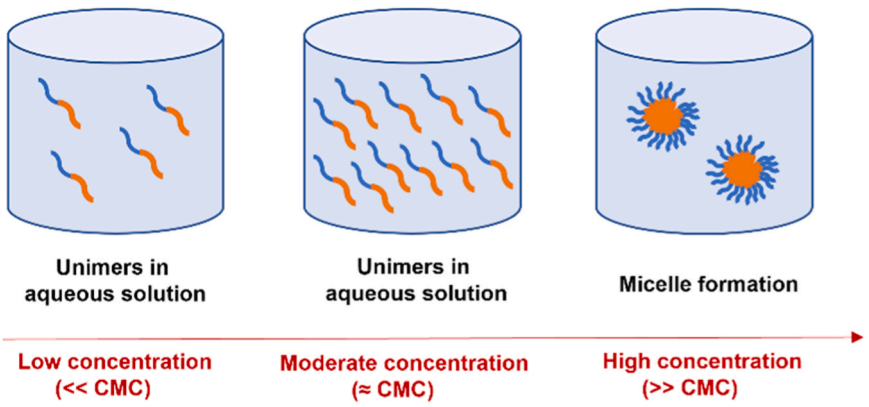

Scheme 9. Formation of a micelle and critical micelle concentration (CMC).

more thermodynamically stable the micelle. Hence, polymeric micelles with low critical micellar concentration, are thermodynamically stable and offer good drug stability under dilution in biological fluids. While micelles with high CMC tend to easily dissociate, resulting in a dilution effect in the blood. [109,110] The CMCs of block co-polymer micelles are typically in the range of 10^{-6} to 10^{-7} M. The micellar association number is the number of unimers needed to form a micelle. Micelles are generally made up of 50–200 unimers and the radius of the spherical micelles are almost identical to the length of a fully extended unimer (1–3 nm). The molecular size and geometrical properties of the unimers determine the size of the micelle. [111] The particles sizes and polydispersity of the micelles can also be influenced by the choice of synthetic strategy (nature of blocks and solvent, concentrations, addition order, etc.).

Several techniques are used to measure the CMC and micellar association number, such as surface tension, [112] conductivity, [113] light scattering, [114] and fluorescence methods. [115,116] The fluorescence technique is routinely employed for CMC determination. Different fluorescent probes are available, such as the coumarin-153, eosin, Nile Red or Pyrene. Pyrene is frequently used as a probe following the I1/I3 method because of its high quantum yield and spectral response. [117] The ratio of the fluorescence intensities of the first (I1) and the third (I3) vibronic peaks of pyrene reflects the environmental polarity of the probe (herein micellar formation). The fluorescence intensity of pyrene increases dramatically to the red shift wavelengths excitation spectra when it is in a non-polar environment, thus when micelle formation occurs and traps the probe in its core. This shift causes a change in the vibrational structure of the emission spectra of pyrene, allowing CMC determination. In other words, when the concentration of the polymer units reaches its CMC, a sudden drop in the fluorescent intensity ratio is observed due to the transfer of the fluorescent probe from a polar to a non-polar environment upon its trapping in the as-formed micelle. From a practical point of view, a fixed diluted concentration of a fluorescent probe is added to a unimer solution at different concentrations. The emission intensities of I1 (374 nm) and I3 (483 nm) vibronic bands of the probe are then measured under excitation at 336 nm. Micelle formation at the CMC is followed by a decrease in the I1/I3 ratio (Fig. 6A). The CMC is determined where a stationary curve appears on the spectra related to a stable electronic effect. The fluorescence spectrum of the solution is measured by a spectrophotometer in quartz cuvette and analyzed for CMC calculation. However, although the high quantum yield and partitioning of pyrene in most micellar cores allows for versatility and little interference with the micellization process, this method suffers from low reproducibility and difficulties in spectra interpretation because of the number of signal shifts. The pyrene assay requires fluorometers with multiwavelength capabilities, which is not a standard filter-based plate reader. Recently, a robust method for critical micelle concentration determination using coumarin-6 as fluorescent probe was performed in a plate reader, simplifying the experimental process. [118] The CMC can also be obtained studying the surface tension of the sample (Fig. 6B).

For instance, for the AN-loaded HEP **8** which self-assembles into micelles,[98] the crossover point of the two straight lines indicated a CMC of 20 μg.mL^{-1} (Fig. 7, A), which is relatively low compared to other antimalarial-drug loaded DDS (CMC ranged from 0.16 to 2 mg.mL^{-1}). For the PVP-*b*-PVL/VE-LUM micelle **21** (described in section 2.2.3)[143] the AM drug-loaded micelle (CMC = 2 mg.mL^{-1}) showed greater thermodynamic stability than the empty micelle (CMC = 5.2 mg.mL^{-1}) (Fig. 7, B), a classical phenomenon observed with micelles. [119]

3.2.2. *From drug encapsulation to drug release*

As Judefeind and de Villiers elegantly explained it in their review, [120] drug loading during the preparation of a drug delivery system and subsequent drug release after administration are two critical properties for the efficiency of such systems. *"Drug loading is the process of incorporation of the drug into a polymer matrix. Drug release is the reverse process by which the drug molecules are liberated from this polymer matrix and become available for absorption and pharmacological action. Drug loading and release are highly related to each other because both depend on the physicochemical properties of the matrix, the physicochemical properties of the drug and the interaction between the matrix, drug and the environment."* This section provides an overview of the different methods of drug-encapsulation into micellar systems as well as the techniques used to assess the efficiency and stability of this drug loading.

3.2.2.1. Drug encapsulation methods. The notion of encapsulation refers to the enclosing or trapping of one or more substances within a matrix. Unlike drug-polymer conjugates, the drug is not covalently linked to its vector but maintained in the nanoparticle through more or less strong physical interactions. The incorporation and retention of the drug within the vector can thus occur through hydrogen bonding, ionic interaction, dipole-dipole interaction, hydrophobic interactions, physical entrapment, precipitation, or it can be adsorbed to the surface (Fig. 8).[120, 121] Most of the time, several loading mechanisms are involved. As with other DDS, the objective is to protect the active substances from external factors (for example, to decrease physiological degradation) and/or to control their course to a precise therapeutic target and their release. There are different polymeric matrix systems allowing this kind of encapsulation, but most common being micelles (Section 2.2) and dendrimers (Section 2.3).

Several processes are available to encapsulate a drug into polymeric nanoparticles. [122–124] The choice of encapsulation method is widely correlated to the solubility of the drug and to the physicochemical properties of the polymeric structure. Formation of drug-loaded micelles or dendrimers involves simple procedures that can be divided into four major groups: 1) the nanoprecipitation method, 2) the solvent

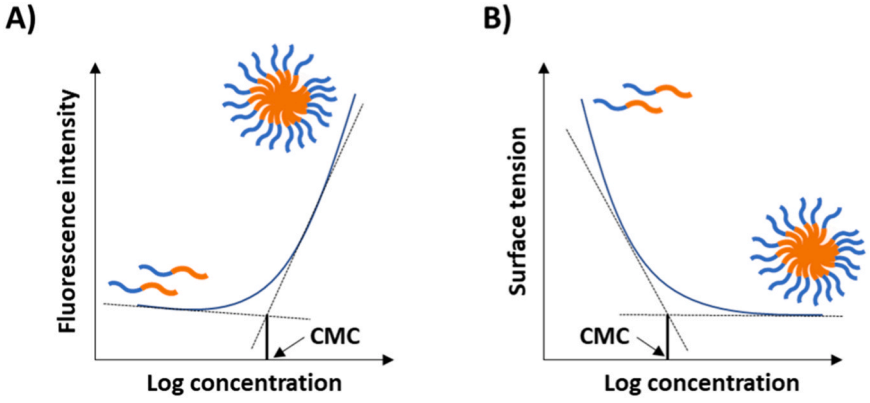

Fig. 6. A Fluorescence intensity (or B: Surface tension) *versus* logarithm of the surfactant concentration for CMC determination.

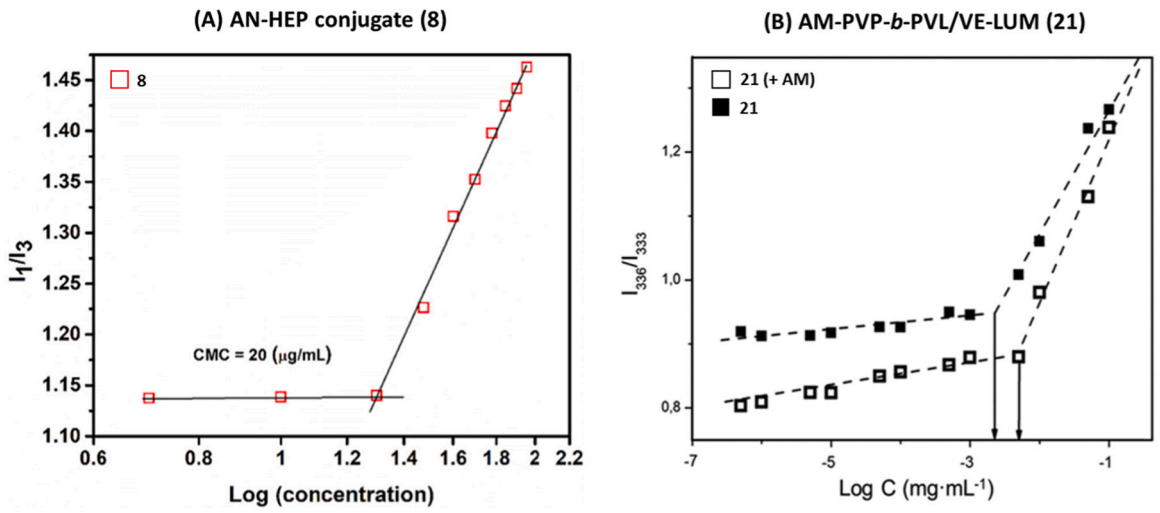

Fig. 7. A: CMC spectrums of the AN-poly(heparin) conjugates **8** (*Reproduced from ref.* 98 *with permission from Elsevier*) and **B**: the AM-loaded and free PVP-*b*-PVL/VE-LUM micelles **21** (*Reproduced from ref.* 143 *with permission from the American Chemical Society*).

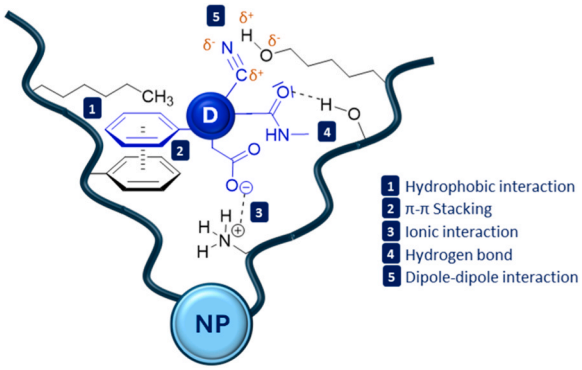

Fig. 8. Examples of intermolecular interactions for drug encapsulation.

evaporation method, 3) the oil-in-water method and 4) the dialysis (Scheme 10). The method chosen for the formation of drug-encapsulated nanoparticles can alter the physicochemical properties of the nanoparticles as well as encapsulation efficiency (EE) and drug loading (DL), (described in section 2.2.2.2). Final drug-loaded nanoparticles are generally lyophilized at the end of each method to remove solvent excess.

1) The nanoprecipitation method is generally employed for lipophilic drugs. In the case of micelles, the drug and the amphiphilic co-polymeric unimers are first dissolved in a water-miscible organic solution (methanol, acetonitrile, tetrahydrofuran, etc.). The organic solution is then drop-wise added to an aqueous medium under stirring to form droplets in suspension. The organic solvent is slowly evaporated at room temperature allowing the encapsulation of the drug upon formation and precipitation of the micelles.
2) The thin film method, or solvent evaporation method, is generally applied for hydrophilic drugs. An organic solution containing a mixture of the amphiphilic unimers, and the drug is evaporated under vacuum to form a thin film layer. The dried film is then hydrated by addition of water with a buffer of the appropriate pH. Sonication of the aqueous mixture generates the drug-loaded micellar nanoparticles. This technique can be used only if both the block co-polymers and the drug dissolve in the same solvent.
3) The oil-in-water emulsion method (O/W) is another kind of technique for hydrophobic drug-encapsulation using a water non-miscible organic solvent to form an emulsion in water. This method consists in the preparation of a solution of the co-polymers and the drug in a volatile organic solvent (such as dichloromethane, ethyl acetate, etc.). This organic mixture is then vigorously stirred or sonicated within an aqueous medium to form an emulsion where the drug and the unimers are trapped in droplets. Because of the instability of these emulsions, this method generally requires the use of amphiphilic surfactants in the aqueous phase to prevent droplet-coalescence. The surfactants align themselves at the surface of the droplets to increase their stability by decreasing the free energy at the interface of the organic and aqueous phases. Finally, slow evaporation of the organic solvent from the as-formed emulsion droplets traps the insoluble drug in the polymeric particles. The water phase is then extracted or evaporated to isolate the solid drug-loaded polymer nanoparticles.
4) In the dialysis method (dialysis bag or "equilibrium dialysis"), a solution of copolymeric unimers and free drug in a water miscible organic solvent is poured into a dialysis bag. This bag is then immersed in water. The aqueous phase is changed every couple of hours until the organic solvent has completely left the dialysis bag by simple diffusion through the membrane. This slow diffusion of the organic solvent to the water solution leads to precipitation of the co-polymers and thus, to the formation of the micelles. While these high molecular weight drug-loaded particles stay stuck in the dialysis bag, the non-encapsulated drugs and other impurities can escape to the aqueous phase through the dialysis bag membrane. At the end of the process, the dialysis bag is retrieved from the water phase and contains only the pure drug-loaded DDS. Finally, the dialysis bag content is collected, centrifuged, evaporated, and lyophilized to isolate the solid drug-loaded DDS. This method is commonly employed for poorly soluble components (drugs and copolymers).

This dialysis bag method can also be employed for further purification of pre-formed drug-loaded DDS. Hence, drug-loaded nanoparticles, can be placed into a dialysis bag and immersed in water in order to remove the excess free drug or other impurities. This purification step can also be carried out using other techniques such as ultracentrifugation, chromatography, membrane filtration, etc. [125] The dialysis technique is also a method widely used for the *in vitro* determination of drug-release kinetics from a drug-delivery system. [126] The content of the supernatant may be analyzed for drug loading assays and stability studies. It provides information on the most appropriate physiological conditions for the release of the drug from the polymer matrix (temperature, pH, etc.).

In the case of malaria studies, the main methods used for the

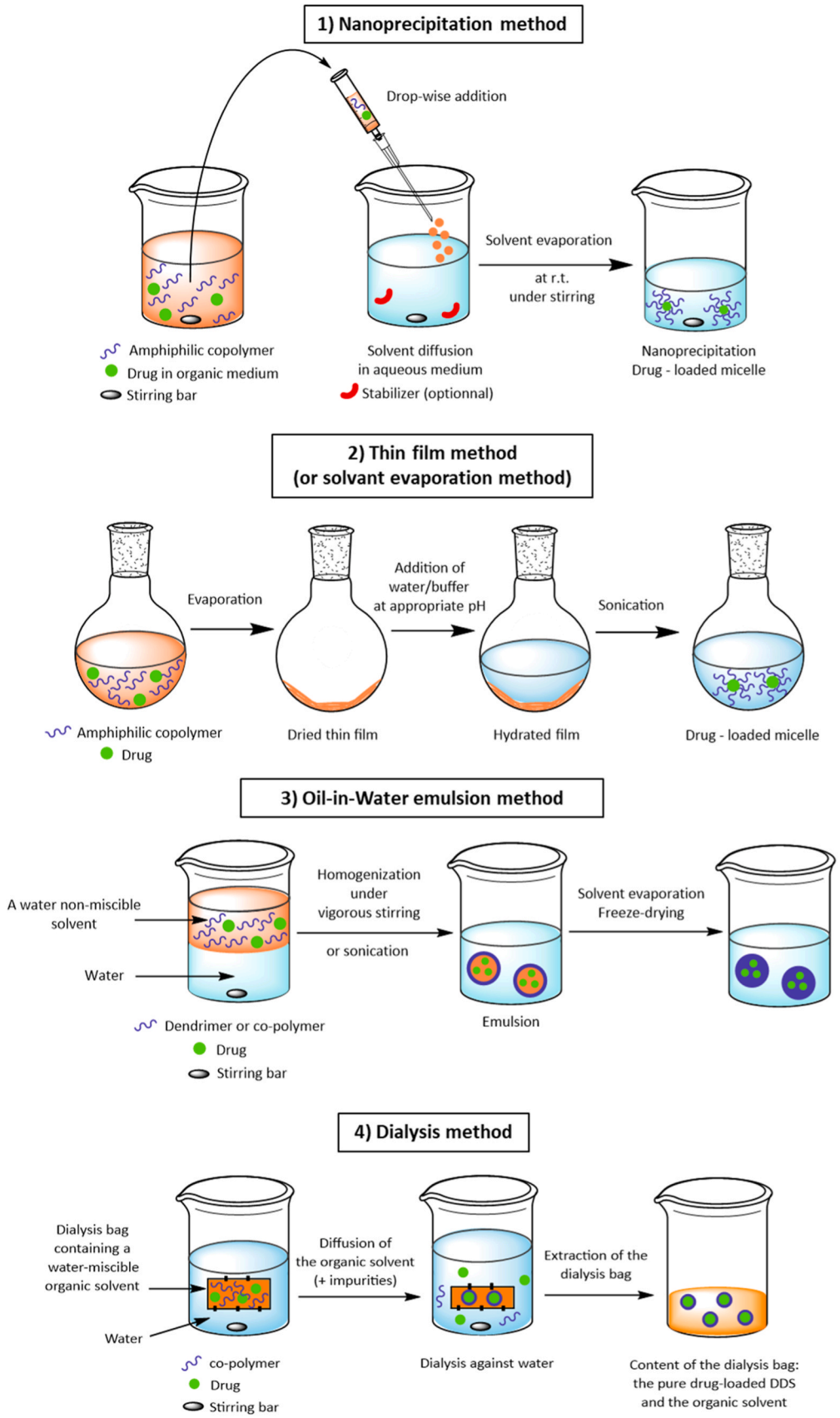

Scheme 10. Drug-encapsulation methods: Nanoprecipitation, thin film, oil-in-water, and dialysis methods.

encapsulation of antimalarial drugs in micelles are the nanoprecipitation and the thin film method (solvent evaporation). The nanoprecipitation method is generally employed for lipophilic antimalarial drugs such as ART, AR or SHMT inhibitor. While the thin film method is used for hydrophilic drugs such as CQ or PQ. [127] The oil-in-water (O/W) procedure is commonly used for drug-encapsulation into dendrimers.

3.2.2.2. Drug loading (DL) and encapsulation efficiency (EE). Drug-loading efficiency (DL, sometimes called DLC Drug-loading content) and encapsulation efficiency (EE, sometimes called DLE Drug-loading efficiency) are two major parameters for the characterization of drug-loaded systems and to assess the efficiency of an encapsulation method. DL and EE are both indirectly obtained by calculating the amount of free drug (non-loaded) found in the eliminated aqueous phase, as in the dialysate after purification by the dialysis bag method. The concentration in free drug of the solution is determined by high-performance liquid chromatography (HPLC) and/or by UV–VIS spectrometry (at a specific wavelength corresponding to the drug-absorption wavelength). Sometimes, Energy-Dispersive X-ray (EDX) Spectroscopy (section 3.2.4.) can also be used to confirm the presence of the drug in the vector by an elemental analysis of the sample.

The drug loading percentage (DL) corresponds to the weight of entrapped drug divided by the total weight of the resulting drug-loaded nanocarrier (Eq. 1). $m_{(entrapped\ drug)}$ is obtained from the initial weight of added drug minus the weight of free non-loaded drug retrieved from the aqueous phase. This DL percentage reflects the proportion of encapsulated drug in relation to the whole drug-loaded nanovector. DL is frequently calculated for systems where the drug is incorporated at the same time than the nanocarrier is formed (e.g. micelles, polymer-drug conjugates). As the mass of the drug-loaded macromolecular vector remains largely superior to the mass of the drug, most nanoparticle systems have relatively low drug loading (DL <30 wt%) and examples of nanoparticles with high drug loading capacities are attracting increasing interest. [128,129] For systems that are preformed prior to the drug encapsulation (e.g. dendrimers), we however noticed that authors prefer to use weight/weight ratios (W/W) to discuss the proportion of the drug in their systems. W/w ratios are calculated by dividing the weight of entrapped drug by the weight of the empty nanocarrier (Eq. 2). W/w percentages are therefore generally higher than DL percentages as the weight difference between the drug and the vector is less pronounced. The nanocarrier can even carry a weight of drugs higher than their own weight, especially if they are hollow inside, resulting in a w/w loading capacity superior to 100%. In contrast, a DL percentage superior to 100% can never be obtained. In this review, we specify for each DDS if the drug loading capacity is calculated according to Eq. 1 (DL) or Eq. 2 (W/W). Unfortunately, authors do not always specify the method of calculation of the drug loading values they discuss in their publications. The terms used (DL, w/w ratio, loading capacity, loading entrapment, etc) are uniformly applied and do not allow to distinguish the equation used either. It can therefore be very difficult to evaluate and compare the relative drug-loading values of different drug-loaded nanocarriers.

On the other hand, the encapsulation (or entrapment) efficiency percentage (EE) reflects the percentage of drug that is successfully entrapped into the polymer matrix compared to the amount that was initially added during preparation. It guarantees the efficiency of the encapsulation method and the stability of the drug-matrix interactions under the chosen conditions. To calculate EE, the weight of entrapped drug ($m_{(entrapped\ drug)}$) is divided by the total weight of initially-added drug in the solution (Eq. 3). The percentage of EE can be very high (up to 85–95%) when the drug is successfully loaded (or when a small amount of drug is loaded compared to the vector capacity…).

$$DL(wt\%) = \frac{m(entrapped\ drug)}{m(drug-loaded\ nanocarrier)} x \quad 100 \tag{1}$$

$$W/W \quad (wt\%) = \frac{m(entrapped\ drug)}{m(initial\ nanocarrier)} x \quad 100 \tag{2}$$

$$EE(\%) = \frac{m(entrapped\ drug)}{m(initial\ drug\ loading)} \quad x \quad 100 \tag{3}$$

These parameters are important to evaluate the performance of the drug delivery system as they will directly impact its biological activity. Ideally, high-drug loading is aimed at ensuring a good therapeutic dose while reducing the amount of polymeric excipient used in the formulation to minimize its toxicity. [7,128] On the other hand, a high encapsulation efficiency is a sign of good entrapment and stability of the drug into the nanocarrier, up to its controlled released under the appropriate conditions. High EE also ensure an economical formulation process by reducing drug losses. Both drug loading and encapsulation efficiency depend on the strength of the interactions between the drug and the polymer matrix. They are thus strongly related to the structural (type of vector, size and surface functionalization) and the physico-chemical (solubility, global charge) properties of the nanocarrier, as well as the formulation process. The drug loading content can for instance be correlated to the CMC of a micellar system: a high DL improves micelle stability in the blood circulation and can change its pharmacokinetic and pharmacodynamic properties. [130] Adjustment of the pH, temperature, hydrophile/lipophile balance of the solvents, or stirring rate optimization can be employed to ensure uniform distribution of the drug and enhance EE and DL, while minimizing aggregation problems.

As the nanoparticle/drug ratios strongly depend on a multitude of factors in addition to the nature of the vector, it is difficult to compare the DL (or EE) values of different DDS containing the same drug. As well, DL and w/w ratios are not comparable. Nevertheless, as a trend, we can notice from Table 2 that the chloroquine **CQ** (or the primaquine **PQ**) present similar w/w encapsulation rates regardless of the type of nanocarrier (≈ 20–40 wt%). Besides, all these polymeric matrixes contain amine groups that favour the stabilization of the drug through H-bonding interactions. In dendrimers, the drug entrapment usually increases with increase in generations of dendrimers and further with coatings such as with D-galactose coatings (e.g. **27**-**28**). Exceptionally high w/w ratios are moreover obtained with coated dendrimers (78–220 wt%). The size of the nanoparticle is not always a guarantee of high drug loading. The more compact unimolecular micelles (20 nm) of the dendronized hyperbranched polymer **DHP-bMPA 31** allowed higher weight/weight ratio (21–25 wt%) than the large micellar aggregates (178–360 nm) of the hybrid dendritic-linear-dendritic copolymer counterpart **32b** (W/W = 12–14 wt%), yet functionalized with the same bis-MPA polyester dendrons. Substitution of these polyester dendrons by poly(ester amide) dendrons in the almost identical **32a** also allowed to double the drug loading of CQ and even quadruple it for PQ, thanks to the H-bond forming ability of the amide groups.

Table 2
Weight/weight ratios of CQ and PQ drugs encapsulated in different polymeric DDS.

Drug	**CQ**	PQ
PAA 6-7	**6**: 33 wt% **7**: 14 wt%	**6:** 15 wt % **7:** 29 wt %
5.0 G PPI Dendrimer **25-26**	-	5.0 G PPI **25:**18 wt % 4.0 G Gal-PPI: 110 wt % 5.0 G Gal-PPI **26:** 220 wt %
PLys Dendrimer **27-28**	3.0 G PLys: 41 wt % 4.0 G PLys **27:** 46 wt % 4.0 G Gal-PLys **28:** 78 wt %	-
DHP-bMPA **31**	25 wt %	21 wt %
HDLDBC-bGMPA **32a**	31 wt %	41 wt %
HDLDBC-bMPA **32b**	14 wt %	12 wt %

3.2.2.3. Drug release studies. Drug release behavior of a therapeutic delivery system is an important parameter in the last stages of delivery. Drug release refers to the process in which the conjugated or encapsulated drug migrates from its inner position to the polymer's outer surface and to the biological target. [131] It is directly correlated to the drug stability and dynamic characteristics, thereby extending the drug's bioavailability and efficacy. The study of the drug-release kinetics is thus a key parameter to predict the *in vivo* releasing conditions, the final localization and becoming of the drug. All these factors contribute to the development of the appropriate market formulation of the final DDS (drug-dose, pharmacokinetic factors, and storage stability).

The release of the drug from its nanovector is triggered by the response of the DDS to endogenous or exogenous stimuli that occur upon physiological changes, typically in altered and/or healthy tissues. Vectors with sensibilities to very specific conditions reduce the concerns of early drug-leakage and improve drug-bioavailability. Variations of pH, redox or enzymatic reactions, hypoxia, or even mechanical frictions and temperature changes are typical endogenous stimuli that can induce significant changes in the DDS. For example, polymeric particles can dissolve or disintegrate to create pores in their surface-membrane allowing the drug escape. Under the *in vivo* acid conditions, protonation of amino or carboxylate groups, of the drug or the vector, is a typical way to break intermolecular interactions (Fig. 8), such as hydrogen and ionic bonds, and release the encapsulated drug. Moreover, ionization of the polymeric chains of the vector (transformation of the amino groups NH of a dendrimer into ammoniums NH^+ for instance) induce electrostatic repulsions and thus spacing between the chains. This swelling of the nanoparticle favours larger void spaces and facilitates the drug escape. Exogenous stimuli usually involve more advanced smart polymers locally applied on a specific part of the body; they include light irradiations, gases, ultrasounds, or magnetic fields used to induce the release of the bioactive substance upon polymer-bursting. [132]

The releasing kinetic factors are dependent on the solubility and physicochemical nature of the drug, the drug-loading, and the molecular weight, size, and shape of the nanoparticle. The inherent viscosity and the glass transition temperature (Tg) of the polymer can also influence drug-release. Regarding the size of the nanoparticle, it has been demonstrated that small DDS (around 20 μm) are easily metabolized through quick renal and splenic clearance, unlocking the drug from the matrix at the same time. [133,134] However, sizes ranging between 50 and 100 nm are recommended to obtain the full pharmacokinetics advantages of a nanovector. Release studies also allow to bring to the fore the release competition between two drugs encapsulated in the same DDS. [135] This competition often relies on size differences: the smaller drug is generally released faster from the polymer because of its weaker hydrophobic interactions with the inner core of the DDS. This phenomenon could find interest when the sequential release of the different drugs of a combined therapy is sought.

Although it strongly differs depending on the nature of the delivery system, the release profile generally follows one of these three models: 1) desorption of the surface-bound/adsorbed drug; 2) diffusion from the nanoparticles; and 3) polymer erosion (or a combined erosion/diffusion process). [136] In practice, the diffusion from and/or (bio)degradation of the polymer matrix usually govern the process of drug release. The rapid initial release, called burst release, generally observed during the first minutes is often attributed to the release of a fraction of the drug weakly bound to the large surface area of the nanoparticle, rather than to the release of the drug incorporated in the inner core of the nanoparticle.

Drug release can be assessed using various techniques including sample and separate (SS), continuous flow (CF), dialysis membrane (DM) techniques, alone or in combination, as well as novel methods such as voltammetry and turbidimetry.[131] These methods are applicable to both covalent and encapsulated systems (PDC, micelles, dendrimers, …). Most commonly, drug release studies are realized *via* the dialysis-bag method, previously described in the drug encapsulation methods section (section 2.2.2.1). The drug-loaded DDS is solubilized in a phosphate buffer solution (PBS) or in a biological medium to better mimic the physiological conditions and placed inside a dialysis bag (Scheme 11). The dialysis bag can be made of different cut-off size, depending on the average size of the studied polymer matrix. The selected cut-off size must exclusively allow membrane crossing of the drug to the external solution, while keeping the polymeric DDS inside the bag. The whole set-up is then immersed in the external solution and incubated (generally at 37°C) throughout the procedure. Under different operating conditions and time intervals, the content of the PBS-dialysate is analysed by HPLC to determine the concentration of released drug.

In the case of antimalarial DDS, the release studies are usually carried out under neutral or acidic conditions (pH 7.4 or 5.5) to mimic real-life conditions in pRBCs and compare the effect of pH on drug-release. Indeed, the parasitic food vacuole of the parasite is at acidic pH (≈5,5) and contains a high concentration of enzymes (esterase) or reducing agents. [137] The pH-sensitivity of antimalarial DDS would thus allow a specific intracellular activation of the vectorized drug within the parasited RBCs. In the different kinetic studies, relatively fast and efficient drug release from the polymer carrier is generally observed in acidic medium (pH ≈ 5.5) after 24–72 h of incubation while slow drug-release is noted under neutral conditions (Tables 1–5). The drug release mechanism is most of the time associated to preferential degradation of the polymeric chain containing pH-sensitive functional groups which are hydrolysed under acidic conditions. For example, the hydrolysis of the ester groups of the hydrophobic backbones of poly (caprolactone) (PCL) or poly(D,L-lactide) (PLA) polymers leads to distortion of the nanovector shape and thus to drug-release.

3.2.3. Examples of micellar DDS used in antimalarial therapy

Various micelles have been studied for the vectorization of antimalarial drugs. Table 3 summarizes different examples of these micelles and their main physico-chemical and biological properties. In this

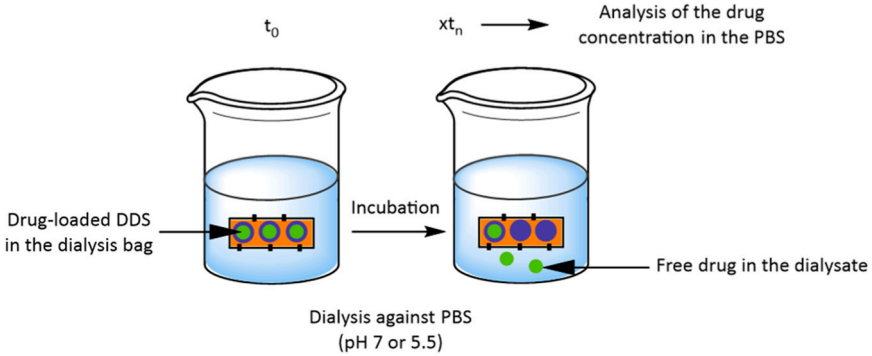

Scheme 11. Dialysis-bag method for drug-release studies.

Table 3
Micelles with antiplasmodial activities.

Entry	1	2	3
Micelles	**PCL-PEG-PCL (12)**	**PMOXA-g(ss)-PCL-PPCL (17)**	**PVP-*b*-PVL/VE (21−22)**
Vectorized drug(s)	Artemisinine (ART)	Serine hydroxy methyltransferase (SHMT inhibitor 1)	Lumefantrine (LUM) + Artemether (AM) (Combo = CoArtem)
Biological target	*Plasmodium falciparum*	*Plasmodium falciparum*	*Plasmodium falciparum*
Polymer synthesis	Anionic ROP	Anionic and cationic ROP + + Thiol-disulfide exchange conjugation of the blocks	RAFT/ROP + Click chemistry for LUM and peptide conjugation
Method of drug incorporation	Nanoprecipitation encapsulation method	Nanoprecipitation encapsulation method	Nanoprecipitation encapsulation method for AM
Critical micellar concentration (CMC)	nd	0.05–0.3 μg/mL	2 μg/mL
Zeta potential (ZP)	-15.4 mV	nd	nd
Sizes	92 nm (DLS)	31–53 nm (DLS)	114 nm (DLS)
(analysis method)	80 nm (AFM)	50–100 nm (TEM)	125 nm (TEM)
Drug loading (DL)	DL = 19 wt%	DL = nd	DL = 14 wt% (AM), 27 wt% (LUM)
Encapsulation efficiency (EE)	EE = 87%	EE = 55%	EE = 60% (AM)
Conditions of drug release	30% at pH 7.4 66% at pH 5.5	Rapid release of the drug in presence of a reducing agent (DTT)	20% at pH 7.4 70% at pH 5.5
Antimalarial activities (IC_{50})	1.85% *of in vivo* parasitemia versus 4.4% for the free ART	4–12 nM (free SHMT: 4–5 nM)	1.6 μM versus 1 μM with the peptide (free combo: 0.86 nM)
Observations	Micelles improve ART water solubility. Higher in vivo antiplasmodial activity (x2) with a dose-dependent effect.	Biodegradable and reduction-sensitive delivery system. Micelles improve SHMT solubility and protection from metabolic instability.	CoArtem-prodrug is less active than the free combo (x1000). Long time required for the release of the CoArtem-prodrug. The micelle decreases hemolysis and toxicity.
References	138–140	141	143

section, the emphasis will be given to their design and strategy of synthesis. Sections 3 and 4 respectively discuss the physicochemical properties and biological characterizations of these antimalarial micelles.

An Artemisinin (ART)-loaded micelle carrier was for instance reported by Kheiri Manjili *et al.* in 2017 (Table 3, entry 1). [138] The poly(ε-caprolactone)-co-poly(ethylene-glycol)-co-poly(ε-caprolactone) triblock **12** (PCL-PEG-PCL) was obtained by anionic ROP of cyclic ε-caprolactone (CL) with PEG-OH as co-macroinitiator and stannous octoate ($Sn(Oct)_2$) as catalyst (Scheme 12). $Sn(Oct)_2$ served as active transesterification agent, first through coordination between the tin metal and the hydroxyl group of PEG (**9**). [139] Then, a subsequent coordination-insertion mechanism of the Sn-PEG intermediate **10** with the carbonyl-functionality of the cyclic monomer promoted the cleavage of the acyl-oxygen bond and thus the ROP of the ε-caprolactone. The resulting triblock co-polymer **12** was purified and collected by precipitation in cold diethyl ether. Finally, PCL-PEG-PCL micelles were assembled, and ART encapsulated by spontaneous self-assembly of the triblock in an aqueous medium (nanoprecipitation method described in section 2.2.2.1).

The diameters of ART-loaded PCL-PEG-PCL micelles were about 92 nm, with a negative zeta potential (ZP) of -15.4 mV (Table 3, entry 1). [140] Micelles with such negative global electrical charge usually exhibit an increased circulation time in the blood, thanks to electrostatic repulsions with the negatively charged surfaces of blood cells and plasma (see Section 3.2.1). The drug loading and encapsulation efficiencies of ART in these micelles were 19 wt% and 87% respectively. The *In vitro* release studies in neutral and acid pH showed that the quantities of ART released from the micelles were of 30% at pH 7.4 and 66% at pH 5.5. The higher release rate of ART under acid conditions was attributed to the degradability of the co-polymer upon hydrolysis. However, drug release kinetics studies suggested that the drug release mechanism mainly depended on diffusion effect rather than polymer core degradation. Regarding the *in vivo* activities, they observed 1.85% of parasitemia on *Plasmodium berghei versus* 4.4% for the free ART.

Meier *et al.* were interested in an innovative amphiphilic block co-polymer micelle **17** as antimalarial vector including a reduction-responsive disulfide bond (Scheme 13, Table 3, entry 2). [141] For the synthesis of the hydrophobic moiety of the micelle (PCL-co-PPCL, **15**), a mixture of caprolactone (CL) and α-benzylcarboxylate-ε-caprolactone (BCL) was randomly polymerized through anionic ROP initiated by the organometallic zinc 2-ethylhexanoate ($Zn(Oct)_2$), to give the intermediate PCL-co-PBCL random co-polymer **13** (Scheme 13). After Pd-catalyzed deprotection of the benzyl group, introduction of a 2-pyridylthio disulfide moiety using cysteamine **14** gave the desired hydrophobic poly(caprolactone)-co-poly(α-pyridylthio cysteamine caprolactone) (PCL-co-PPCL, **15**). For the hydrophilic moiety of the micelle, the poly(2-methyl-2-oxazoline) block (PMOXA) **16**, beforehand prepared by cationic ROP of the 2-methyl-2-oxazoline monomer, was used as an alternative to the classical poly(ethylene-glycol) (PEG). The polymer **15** was conjugated to the PMOXA block **16** by thiol-disulfide exchange to obtain the desired PMOXA-g(SS)-PCL block co-polymer **17**. Finally, the antifolate drug, the serine hydroxy methyltransferase (SHMT inhibitor 1), was encapsulated in the micelle by spontaneous self-assembly of the co-polymer **17** in aqueous medium or through nanoprecipitation method (section 2.2.2.1).

The redox-sensitive disulfide bond used as linker between the PMOXA and PCL-PPCL polymer blocks is cleaved in the cell and thus allows the disassembly of the DDS. Indeed, drug-resistant intracellular malaria parasites are reported to possess increasing cytosolic reduction potentials which may allow the *in vivo* release of the antifolate drug through the reductive cleavage of the disulfide bridge and disassembly of the micelle. For instance, the *P. falciparum* glutathione redox system (GSH/GSSG) is a major redox buffer located in the cytosol and the apicoplast. It plays a key role as an indicator of cellular redox status and oxidative stress, allowing the detoxification of reactive oxygen and nitrogen species (ROS and RNS). [142]

SHMT-loaded micelles, made from the assembly of co-polymer **17**, showed interesting IC_{50} values ranging from 4 to 12 nM, equivalent or even lower than the free SHMT (IC_{50} = 4–5 nM) (Table 3, entry 2). Particle sizes ranged from 27 to 51 nm. To confirm the reductive

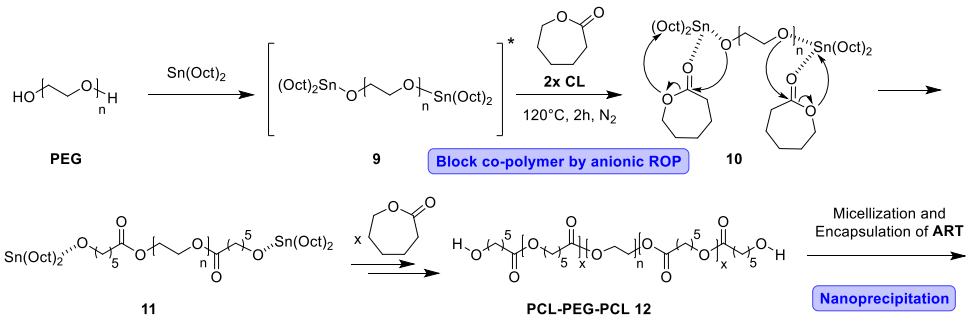

Scheme 12. Synthesis of PCL-PEG-PCL co-polymer **12** by anionic ROP.

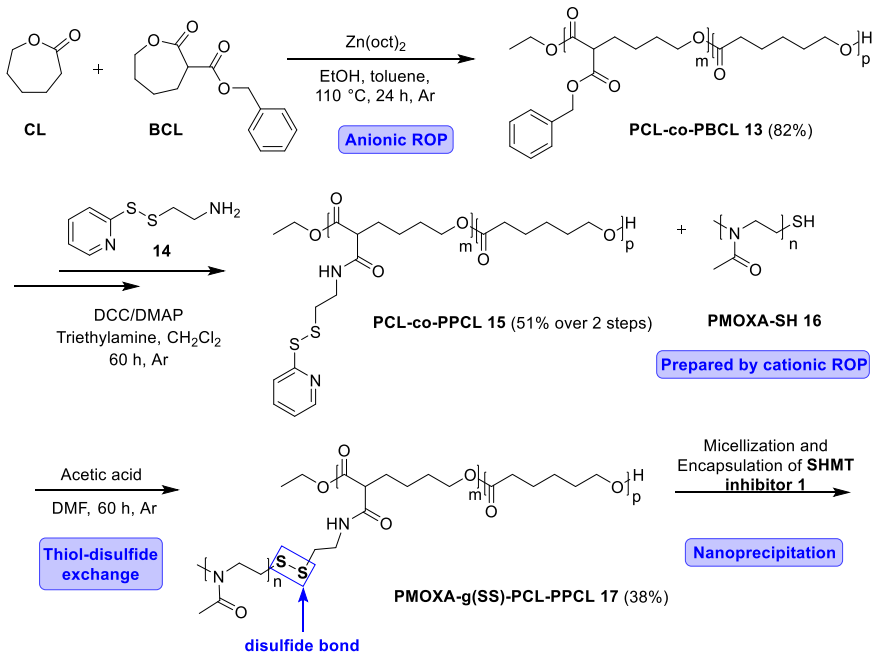

Scheme 13. Key steps of the synthesis of PMOXA-g(SS)-PCL polymer **17**.

degradation of the disulfide bond, a reducing agent like dithiothreitol (DTT) was added to a solution of the nanovector in PBS. The disintegration of the micelles was confirmed by SHMT-drug release and the formation of polymer aggregates.

Micellar DDS can also be designed as hybrid nanocarriers, integrating two types of antimalarial drugs, incorporated through different methods. Depending on their properties (chemical functions, solubility), one drug is usually conjugated to the polymer while the other one is encapsulated. In 2020, the first micellar nanocarrier of the WHO-recommended antimalarial combination of lumefantrine (LUM) and artemether (AM) was reported (Table 3, entry 3). [143] This combination therapy ("Coartem" Novartis 2009[66]) is recommended for uncomplicated malaria cases. To improve pharmacokinetic aspects, Klumperman *et al.* focused on a polymeric carrier PVP-*b*-PVL/VE based on poly(*N*-vinylpyrrolidone) (PVP) and poly(α-allylvalerolactone) (PVL), functionalized with ethylene glycol vinyl ether (VE) (Scheme 14). [143] The *N*-vinylpyrrolidone monomer (NVP) was first polymerized into PVP-OH **19** using a reversible addition fragmentation chain transfer (RAFT) polymerization reaction. RAFT is a powerful polymerization procedure [144] consisting in a reversible deactivation radical polymerization (RDRP), allowing a controlled radical polymerization. RAFT works with a lot of monomers (styrene, nitrile, acrylate, etc.) but the efficiency of the reaction is directly linked to the choice of chain transfer agent (CTA) (trithiocarbonates, dithiobenzoates, xanthates or dithiocarbamate). [145] Xanthate-type CTA as **18** are typical RAFT-agents for monomers like NVP. This PVP **19** was then used as macroinitiator to introduce the second PVL block through anionic ROP of α-allylvalerolactone. Finally, LUM was covalently linked to the PVL moiety of the block PVP-*b*-PVL co-polymer **20** *via* a simple "acetal click-type reaction" (DL = 27 wt%). The resulting acide-labile acetal bond easily dissociate in acid conditions and should thus favour controlled drug release. A slightly hydrophobic peptide ligand (**GSRSKGT**) was then anchored to the surface of the PVP-*b*-PVL/VE-LUM co-polymer **21** to facilitate the self-assembly process into micelles. This peptide can also enhance the uptake into pRBCs. [146] Nanoprecipitation of the peptide-PVP-*b*-PVL/VE-LUM **22**-made micelles ultimately allowed the encapsulation of the second AM drug within the hydrophobic core of the "Coartem" AM/LUM-hybrid micelles. Concomitant self-assembly of the co-polymer **22** and incorporation of AM were made possible by the poor solubility of AM in aqueous medium and its good interaction with the PVL hydrophobic core.

AM loading and encapsulation efficiencies in the hybrid micelle were of 14 wt% and 60%, respectively (Table 3, entry 3). Spherical hybrid micelles of 114 nm in average size were obtained, ideal to avoid recognition by the reticuloendothelial system (RES) and for the passive transport through the NPP of pRBCs (Scheme 1). *In vitro* biological studies showed IC_{50} values of 1 μM for the drug-loaded micelles *versus* 0.86 nM for the free AM/LUM combination

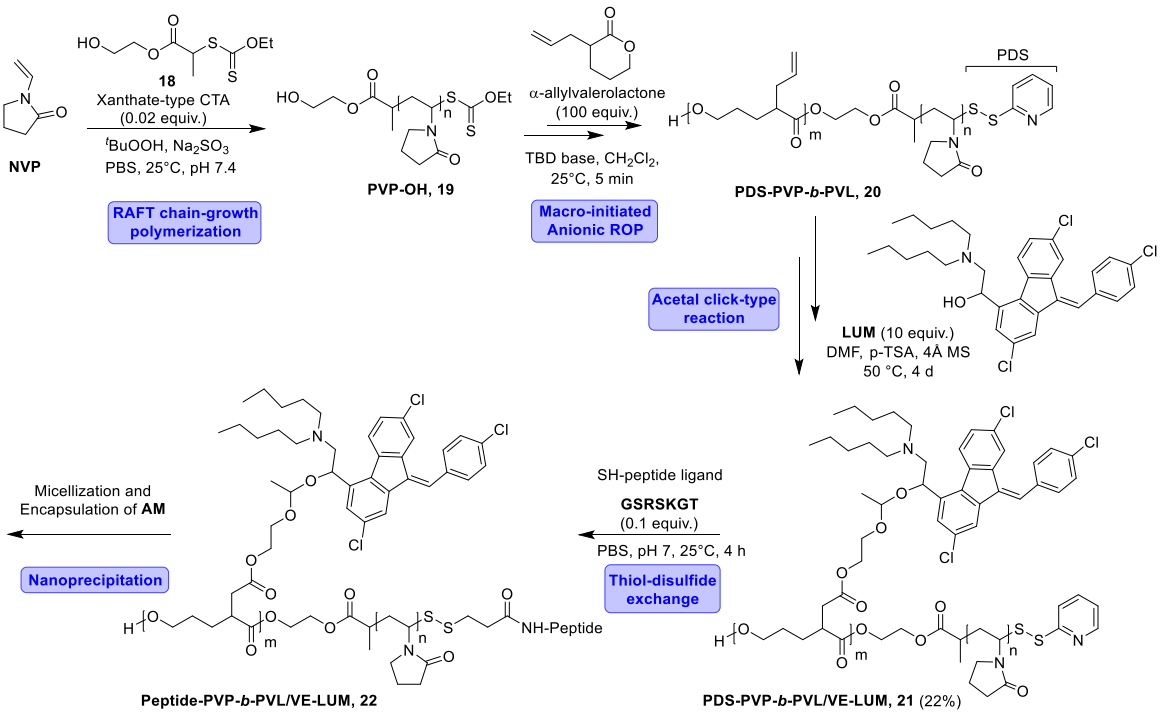

Scheme 14. Key steps of the synthesis of peptide-PVP-*b*-PVL/VE-LUM **22**.

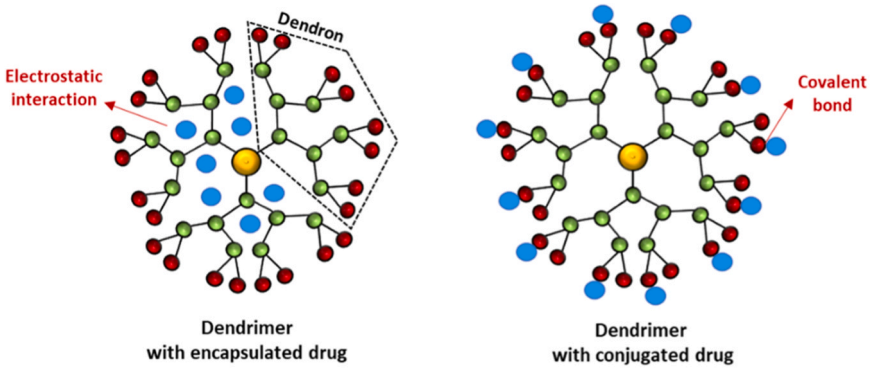

Fig. 9. Dendrimeric DDS with encapsulation (left) or conjugation (right) of the drug.

3.3. Polymeric dendrimers

Dendrimers are architectural polymeric macromolecules characterized by a three dimensional, highly branched, and mono-disperse form (Fig. 9). [147–149] These features make dendrimers different from traditional linear and branched polymers. They are composed of three distinct parts: 1) a central core to which the different branches are growing out, 2) repetitive branching units and 3) terminals, the surface of the dendrimer. The drug can be conjugated to this surface or encapsulated in the void spaces of the central core. Modifications on these three parts modulate the properties of the dendrimer, such as its solubility, its thermal stability, or its electrostatic interactions. [150] Compared to other nano-DDS, the finely controllable structure (leading to low polydispersity index and precise molecular weight), alongside the cooperative multivalency with the biological target, makes dendrimers well-defined and biocompatible vehicle for the vectorization of drugs [151–153] and/or diagnostic imagery agents in various therapeutic fields. [154] As a matter of fact, some dendrimers with promising potentials for the delivery of drugs against influenza virus, COVID-19, inflammatory diseases, cancers or for vaccine delivery are currently under clinical trials (phase 1–3). [155–157]

3.3.1. General strategies for the synthesis of dendrimers

A wide range of polymeric structures, including polyamines, polyesters, polyethers, triazines, carbohydrates, phosphorus groups or even peptides can compose the core of the dendrimer. Although different synthetic methods have been reported for the preparation of dendrimer matrices, divergent and convergent strategies are most commonly employed for the construction of the dendrimeric core. [158–160] In short, the divergent approach consists in a synthesis starting from the inner core of the dendrimer and expanding toward the external core, while the reverse path is followed for the convergent approach. The choice of chemical procedure can impact dendrimer size and the number of generations.

The widely used divergent method consists in dendrimer growth from the central core to the surface (Scheme 15). The core must be multifunctionalized to be extended *via* a step-by-step iterative addition of several monomer units giving the first-generation dendrimer (1.0 G). The external moieties of the dendrimer 1.0 G are then activated to react again with other monomers and form the second-generation dendrimer 2.0 G. These steps are repeated until the desired number of dendrimer generations is obtained. For instance, the amine groups of an ethylenediamine (EDA) central core can add on acrylate monomers (Michael

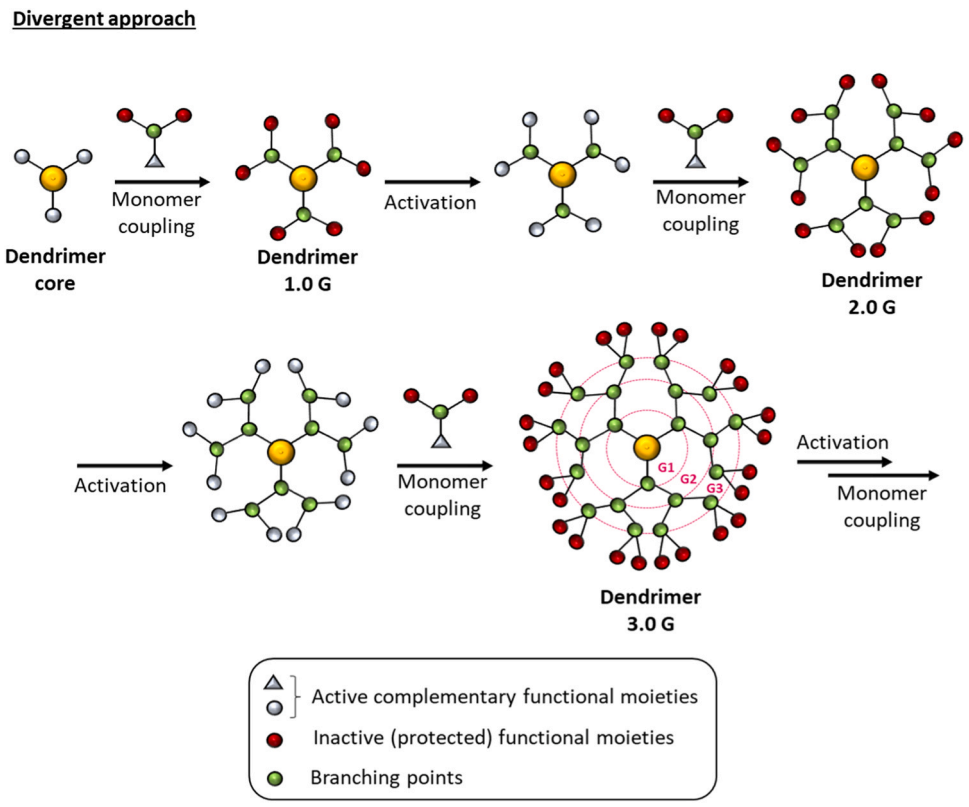

Scheme 15. Preparation of dendrimer matrix by the divergent approach.

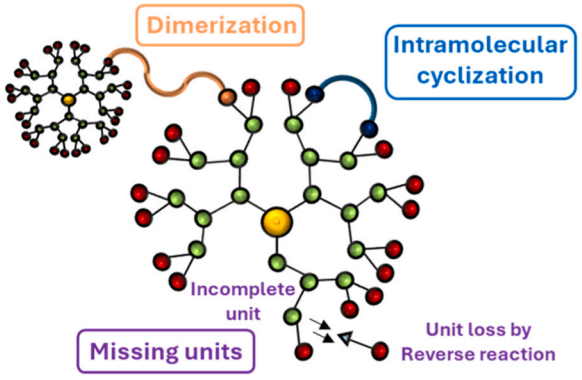

Fig. 10. Common structural defects occurring during dendrimer synthesis.

addition) to form dendrimer 1.0 G. Addition of new molecules of ethylenediamine on the ester moieties activates dendrimer 1.0 G to continue the expansion through amide groups, used as branching connections between generations. The divergent method generally provides high control of the size through stepwise monomer addition and flexibility over dendrimer generation, resulting in high branching rates and well-defined structures.[158] It also makes it possible to introduce a large variety of reactive functional groups at the terminals or into the inner core.

However, the divergent method is often the source of structural defects that impact dendrimer quality and purity. Synthetic failures such as missing units (incomplete branches growth or unit loss), intramolecular or intermolecular cyclization/dimerization (growth stopped) are frequent (Fig. 10).

The typical reactions leading to these defects are depicted in Scheme 16. Thus, incomplete reactions, like the Michael addition, result in asymmetrical dendrimers. Same outcome with the afterward degradation of a branching arm by retro-Michael reaction, ester hydrolysis or amine oxidation. Moreover, dendrimers with missing units can still undergo further growth reactions, leading to additional defects. Elevated temperatures (above 60°C) usually promote retro reactions or intramolecular cyclizations, especially when 1,2-alkylene polyamines are used as core structures. Although reduced temperatures (25–50°C), methanolic conditions, controlled concentrations, or extended reaction times help mitigate these side reactions, they remain common in high-generation dendrimers, where steric hindrance intensifies the issue. The proximity of terminal groups during growth step reactions thus causes both intramolecular cyclization and intermolecular dimerization/cyclization. To avoid these abnormal dendrimer syntheses, accurate monitoring of each reaction step by spectroscopic techniques (^{1}H NMR, FT-IR, and MS, see Section 3.1 for further details) and use of excess reagents are generally recommended, although this may impact the uniformity and purity of the dendrimer.

These defects also complicate the separation of defective dendrimers from the desired ones. Purification methods are restrained and laborious because of the small differences between the two structures. Recent advances in purification process significantly improved the ability to obtain high-purity dendrimers and hyperbranched polymers, a crucial point for effective and safe applications in drug delivery. Conventional techniques such as advanced chromatography, selective precipitation or liquid/liquid extraction can be used.[159,161,162] Alternative and more sophisticated methods based on membrane separation, such as optimized dialysis, [163] nanofiltration or ultrafiltration, [164] and even microfluidic techniques, [165] can be applied to enhance the distinction between the target dendrimer and impurities. All these techniques, especially when combined, address the challenges posed by minimal structural differences among dendrimer variants.

On the other hand, the convergent method a more precise approach developed to overcome the disadvantages of the divergent method, consists in a synthesis from the surface to the inner core of the dendrimer (Scheme 17). [166] The dendrons are independently synthesized and, at

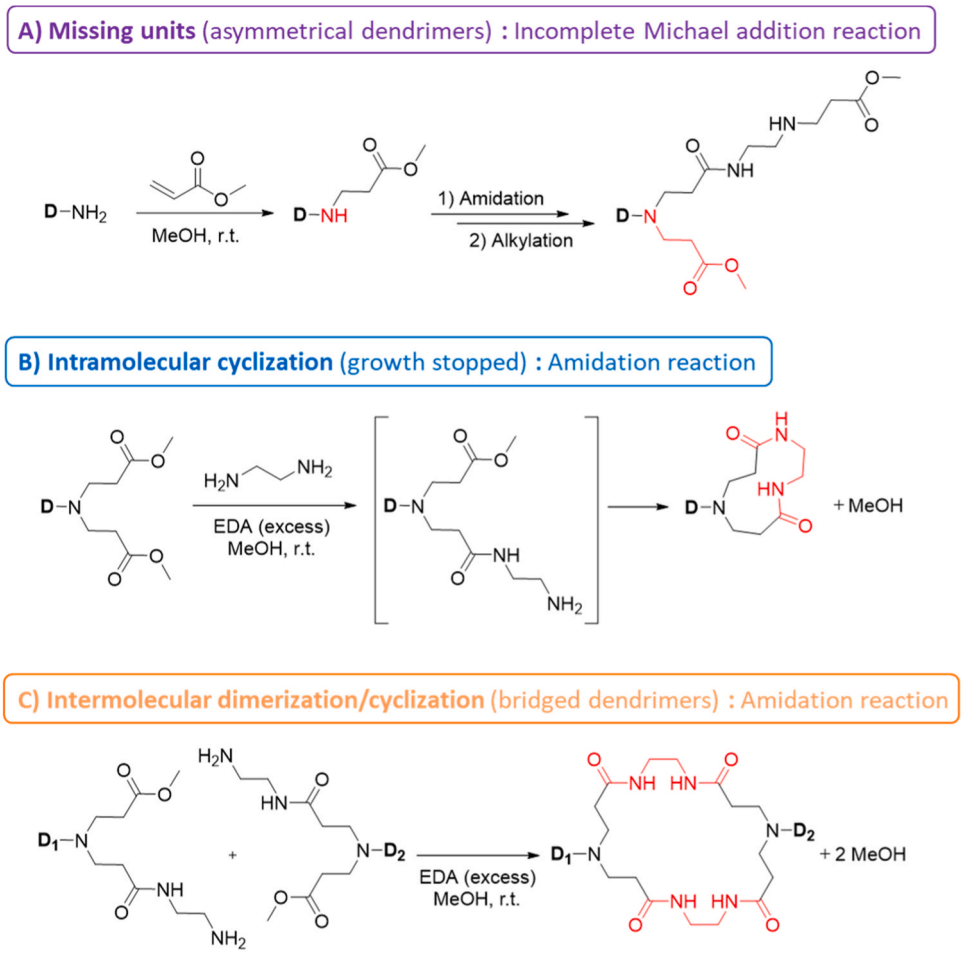

Scheme 16. Typical side-reactions causing defective dendrimer structures.

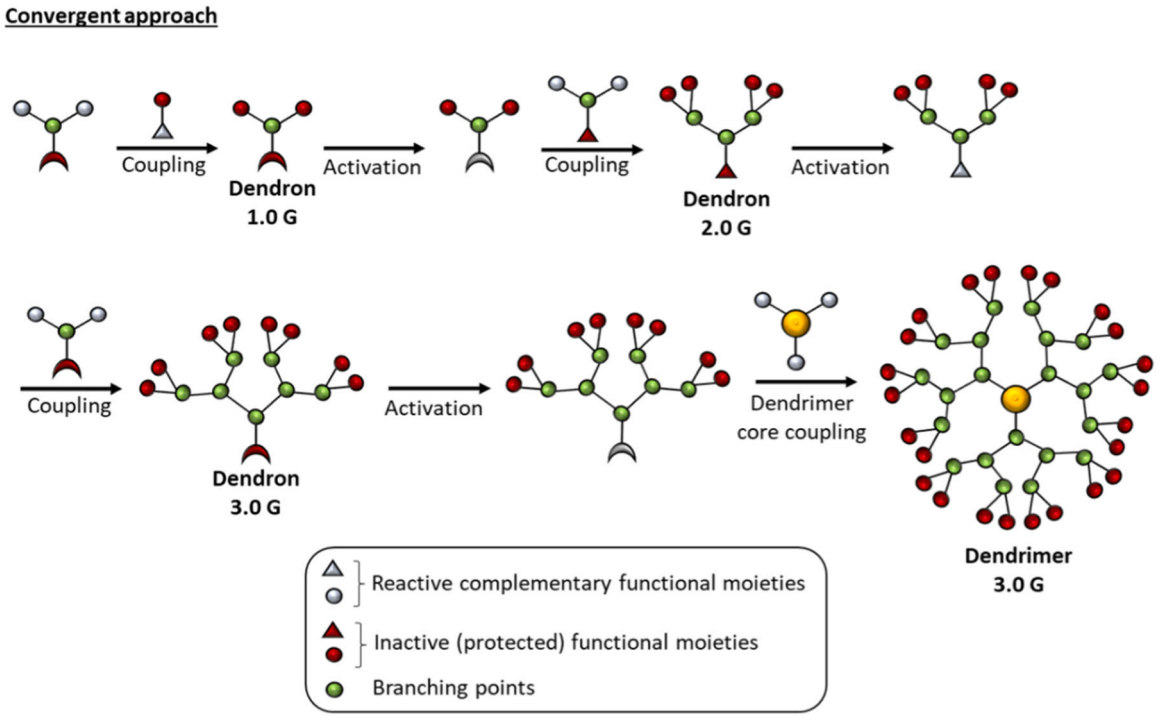

Scheme 17. Preparation of dendrimer matrix by the convergent approach.

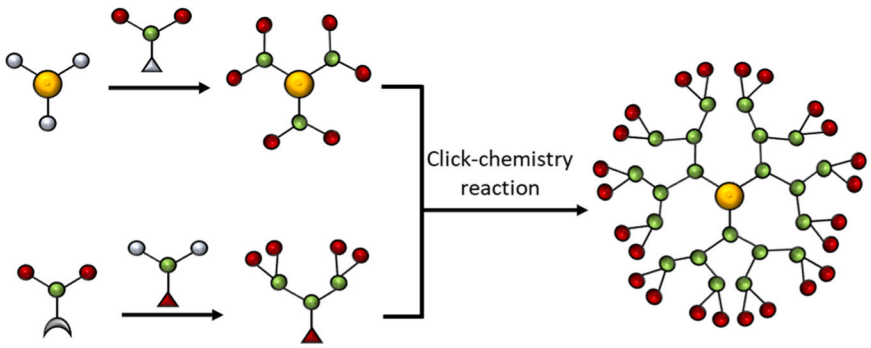

Scheme 18. Combined divergent/convergent synthesis.

the end, all linked together to a central core molecule to form the final dendrimer. The convergent method offers superior molecular and size control, and excels in producing pure and monodisperse (more uniform and symmetric) dendrimers with well-defined structures. This iterative assembly approach also limits the defect rates and thus formation of impurities, facilitating the purification phases of the dendrons. Nevertheless, the process can be more expensive, complex to scale-up and time-consuming with all the separate synthesis and purification steps of each intermediate. The convergent method gives thus smaller dendrimers with lower generations compared to the divergent method and are generally associated to lower overall yields.

A combination of divergent and convergent approaches, called double-stage convergent approach, can also be used to preserve the advantages of each approach (Scheme 18). [167,168] This method enables precise control over dendrimer size and structure, ensuring excellent structural integrity with high-purity and higher yields, while avoiding defects due to rigorous purification steps between stages. It thus enhances the synthesis of large and complex dendrimer structures. The divergent-convergent methods usually rely on environmentally safe and efficient click-chemistry reactions to selectively connect the separately prepared central part and branching units, while minimizing side reactions. [169] Click reactions such as the Copper- or Strain-Catalyzed Azide-Alkyne Cycloaddition (CuAAC, SPAAC), [170] thiol-ene or thiol-yne click reaction (TEC, TYC) thus enable precise structural control, yielding monodisperse products, and facilitates the introduction of various functional groups to tailor properties like solubility and biocompatibility. Moreover, theses mild condition reactions are usually environmentally friendly, energetically efficient and, thus, suitable for sensitive substrates. They rely on fast, room temperature and high atom economy synthesis in aqueous or polar solvents, with limited amount of toxic reagents or hazardous waste. Their selectivity makes them compatible with diverse functional groups, eliminating the need for protecting groups. Their efficiency, reliability and scalability make them suitable for large-scale industrial applications.

To overcome these synthetic limitations, Ling's group also developed a new supramolecular construction approach, consisting of the self-assembly of small, easy-to-synthesize poly(amidoamine) amphiphilic dendrimers (PAMAMs)(Fig. 11). [171,172] The hydrophilic PAMAM dendron part is coupled to a single (or double) hydrophobic alkyl chain *via* CuAAC cycloaddition. Their amphiphilic nature then facilitates their self-assembly into well-defined nanomicelles with large voids and numerous terminal functionalities. These features enable high-load physical encapsulation of drugs, delivery of nucleic acids or conjugation of bioimaging agents on the surface. [173] Moreover, these PAMAM dendrimers exhibit a good biocompatibility profiles and can be tailored to mimic protein properties such as good solubility, stability, and also targeting specificity. The relative small size and easy synthetic routes of these supramolecular dendrimers offer greater versatility in modification while still mimicking the properties of covalent dendrimers. This simplicity often translates into improved purity, scalability and reproducibility in synthesis, crucial for industrial transposition.

3.3.2. *Drug incorporation methods in dendrimers*

After the dendrimer synthesis, the drugs are generally conjugated to the surface of the dendrimer or encapsulated in the void spaces of its central core (Fig. 9).

For surface functionalization, drugs or targeting moieties are anchored by bioconjugation with a specific functional group (amine, ester, alcohol…) of the terminals. As for drug anchoring to polymer backbones (Fig. 4), formation of these covalent bonds through amide, ether or ester groups usually applies condensation or addition reactions on the dendrimer terminals. The choice of terminals also has an impact on the biological activities of the dendrimer. Hydroxyl (-OH), carboxyl (-COOH), or amine (-NR) terminals significantly increase its solubility in aqueous biological environments and its biodistribution. The nature of the terminals can also improve its biocompatibility, minimizing side cytotoxicities and facilitating the desired interactions with the therapeutic target. They can directly impact the composition of the protein

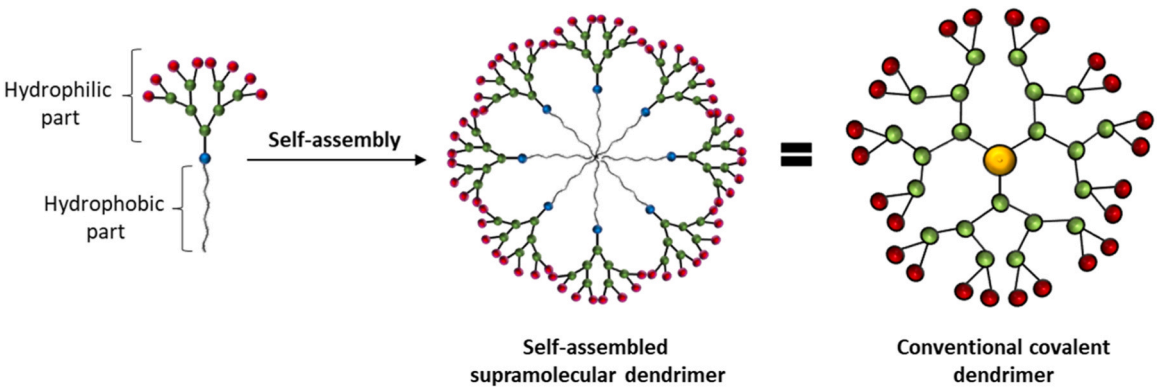

Fig. 11. Self-assembled supramolecular dendrimers mimicking conventional dendrimers.

Table 4
Glycodendrimers with antiplasmodial activities.

Entry	1	2
Dendrimers	**5.0 G PPI, 25** **5.0 Gal-PPI, 26**	**4.0 G Plys, 27** **4.0 Gal-Plys, 28**
Vectorized drug(s)	Primaquine (PQ)	Chloroquine (CQ)
Biological target	*Plasmodium falciparum*	*Plasmodium falciparum*
Polymer synthesis	Divergent method with EDA as central core	Divergent method with PEG as central core
Method of drug incorporation	Dialysis encapsulation method	Dialysis encapsulation method
Sizes (analysis method)	< 50 nm (DLS)	< 50 nm (DLS)
W/w ratio (W/W) Encapsulation efficiency (EE)	W/W = 18 wt% (**25**) W/W = 220 wt% (**26**)	W/W = 46 wt% (**27**) W/W = 78 wt% (**28**)
Conditions of drug release	At pH 7 (storage conditions): **25**: 85% (48 h) **26**: 89% (6 days)	At pH 7 (storage conditions): **27**: 40% (7 h) **28**: 40% (24 h)
Antimalarial activities (IC_{50})	nd	nd
Observations	Significant decrease in release rate with high generation and Gal-coated PPI dendrimers	Significant decrease in release rate with high generation and Gal-coated PLys peptide dendrimers
References	180	181

corona coating (presented in section 2.1.2) and thus favour an *in vivo* protection shield of the dendrimer to reduce the immune response and improve its bioavailability. Weil and coworkers demonstrated that the surface charges and hydrophobicity of amphiphilic dendrimers could alter the protein corona binding around dendrimer-coated liposomes. [174] They reduced binding of opsonin proteins but increased the adsorption of proteins controlling cellular uptake. Biocompatible moieties or targeting ligands, such as carbohydrates (glucose, galactose, mannose, etc.), amino-acids, or peptides, can also reduce the toxicity and extend the circulation time. More recently, specific biomimetics or human cell-derived membranes (mitochondrial or red blood cell membranes) have been used as innovative coatings. [175] Although in the past there had been some concerns about the toxicity of dendrimers (especially for positively charged dendrimers bearing primary amine terminals), [176,177] nowadays, these various chemical surface modifications approaches have been effectively employed to avoid *in vitro* and *in vivo* toxicities while enhancing safety. [178] Core modifications or increased generation layers can also influence the behaviour of the dendrimer in the body and minimize its toxicity.

With their multivalent building block structures and void spaces, dendrimers also easily provide accessible spaces to encapsulate drugs. [153] The drug is more generally maintained inside the voids of the dendrimers through intermolecular interactions (Fig. 8). The different general methods of drug encapsulation described for micelles (section 2.2.2.1) can also be applied to dendrimers. These techniques allow the formation of a supramolecular complex through non-covalent interactions between the drug and the inner voids of the dendrimer. Among them, the oil-in-water emulsion and the dialysis methods have been widely used for the encapsulation of antimalarial drugs into polymeric dendrimers such as aminoquinoline and its derivatives

Table 5
Hybrid dendronized co-polymer with antiplasmodial activities.

Entry	1	2	3
Dendrimers	**DHP-bMPA** X = 4 **(31)**	**HDLDBC-bGMPA** **(32a)**	**HDLDBC-bMPA** **(32b)**
Vectorized drug(s)	Primaquine (PQ) or Chloroquine (CQ) or Quinacrine (QN)	Primaquine (PQ) or Chloroquine (CQ) or Quinacrine (QN)	Primaquine (PQ) or Chloroquine (CQ) or Quinacrine (QN)
Biological target	*Plasmodium falciparum*	*Plasmodium falciparum*	*Plasmodium falciparum*
Polymer synthesis	Convergent method Click-chemistry: CuAAc	Convergent method Click-chemistry: CuAAc	Convergent method Click-chemistry: CuAAc
Method of drug incorporation	Oil-in-water encapsulation method	Oil-in-water encapsulation method	Oil-in-water encapsulation method
Sizes (analysis method)	13.5 nm (empty) 19 nm (PQ) (TEM) 20 nm (CQ) (TEM) 12 nm (QN) (TEM)	13 nm (empty) 11 nm (PQ) (TEM) 17 nm (CQ) (TEM) 14 nm (QN) (TEM)	178 nm (PQ) (SEM) 360 nm (CQ) (SEM)
W/w ratio (W/W) Encapsulation efficiency (EE)	W/W = 21 wt% (PQ), 25 wt% (CQ), 23 wt% (QN) EE= 60% (PQ or CQ), 37% (QN)	W/W = 41 wt% (PQ), 31 wt% (CQ), 48 wt% (QN) EE= 41% (PQ), 31% (CQ), 48% (QN)	W/W = 12 wt% (PQ), = 14 wt% (CQ), EE= 92% (PQ), 100% (CQ)
Conditions of drug release	At pH 7, over 72 h: 60% (CQ) (nd for PQ)	At pH 7, over 72 h: 60% (CQ) (nd for PQ)	At pH 7, over 48 h: = 100% (CQ) = 100% (PQ)
Antimalarial activities (IC_{50})	69 nM for **CQ-31** (vs Free CQ: 32 nM) 12.4 μM for **PQ-31** (vs Free PQ: 7 μM) 13.7 nM for **QN-31** (vs Free QN: 27 nM)	46 nM for **CQ-32a** (vs Free CQ: 32 nM) 11.9 μM for **PQ-32a** (vs Free PQ: 7 μM) 27.5 nM for **QN-32a** (vs Free QN: 27 nM)	4 nM for **CQ-32b** (vs Free CQ: 13.6 nM) 20.5 μM for **PQ-32b** (vs Free PQ: 4.9 μM)
Observations	More compact and sealed architecture with high generation and coated dendrimers.	Dendrimer carriers are biocompatible and exhibit appropriate sizes to enter into all stages of pRBCs.	Dendrimers reduce hemolysis and toxicities and offer a new way of treating G6PD deficient patients.
References	183	183	185

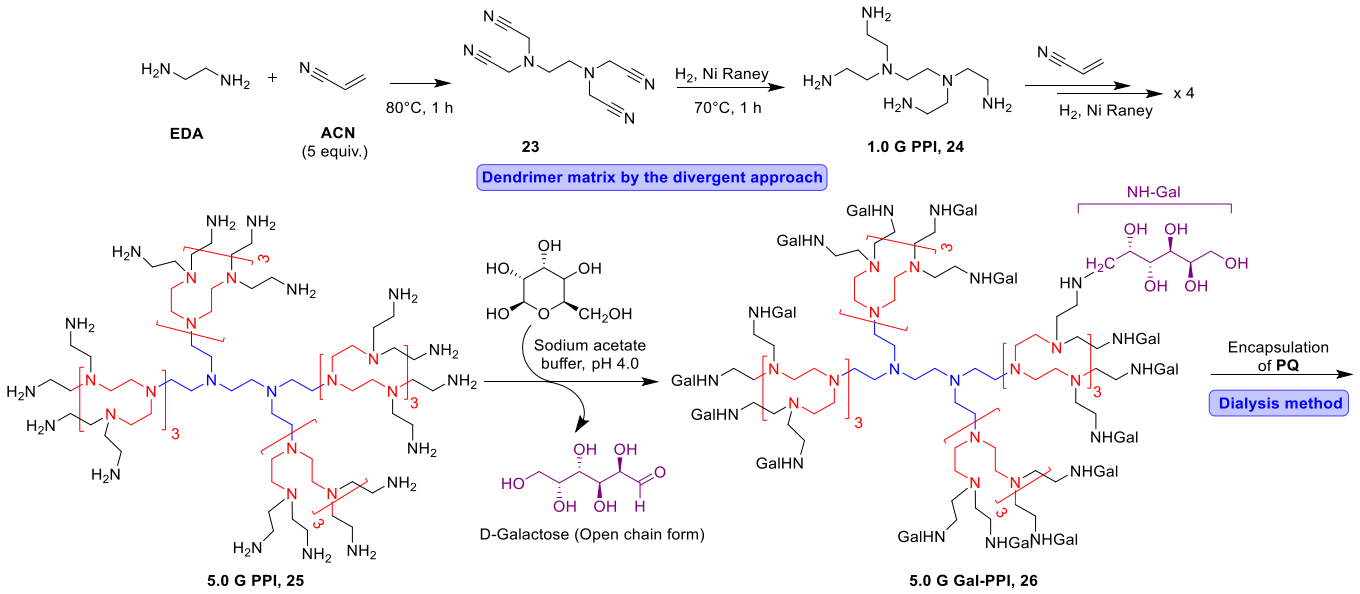

Scheme 19. Synthesis of 5.0 G galactose-coated poly(propylene imine) dendrimer **26.**

(chloroquine, primaquine and quinacrine). In the case of the oil-in-water method, the non-water-miscible solvent phase contains the dendrimer while the water-soluble drug is in the aqueous phase (Scheme 10). Vigorous stirring of these two phases, present in a specific ratio, creates an emulsion that is maintained until complete evaporation of the organic solvent. Finally, the drug-loaded dendrimer is generally separated from the emulsion after simple solvent evaporation or *via* the dialysis bag method, in order to remove non-loaded drugs. As with micelles, drug loading (DL), w/w ratio (W/W) and encapsulation efficiency (EE) in dendrimers are determined as described in section 2.2.2.2.

3.3.3. *Examples of dendritic DDS used in antimalarial therapy*

Different dendrimers have been studied for the vectorization of antimalarial drugs. This section describes their design and the strategies for their synthesis. Their main physicochemical and biological properties are summarized in Tables 4 and 5.

In the field of dendritic DDS, glycodendrimers have attracted some interest in the delivery of antimalarial drugs (Table 4). Notably, D-galactose is a promising sugar ligand [179] to target the Asialo-glycoprotein (ASGP) receptors overexpressed in human hepatocytes. Hepatic ASGP receptors allow the endocytosis into cells of proteins containing a terminal galactose moiety. Moreover, galactose-coated dendrimers are less prone to phagocytosis thanks to their high polymer density and more hydrophobic surface, which reduce their hemolytic toxicity and immunogenicity.

Hence, Jain and co. synthesized D-galactose-coated poly(propylene imine) matrix (Gal-coated PPI **26**) *via* the divergent method and used it to encapsulate primaquine (PQ) (Entry 1). [180] The fifth-generation dendrimer matrix was synthesized upon Michael addition of an ethylenediamine central core on acrylonitriles (Scheme 19). The nitrile groups of the tetra nitrile derivative **23** were then reduced by hydrogenation under Raney nickel catalysis. Once this first generation of dendrimer obtained (1.0 G PPI, **24**), these steps were consecutively repeated four times to synthesize the 5.0 G PPI dendrimers **25**. The D-galactose ligands were finally introduced at the surface of the 5.0 G PPI upon ring-opening of the galactose with a sodium acetate buffer solution (pH 4.0), and addition of the amino groups of **25** on the aldehyde group of the opened D-galactose. The as-formed Schiff's base (-N=CH-) were subsequently reduced into secondary amines under these conditions to form 5.0 G Gal-PPI **26**. Primaquine (PQ) was then encapsulated through the dialysis method (section 2.2.2.1).

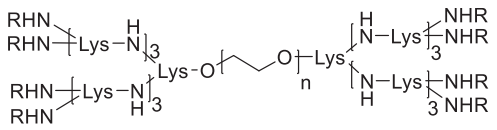

Fig. 12. Galactose-coated poly-L-lysine dendrimer **28**.

Encapsulation rate of PQ increased in Gal-coated dendrimers and along with the generations of the dendrimer (0.18 g of PQ/g of non-coated 5.0 G PPI **25**; 1.1 g of PQ/g of coated 4.0 G Gal-PPI; 2.2 g of PQ/g of coated 5.0 G Gal-PPI **26**) (Table 4, entry 1). In molar ratio, it corresponded to high rate of drug loading content of 30–60 molecules of PQ for one molecule of Gal-PPI. A higher number of generations, as well as hindrance of the dendrimer surface with sugar coating, increased the drug entrapment rate. The more compact structures of large dendrimers also provide a steric hindrance that prevents drug release, compared to more open structures. Release studies showed a significant decrease in the release rate of PQ from high generation and Gal-coated PPI dendrimers (85% of release in 48 h for non-coated 5.0 G PPI **25**; 88% in 5 days for coated 4.0 G Gal-PPI or 89% in 6 days for coated 5.0 G Gal-PPI **26**).

Jain and co. also reported the glycodendrimer **28** based this time on a peptide matrix, for the encapsulation of chloroquine (CQ) (Fig. 12, Table 4, entry 2). [181] Peptide dendrimers are biomaterials frequently employed as proteins and liposomal mimetics. Thanks to their polyvalency, peptide dendrimers can improve affinity, through specific interactions with peptides, proteins, or carbohydrates. [182] Following a similar divergent method, the 4.0 G galactose-coated peptide dendrimer **28** was assembled around a PEG_{1000} unit as central core and poly-L-Lysine units for the branches. The chloroquine (CQ) was then encapsulated through the dialysis method (section 2.2.2.1). Higher nanometric sizes were obtained for these Gal-coated dendrimers. As for the PPI-dendrimer **26**, drug loading also increased with dendrimer generations and in Gal-coated dendrimer (41 wt% for 3.0 G PLys and 64 wt% for 3.0 G Gal-PLys *versus* 46 wt% for 4.0 G PLys **27** and 78 wt% for 4.0 G Gal-PLys **28**) (Table 4, entry 2). In addition, *in vitro* release studies highlighted a significant decrease in release rate of CQ in sealed architectures of high generation or Gal-coated PLys dendrimers compared to non-coated PLys (95% for 3.0 G PLys and 75% for 3.0 G Gal-PLys in 7 h *versus* 40% for 4.0 G PLys **27** in 7 h and 40% for

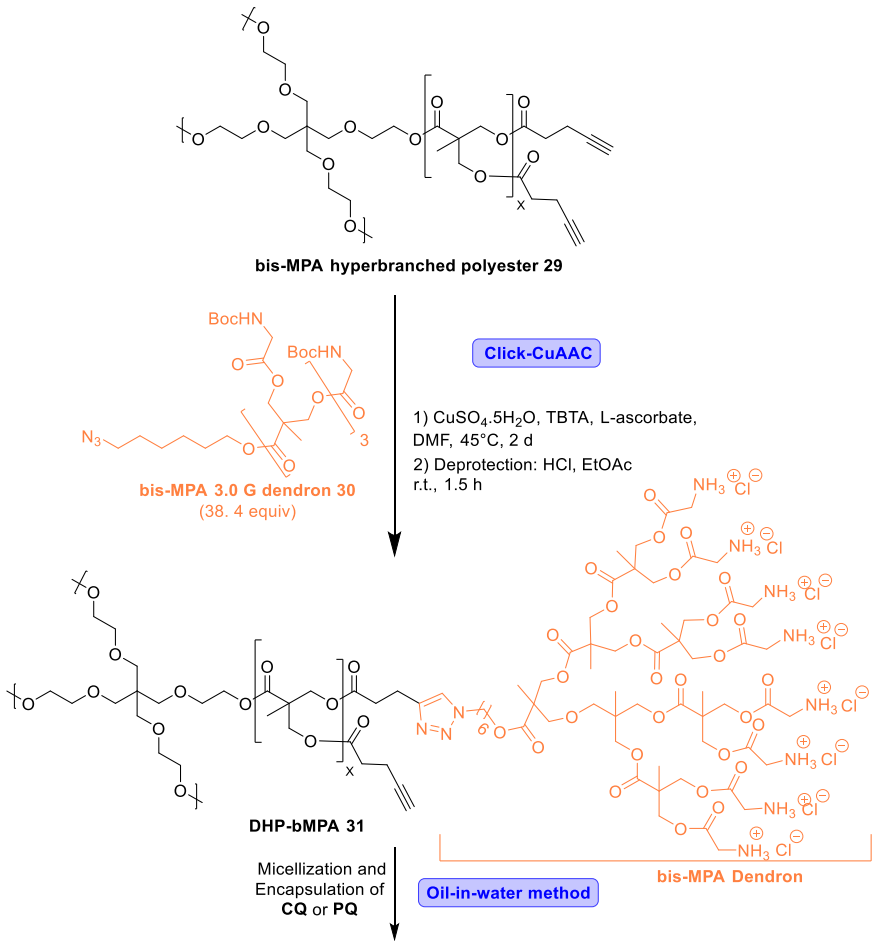

Scheme 20. Synthesis of the **DHP-bMPA** hybrid dendronized-polymer **31**.

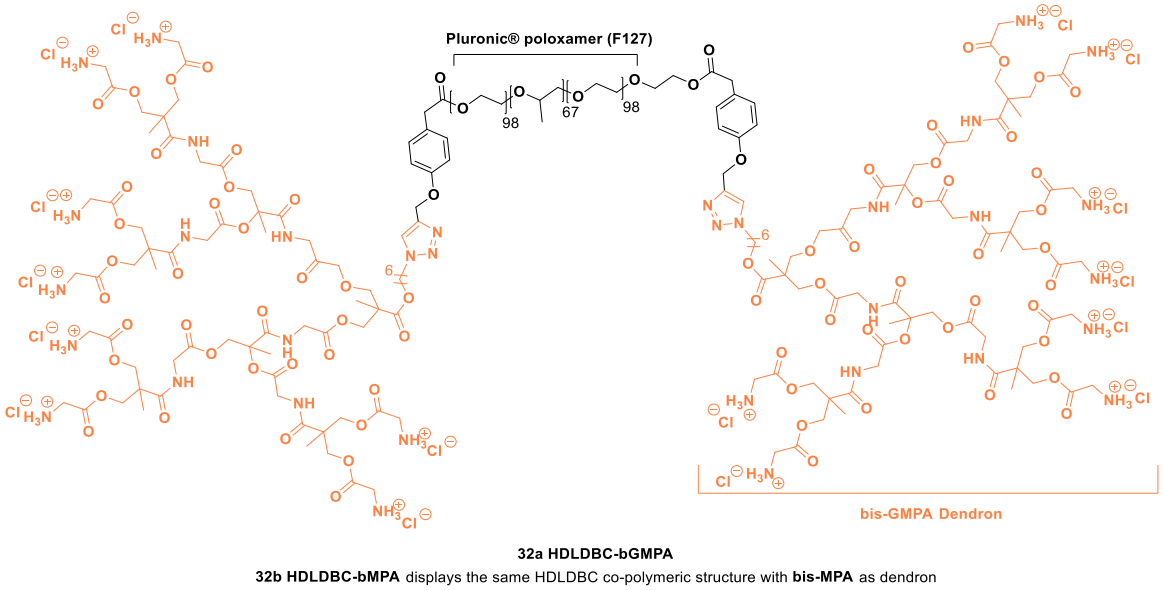

Fig. 13. HDLDBC-bis-(G)MPA dendrimers **32a-b** (see Scheme 20 for the structure of bis-MPA dendron).

4.0 G Gal-PLys **28** in 24 h).

Polymer and dendrimer strategies can also be combined to design hybrid dendronized-polymer DDS with original shapes. Sierra *et al.* synthesized dendronized hyperbranched polymers (DHP) **31** derived from 2,2'-bis(hydroxymethyl) propionic acid (bis-MPA) hyperbranched polymers (Table 5, entry 1). [183] The **bis-MPA** polyester dendron combines the advantages of the hydrolytic degradability of ester linkages, and the end-group functionalization with glycine groups to favour their self-assembly in water into globular unimolecular micelles, of appropriate size to facilitate their entry into pRBCs (Scheme 20). For this

convergent approach, the copper-catalysed azide-alkyne cycloaddition reaction (CuAAC, regioselective formal Huisgen 1,3-dipolar cycloaddition) was employed as a key step to graft a *N*-Boc-protected bis-MPA 3.0 G dendron **30** on the bis-MPA hyperbranched polyester **29**. [184] Selective formation of the 1,4-triazole linker and Boc-deprotection under acidic conditions gave the final **DHP-bMPA** pseudodendrimer **31**. According to the number of generations in **29** (X = 2.0–4.0 G), the resulting DHP **31** theoretically bear 128, 256, and 512 glycine moieties. Chloroquine (CQ) or primaquine (PQ) were then encapsulated in the dendrimer *via* an oil-in-water procedure (section 2.2.2.1). Drug loadings were around 20% in weight and encapsulation efficiencies (EE) of 60% for both PQ and CQ (Table 5, entry 1).[183] The PQ- or CQ-loaded-dendrimers presented similar sizes: 19 nm for PQ-**31** and 20 nm for CQ-**31** (measured by TEM method). At neutral pH, stability studies showed 60% CQ release over 72 h.

Sierra et al. also employed this CuAAC strategy for the preparation of other hybrid dendritic-linear-dendritic block co-polymers (HDLDBC, Janus-type dendrimers) based on **bis-MPA** polyester or **bis-GMPA** poly (ester amide) dendrons (bis-GMPA = 2,2′-bis(glycyloxymethyl) propionic acids) (Table 5, entry 2–3).[183,185] The amphiphilic cationic hybrid dendronized co-polymers **HDLDBC-b(G)MPA 32a-b** were used to encapsulate antimalarial drugs such as chloroquine (CQ) and primaquine (PQ). A similar three-step convergent procedure and CuAAC step were used to prepare and incorporate the three-generation dendron on the commercial amphiphilic Pluronic® poloxamer (F127) (Fig. 13). Poloxamers are nonionic triblock copolymers, typically composed of a central hydrophobic block of poly-propylene glycol flanked by two external hydrophilic blocks of poly-ethylene glycol (PEG). The ammonium end-chains of **32a-b** favour their self-arrangement in aqueous solutions into micelles with glycine groups at the surface, and a good encapsulation of CQ and PQ with the oil-in-water procedure (section 2.2.2.1). The drug-loaded dendrimer **HDLDBC-bGMPA 32a** had average diameters of 11 nm with PQ and 17 nm with CQ (measured by TEM) (Table 5, entry 2).[183] Drug loadings in weight and encapsulation efficiencies (EE) in **32a** were both 41% for PQ and 31% for CQ. This Janus-type HDLDBC dendrimer thus presented higher loading capacities than the **DHP-bMPA** counterpart **31**. *In vitro* drug release studies showed a drug release in neutral medium over 72 h of 60% for CQ. After this period, the remaining encapsulated CQ stayed in the dendrimer.

The consecutive studies carried out by Sierra and Fernàndez-Busquets on these two similar amphiphilic dendronized-polymer **HDLDBC-bGMPA 32a** and **HDLDBC-bMPA 32b** underline the importance of the dendron structure for the drug-encapsulation (Table 5, entry 2 *vs.* 3). [183,185] Introduction of the poly(ester amide) dendrons in **32a** allows to double the drug loading of CQ and even quadruple it for PQ, thanks to the H-bond forming ability of the amide groups. The poly(ester amide) dendrons also had a strong effect on the size and stability of the self-assembled micelles, given the additional H-bonding interactions. Compared to the very large size micelles formed by polyester **32b** (178 and 360 nm), poly(ester amide) **32a** generated much smaller micelles of 11–17 nm after drug loading. Both dendrimers **32a** and **32b** presented low cytotoxicity profiles (CC_{50} up to 0.15 mg.mL^{-1}) and exhibited no hemolysis effect. Compared to CQ-**32a** (IC_{50} = 46 nM *versus* free CQ: 32 nM), CQ-**32b** displayed an antiplasmodial activity increased by a factor of ten (IC_{50} = 4 nM). This enhanced activity may be attributed to an additional intrinsic activity of dendrimer **32b** (IC_{50} = 0.2 mg.mL^{-1}) associated with a more specific targeting for pRBCs over healthy RBCs. Promising *in vivo* results on Plasmodium-infected mice confirmed these findings. Better overall health and higher survival rates were observed after treatment with these CQ-dendrimers.

DDS can also take the form of dendritic system of smaller generations, involving de facto the conjugation of the drug to the dendrimer. Tsogoeva and co-workers reported the synthesis of dendritic dimers and trimers for the vectorization of conjugated artemisinin (ART) and artesunate (AN) [186] (Fig. 14). In recent years, dimerization of natural or synthetic drugs has become a powerful strategy to increase the biological potential of medicinal compounds, while reducing synthesis efforts and costs. [187] The concept of dimerization has the potential to improve the pharmacological properties of monomeric drugs, leading to better biological activity, metabolic stability and bioavailability, or reduced toxicities. ART and AN drugs are interesting candidates for this dimerization approach. [188–190] as they contain useful functional groups (alcohol and carboxylic acid) to facilitate the formation of covalent bonds with the small dendritic matrix. The tris- and tetra-substituted dendritic oligomers **33-35** were thus prepared in 2–4 steps using a succinic skeleton to combine three or four molecules of artemisinin (ART) and artesunate (AN) around a polyester dendron (Fig. 14).[186] These ART and AN-conjugated dendrimers were evaluated for their *in vitro* biological activities towards *Plasmodium falciparum* 3D7 parasite-invaded red blood cells (pRBCs). Higher antimalarial activities were observed for AN-DDS (IC_{50}= 5.4 nM for **34** and 5.7 nM for **35**) compared to ART-DDS (IC_{50}= 343 nM for **33**) (Free AN: 9 nM). They

Table 6
List of methods for DDS physico-chemical characterizations.

Methods	Determined parameters	Objectives and information
Dynamic light scattering (DLS)	Hydrodynamic diameter and electrophoretic mobility in solution Zeta potential (ZP)	Particle size Surface charge Stability
Size exclusion chromatography (SEC)	Average mass and dispersity of the polymer	Molecular weight Chain lengths
Ultracentrifugation (UCA)	Density and hydrodynamic diameter	Particle size
Spectrophotometry	Fluorescence of the probe (generally: pyrene)	Critical micelle concentration (CMC)
Atomic force microscopy (AFM) Transmission electron microscopy (TEM) Scanning electron microscopy (SEM)	Homogeneity, height Overall shape and size of the particles Particle surface morphology	Particle morphology/form (image of the particles)

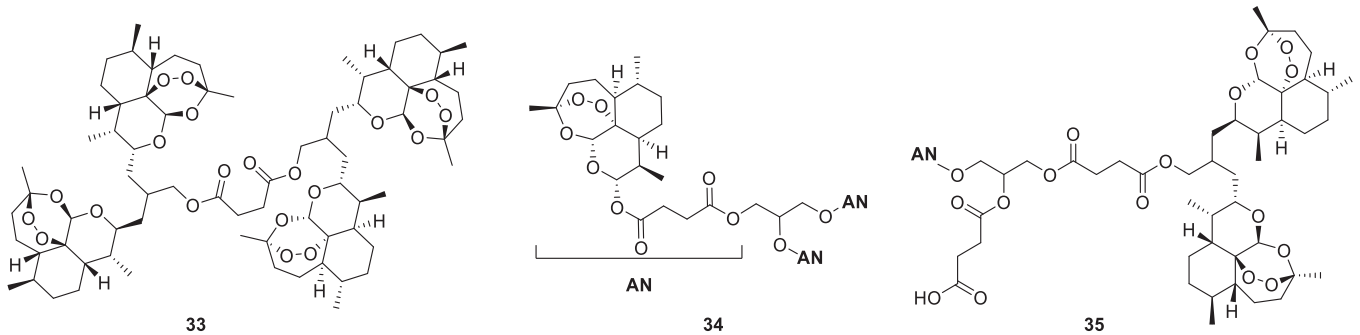

Fig. 14. ART- and AN-conjugated dendrimers of small generation **33-35.**

concluded that artesunate (AN) should be considered as a *via*ble alternative to artemisinin derivatives, although artesunate ester derivatives are less hydrolytically stable.

In summary, two main families of antimalarial compounds are frequently incorporated in these DDS vectors: aminoquinoline derivatives, such as chloroquine (CQ) and primaquine (PQ), and artemisinin derivatives, notably artemisinin (ART) and artesunate (AN). In addition, there seems to be a correlation between the type of molecule and the choice of method of incorporation. For instance, compounds with a "conjugable" functional group such as a primary amine (-NH_2) (pyrimethamine (PYR)), or an alcohol (-OH) (lumefantrine (LUM)) or a carboxylic acid (-COOH) (artesunate (AN)) are typically incorporated in polymer-drug conjugates (PDC). For other kinds of drugs where the conjugation appears to be more complex and could require different preliminary steps of synthesis, encapsulation is preferred.

For encapsulating systems, the choice of vector type and method of drug incorporation depends directly on the solubility of the drug. Regarding dendrimers, a particular profile emerges with the systematic encapsulation of water-soluble molecules such as aminoquinolines derivatives. Unlike micelles which are more amphiphilic, dendrimers are relatively lipophilic structures, *de facto* impeding the encapsulation of hydrophobic compounds. Thus, the oil-in-water or dialysis methods are very widespread methods for the encapsulation of drugs in dendrimers. In the case of micelles, the choice of the drug is less limited as incorporation relies on simple self-association of the unimers, linked to their solubility and electrostatic interactions. For micellar DDS, the nanoprecipitation method is widely used, followed by the thin film method.

4. Physicochemical characterizations of polymeric DDS

The dynamic nature of polymeric DDS makes it difficult to fully characterize them by the conventional techniques used for small molecules. This section summarizes several methods used for the physicochemical characterization of macromolecular DDS, including standard or more advanced techniques. Although each of these methods has its own advantages and disadvantages, it should be kept in mind that the characterization of a macromolecular polymer cannot be accomplished with a single method, but rather by combining different methods for conclusive results. The most common methods and their purpose are listed in Table 6.

4.1. Characterization of the chemical structure

Several chemical tools are available to characterize the nature of the polymeric backbone and confirm the drug incorporation.

4.1.1. Nuclear Magnetic Resonance (NMR)

Proton (^{1}H) and carbon (^{13}C) nuclear magnetic resonance (NMR) is traditionally considered as a spectroscopic method of choice to assign the atoms along the polymer backbone and side chains, and thus confirm the chemical compositions of (co)polymers, micelles, and dendrimers. [191] In addition to the usual information on the atomic structure, the relaxation times measured when the excited nuclei return to their thermodynamically stable states reveal valuable information for studying macromolecular dynamics. NMR spectroscopy can thus provide detailed and quantitative information on the topology, dynamics, and three-dimensional structure of molecules in solution and the solid state. Moreover, NMR can be used to monitor the progress of polymerization reactions by determining monomer conversion into polymer or to calculate monomer ratios in copolymers (relying on the quantitative analysis of signal intensities). However, this method remains limited by its mid sensitivity, which generally results in NMR spectra characterized by a low signal-to-noise ratio (S/N). Information on the nature and position of the few covalent bonds formed between the end/side-chain groups and the polymeric backbone can thus be difficult to obtain by NMR. Recent promising NMR techniques, such as Dynamic Nuclear Polarization (DNP) can be used to increase signal sensitivity and intensity. [192]

Hence, the successful preparation of LUM-polymer conjugate **21** [143] was confirmed by ^{1}H NMR spectroscopy at each step of the synthesis with the disappearance of the characteristic signals of the different intermediates **20a**-**20c** (allyl protons (a), carboxylic acid (b), methylene and vinylic protons (c)) and the appearance of characteristics signals of LUM drug (d)(Fig. 15).

In the case of dendrimer synthesis, ^{1}H NMR is an indispensable technique to monitor at each step the progress of the branches growth

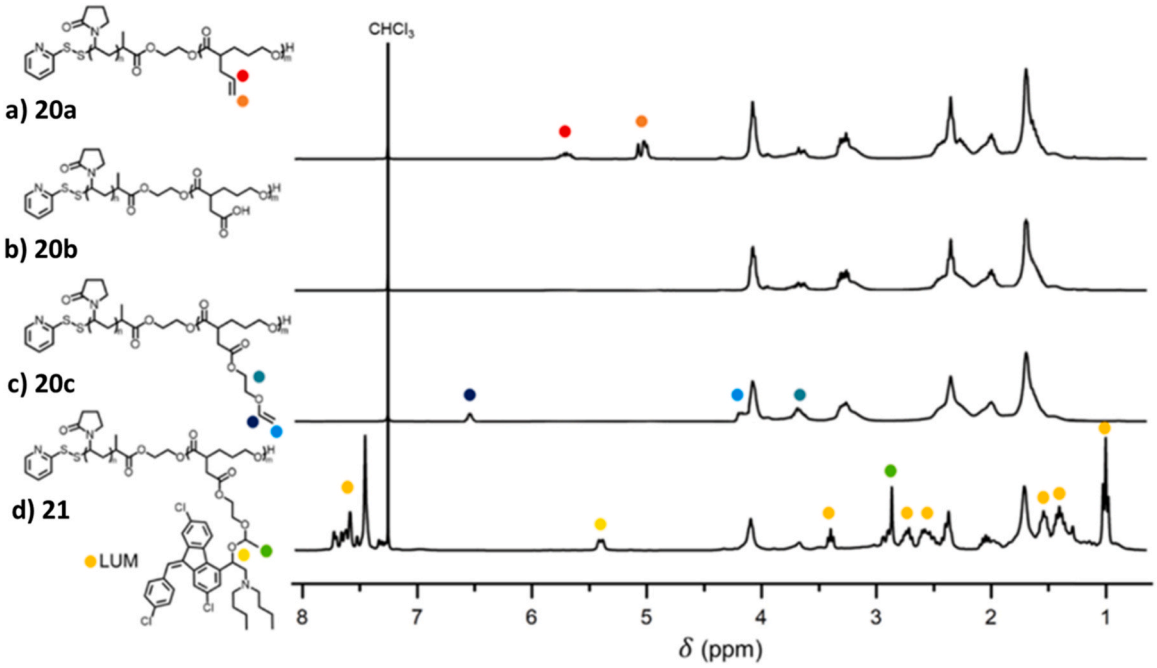

Fig. 15. ^{1}H NMR spectra and chemical structures of (a) allylated PVP-*b*-PVL **20a**, (b) carboxylated PVP-*b*-PVL **20b**, (c) vinyl ether-functionalized PVP-*b*-PVL **20c**, and (d) LUM-polymer conjugate **21** ($CDCl_3$, 400 MHz). (*Reproduced from ref.* 143 *with permission from the American Chemical Society*).

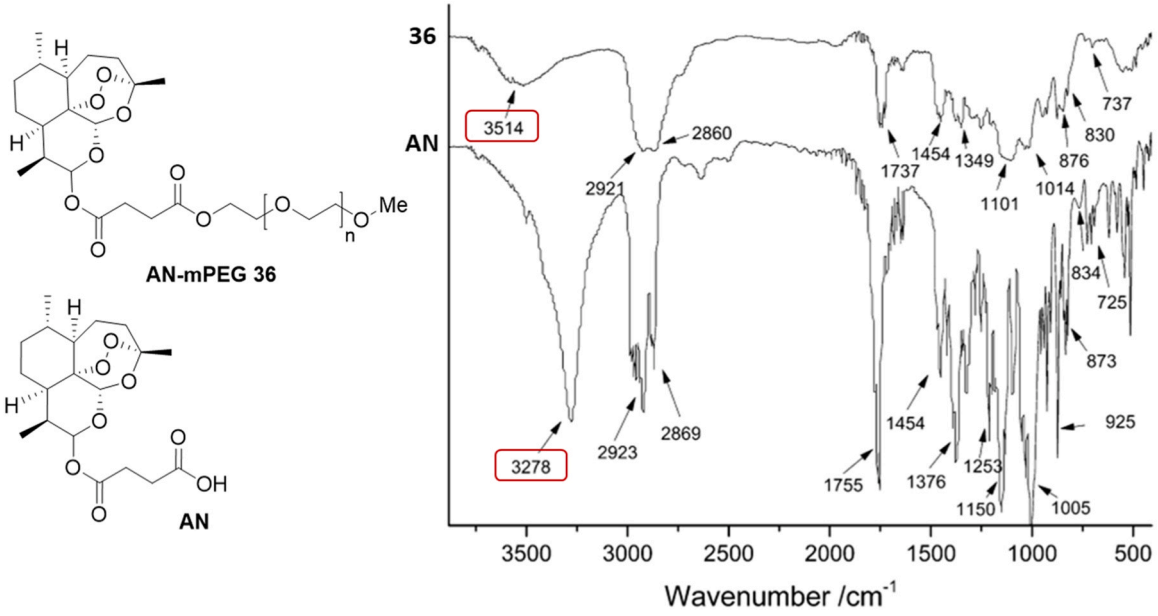

Fig. 16. FT-IR spectra of AN-mPEG (**36**) and free AN.
(a) (*Reproduced from ref.*193 *with permission from Elsevier*).

and rapidly identify the synthetic failures. Detailed information on the chemical environment and integration of hydrogen atoms helps discerning missing branching units or abnormal terminal functionalizations. Differences in chemical shift and pic shapes allow identifying intramolecular cyclization. Finally, ^{1}H NMR can also be useful for the detection of impurities due to external contaminations or side reactions. Thus, Sierra and Fernàndez-Busquets confirmed by ^{1}H NMR the efficiency of the click CuAAC step between the **bis-GMPA** dendron and the poloxamer chain of **HDLDBC-bGMPA 32a**, through identification of the small hydrogen signals of the triazole.[183]

4.1.2. *Fourier Transform Infrared Spectroscopy (FT-IR)*

Fourier Transform Infrared Spectroscopy (FT-IR) is used to determine the chemical composition of a sample through the identification of the molecular vibrations created by infrared light irradiations. Each band is characteristic of a type of chemical bond, and combined, they form a molecular "fingerprint" of the sample.In the case of polymers, FT-IR is usually used for the validation of heteroatom functional groups such as hydroxyl, ether, carbonyl, or carboxylic acid groups found in polymers like PEG or PCL. It can also confirm drug-polymer coupling. For example, on the spectrum of the artesunate- conjugated poly(ethyleneglycol) monomethyl ether AN-mPEG **36**, Muir and co-workers observed the disappearance of the characteristic O-H absorption band (3278 cm^{-1}) of the carboxylic group of the free AN, and the simultaneous appearance of a new band (3514 cm^{-1}), typical of strong inter- and intra-molecular hydrogen bonds found in the link between AN and the polymer (Fig. 16). [193] The AN-mPEG **36** also showed intense characteristic stretching bands of mPEG at 2860 and 1100 cm^{-1} and the typical peaks of the AN-peroxy bridge bonds at approximately 830 and 737 cm^{-1}. This FT-IR spectra confirmed the conjugation of the mPEG to the AN backbone.

In the case of dendrimers, FT-IR is employed to validate the transformation of specific functional groups such as alcohols into esters, or amines into amides or nitriles. Due to its low sensitivity, FT-IR usually does not allow the observation of most frequent defects such as missing units, cyclization or dimerization, supporting the essential role of ^{1}H NMR and MS analysis for this purpose.

4.1.3. *Steric exclusion chromatography (SEC)*

Steric exclusion chromatography (SEC) (also called Gel permeation chromatography (GPC)) is a liquid chromatography technique based on the separation by size (hydrodynamic volume) of dissolved macromolecules, during their elution through a column filled with porous gel beads (stationary phase). Large polymers of molecular weight that are above the column exclusion limit are not trapped and are rapidly eluted in the dead volume. Polymers small enough to penetrate the pores of the

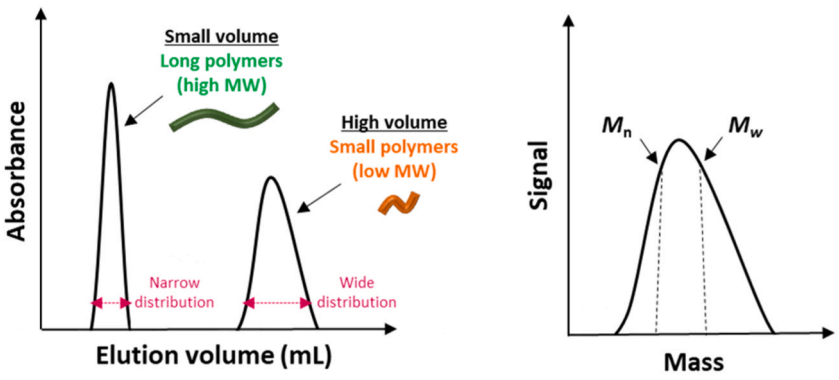

Fig. 17. Size-Exclusion Chromatography (SEC) chromatograms.

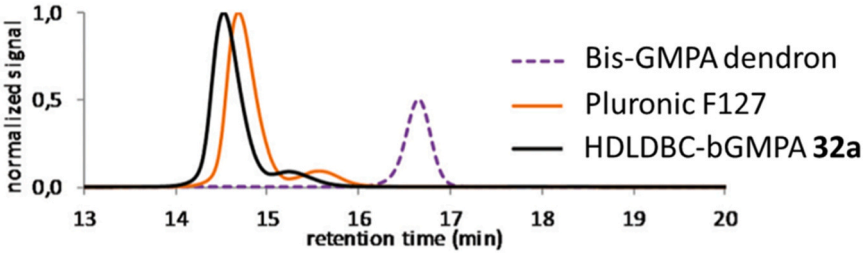

Fig. 18. SEC chromatograms of dendrimer **32a** and its dendrons bis-GMPA and F127. Reproduced from ref. [183] with permission from the Royal Society of Chemistry.

stationary phase are trapped, to varying degrees depending on their size, and will thus be ejected from the column at different elution volumes (Fig. 17). The number average molecular weight (M_n), the weight average molecular weight (M_w) and the dispersity ($Đ$) of the polymers are deduced from this chromatogram. [194]

The number average molecular weight (M_n) represents the statistical average molecular weight of all the polymer chains in the sample and influences the thermodynamic properties of the polymer (*eq 4*). While the weight average molecular weight (M_w) considers the molecular weight of each chain in determining their contribution to the molecular weight average, rather than just their number (*eq 5*). The more massive the chain, the more the chain contributes to molecular weight. M_w better reflects the proportion of large polymer and influences the bulk properties and toughness of the polymer. M_w is always greater than M_n unless the polymer is completely monodispersed ($Đ=1$, all the chain lengths are equal). Finally, the ratio of M_w to M_n is also used to calculate the polydispersity index (PDI) of a polymer (Eq. 6), also called dispersity $Đ$. The dispersity represents the homogeneity of a polymeric population according to the range of molecular weights. The wider the molecular weight distribution, the larger the PDI and the less homogeneous the population.

$$Mn = \frac{\sum Mixni}{\sum ni} \quad (eq4) Mw = \frac{\sum Mi^2 xni}{\sum Mixni} \quad (eq5) Đ = \frac{Mw}{Mn} \qquad (6)$$

SEC can be useful to monitor the progression of a (co)polymerization by observing the increase in molar masses. For instance, the final HDLDBC-bGMPA dendrimer **32a** was eluted faster than its dendrons bis-GMPA and F127 poloxamer (Fig. 18),[183] confirming its higher molecular weight.

Due to the poorly defined macromolecular structures and relatively high molecular weights of polymers, mass spectrometry (MS) analysis, including high-resolution mass spectrometry (HRMS), are generally not methods of first choice for the mass determination of polymers.

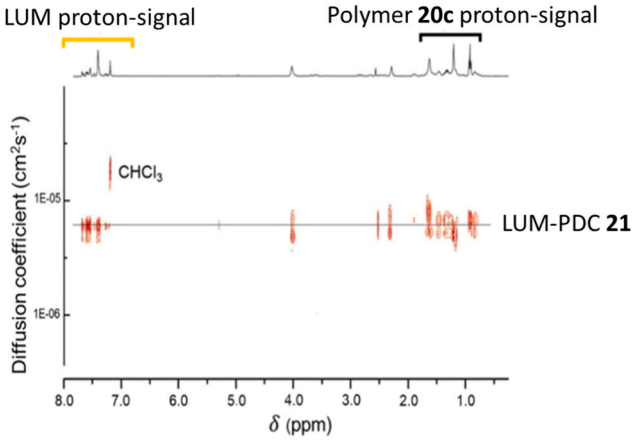

Fig. 19. DOSY spectrum of LUM and the PVP-*b*-PVL/VE-LUM copolymer **21.** (*Reproduced from ref.* 143 *with permission from the American Chemical Society*).

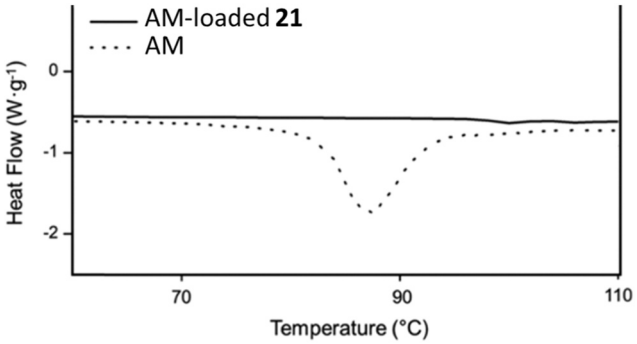

Fig. 20. DSC thermograph of AM-loaded **21** and free AM. (*Reproduced from ref.* 143 *with permission from the American Chemical Society*).

However, in the case of the well-defined structure of dendrimers, mass spectrometry is important to determine their precise molecular formula and molecular weight. The sensitivity of the technique and the precise information on the different masses of a mixture of dendrimers also make it possible to detect the presence of defective dendrimers and to identify their structural defects. Identification of cyclized or dimerized dendrimers is thus easier by mass spectrometry than by ^{1}H NMR. The efficient conjugation of drugs or targeting ligands on a dendrimer surface can also be confirmed and quantified by mass spectrometry.

4.1.4. Diffusion-ordered spectroscopy (DOSY)

Diffusion-ordered spectroscopy (DOSY) seeks to separate the NMR signals of different species according to their diffusion coefficient. [195] This analytical method produces a two-dimensional correlation spectrum with chemical shifts on the horizontal axis and diffusion coefficients on the vertical axis. Hence, nuclei that are distinct but structurally correlated in the same molecule display NMR signals at the same diffusion coefficient. DOSY experiment has been, for example, performed to confirm the successful conjugation of lumefantrine (LUM) to the polymeric backbone of **20c** (Fig. 19).[143] The same translational mobility was observed for both proton NMR signals of LUM and the polymer, testifying the covalent binding between these two components to form LUM-polymer conjugates **21** (Fig. 19).

4.1.5. Differential scanning calorimetry (DSC)

Differential Scanning Calorimetry (DSC) is used to determine the stability of biomolecules directly in their native form, as well as their purity, their polymorphic forms, or their molecular interactions. It is based on the measurement of the heat variation associated with the thermal denaturation of a molecule subjected to constant heating. DSC is also used to gain information on drug-polymer interactions as well as the physical changes occurring on the drug or the polymer during the thermal analysis. For instance, DSC can be used to compare the stability of drug-loaded micelles against their free drugs. For the AM-loaded LUM hybrid micelle **21** (Coartem combination), DSC analysis indicated an increased stability of the drug encapsulated in the micelle, reflected by a

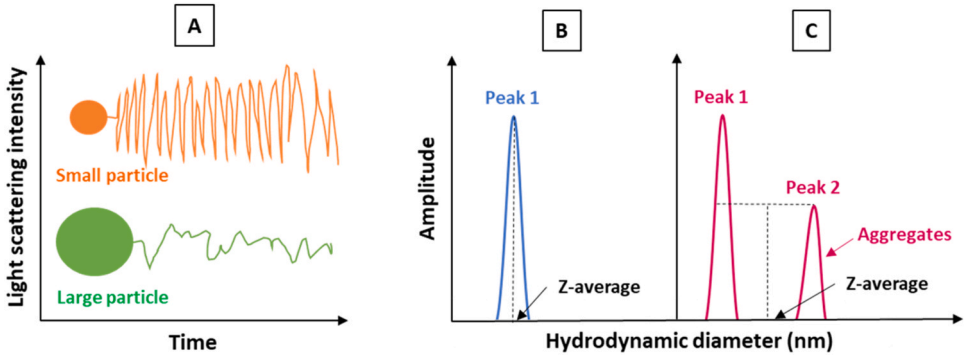

Fig. 21. A: Light scattering intensity of small vs large particles, B: DLS of monodisperse sample, C: DLS of polydisperse sample with aggregates.

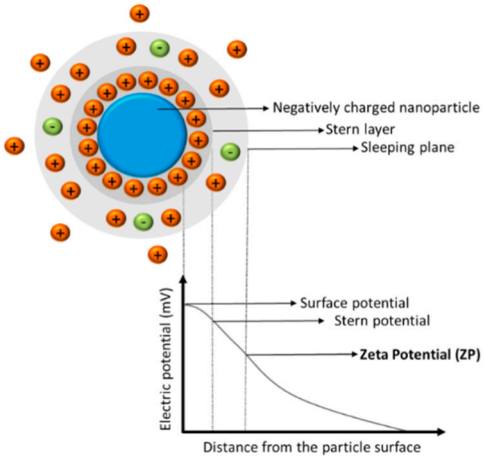

Fig. 22. Zeta Potential of a negatively charged nanoparticle.

higher melting point (Fig. 20).[143]

4.2. *Characterization of the physical properties*

Parameters such as the size and the shape of the nanoparticle are strongly influenced by the synthetic pathways used to obtain the polymer backbone, by the method of drug insertion, or by the intrinsic nature of the polymeric nanovector or the drug. Several physical methods can give valuable information on the size, shape, and surface charge of the nanoparticle.

4.2.1. *Dynamic light scattering (DLS) and zeta potential (ZP)*

Dynamic Light Scattering (DLS) (also called Photon Correlation Spectroscopy PCS or Quasi Elastic Light Scattering QELS) is a spectroscopic method used to evaluate the size distribution profile and the zeta potential of particles in suspension. [196] DLS is a label-free, non-destructible, rapid, and accessible method broadly compatible a large array of particles of nano to sub-micrometer sizes. It is also a reproducible technique that does not require high concentrations of product (less than 5 mg/mL). In practice, the particle size is determined by measuring changes in laser light intensity, perpetrated by the random movement of particles in the suspension (known as Brownian motion). Rapid changes in light intensity indicate rapid changes in relative positions, characteristic of small particles, while large particles tend to move around more slowly (Fig. 21, A). This hydrodynamic size is dependent of the temperature and viscosity of the solution and its standard deviation can be correlated to the width of the size distribution and converted to a polydispersity index (PDI). DLS experiment can also allow the detection of aggregates, as it provides size distribution through the Z-average and/or directly through the peak size value. For a perfectly monodisperse sample (only one population of peak), the size values obtained by Z-average and peak size are substantially the same (Fig. 21, B). However, for a polydisperse sample such as in aggregates, the values are different from the different population peaks (at least two populations, Fig. 21, C). In this case, the Z-average value is irrelevant and only the corresponding peak sizes must be considered.

DLS can also be used to determine the zeta potential (ZP) of the sample (also called electrokinetic potential), which represents the global electrical charge of a nanoparticle in suspension as a function of ions surrounding it (Fig. 22). The mobility of the charged particles under the effect of an electric field (such as electrostatic repulsion between adjacent and similarly charged particles) is converted into a zeta potential according to Henry's equation. It is one of the fundamental parameters employed to determine the stability of colloidal dispersions or estimate the surface charge of a particle. [197,198] High zeta potential (negative or positive) implies highly charged particles, a key parameter to obtain stable nanoformulations. Indeed, the strong electrostatic repulsions between highly charged particles prevent the aggregation of the particles and thus maintain good nanosuspension stability. Generally, nanoparticles whose ZP is more positive than +30 mV (or more negative than −30 mV) are considered stable. On the other hand, a low ZP (from −30 mV to +30 mV) implies that attractions between the particles overcome the repulsions, thereby favoring particle aggregation in the mixture.

ZP-negative nanoparticles are known for having an increased lifetime in the blood thanks to moderate interactions with blood components, as well as weak cell internalization. Indeed, the negatively charged surfaces of the plasma and the blood cells lead to electrostatic repulsions with the ZP-negative nanoparticles, thus decreasing nonspecific interactions. The high reticuloendothelial uptake adsorption of negatively charged nanoparticles has nevertheless been reported to favour their endocytosis and thus, their final elimination.

On the other hand, positively charged nanoparticles can easily interact and agglomerate with the negatively charged plasma proteins or cell membranes. These electrostatic attachments favour fast endocytosis or direct penetration of the nanoparticle in the cell. However, for the same reasons, cationic nanoparticles are generally more toxic than negative ones. Their ability to rapidly penetrate cells can cause plasma-membrane integrity disruption or strong mitochondrial and lysosomal damages. [199] Determination of the zeta potential is thus useful to anticipate the particles behaviour in biological fluids. [200]

In the case of antimalarial DDS, DLS has primarily been used to determine particle size distribution and measure their zeta potentials. The DLS results are often compared to those from other similar techniques, such as Atomic Force Microscopy (AFM) or Transmission Electron Microscopy (TEM). For instance, the Z-average (83 nm) and the zeta potential (-15.4 mV) of the PCL-PEG-PCL co-polymer **12** were determined by DLS (Fig. 23).[138] DLS measurements can also be used to confirm the encapsulation of a fluorescent dye into a polymeric system. For instance, encapsulation of the cisplatin dye (Platinol® or

			Size (d.nm)	Intensity (%)	St Dev (mV) (d.nm)
Z-average (d. nm)	**83.22**	Peak 1	112.2	100.0	65.88
PDI	0.22	Peak 2	0.000	0.0	0.000
Intercept	0.938	Peak 3	0.000	0.0	0.000
Result quality	Good				

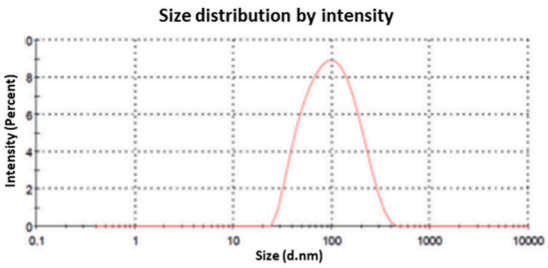

			Mean (mV)	Area (%)	St Dev (mV)
Zeta Potential (mV)	**-15.4**	Peak 1	-15.4	100.0	5.81
Zeta Deviation (mV)	5.81	Peak 2	0.000	0.0	0.000
Conductivity (mS/cm)	0.938	Peak 3	0.000	0.0	0.000
Result quality	Good				

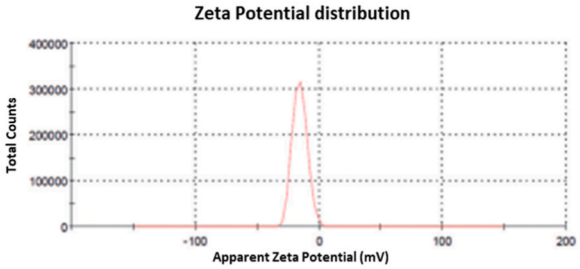

Fig. 23. DLS spectra of PCL-PEG-PCL **12** (Z-average and Zeta potential). (a) (*Reproduced from ref.* 138 *with permission from Taylor & Francis*).

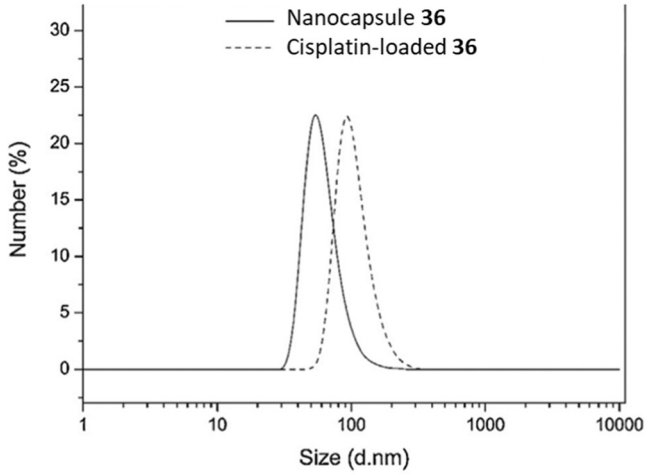

Fig. 24. DLS spectra of free *versus* cisplatin-loaded nanocapsules **36**. (*Reproduced from ref.* 193 *with permission from Elsevier*).

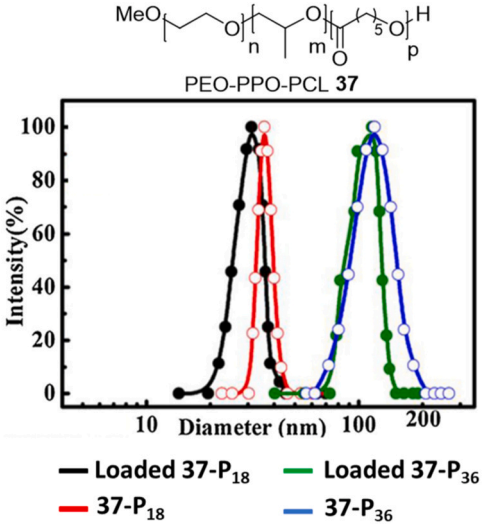

Fig. 25. DLS spectra of DTX/CQ-loaded and free **37-P$_{18/36}$**. (a) (*Reproduced from ref.* 127 *with permission from Elsevier*).

generic name: CDDP) within the liposome-like nanocapsules AN-mPEG **36** (Fig. 16) was confirmed by DLS analysis of the hydrodynamic diameters of the free *versus* cisplatin-loaded nanocapsules (Fig. 24).[193] After encapsulation of cisplatin, the hydrodynamic diameter of the nanocapsules **36** increased to an average diameter of 103 nm compared to an average diameter of 89 nm for the empty ones. A negative zeta potential of −12.4 mV was measured for the cisplatin-loaded nanocapsules, foreshadowing a potentially high circulation time in the blood.

In the case of poly(ethylene-oxide)-co-poly(propylene-oxide)-co-poly(ε-caprolactone) micelles (PEO-PPO-PCL) **37** (Fig. 25), [127,201] DLS was used to confirm drug encapsulation of chloroquine (CQ) and an antitumoral agent (docetaxel, DTX) by the thin film method. Two co-polymers were particularly compared: the hydrophilic PEO_{68}–PPO_{34}–PCL_{18} and the more hydrophobic (containing more PCL) the PEO_{68}–PPO_{34}–PCL_{36}. DLS showed that particle sizes increased with the amount of PCL blocks (Ø **37-P$_{36}$** > Ø **37-P$_{18}$**), (Fig. 25). However, in both cases, the drug encapsulation process slightly decreased the hydrodynamic diameter of the particles. DTX/CQ-loaded micelles displayed slightly lower diameters than the corresponding free micelles (Ø (loaded-**37-P$_{18}$**) = 31 nm *vs* Ø (empty **37-P$_{18}$**) = 36 nm and Ø (loaded-**37-P$_{36}$**) = 115 nm *vs* Ø (empty **37-P$_{36}$**) = 119 nm). This size reduction was attributed to the strong attractive hydrophobic interactions between the encapsulated drugs and the inner core, causing micelle shrinkage. Their study also highlighted the impact of the size of the hydrophobic PCL polymeric part on the drug-loading, the encapsulation efficiency and the drug release. DL and EE parameters increased with the size of the PCL block: DL = 3%, EE = 77% in **37-P$_{18}$** < DL = 6%, EE = 95% in **37-P$_{36}$**. As well, *in vitro* release of both drugs at pH 7.4 was always faster with P_{18}-block micelles (76% DTX in 48 h, 75% CQ in 24 h), while larger and more hydrophobic P_{36}-block micelles better controlled the burst drug release effect (76% DTX in 72 h, 72% CQ in 36 h). Note that the smaller chloroquine CQ was released twice faster than docetaxel DTX. The authors also attributed it to the weaker interactions of CQ with the inner polymer core.

DLS was further used to investigate the sensitivity to reduction of the disulfide bridge present in the PMOXA-g(SS)-PCL micelles **17** (which is essential for drug-release) in presence of reducing agent like dithiothreitol (DTT), mimicking the physiological cytosolic conditions of

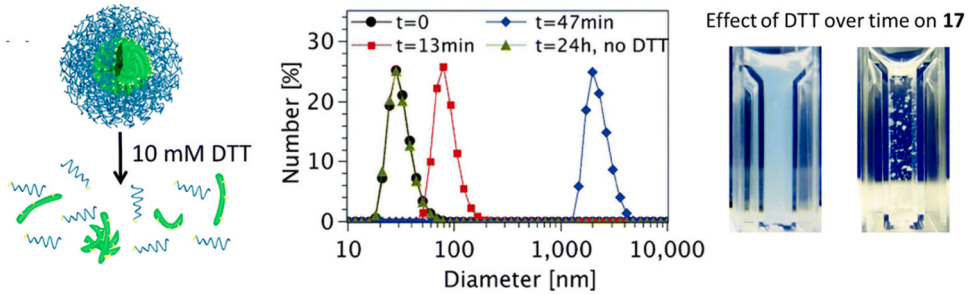

Fig. 26. Effect of DTT on the stability of micelles **17** followed by DLS. (*Reproduced from ref.* 141 *with permission from the Royal Society of Chemistry*).

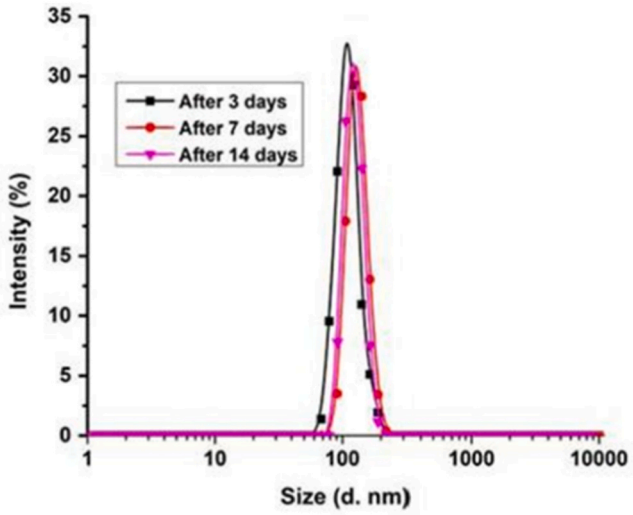

Fig. 27. Storage stability studies of AN-poly(heparin) conjugate **8** by DLS. (a) (*Reproduced from ref.* 98 *with permission from Elsevier*).

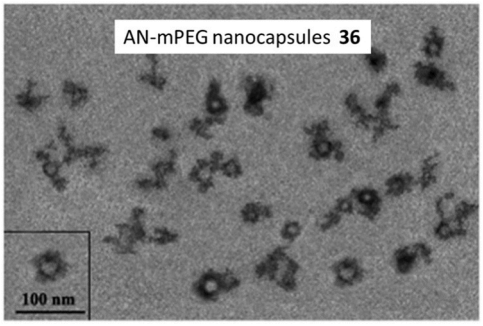

Fig. 28. TEM image of AN-mPEG nanocapsules **36** stained with cisplatin. (*Reproduced from ref.* 193 *with permission from Elsevier*).

malaria parasites (Fig. 26).[141] DLS analysis revealed that the micelles **17** remained stable for at least 24 hours in the absence of reducing agent (black and green curves) but were quickly destabilized by the reducing agent (red and blue curves). During time exposure, the diameter of the nanoparticles increased so drastically that a high turbidity appeared, and precipitates were visible to the eye. These precipitates were attributed to aggregates of insoluble PCL after cleavage of the hydrophilic blocks (PMOXA) from the co-polymer. This DLS study clearly indicated that the disulfide bridge between PMOXA and PCL units was well reduced in the presence of a reducing agent, leading to the disintegration of the micelles that allowed drug-release.

Finally, DLS can also help provide information on storage stabilities. The stability of AN-poly(heparin) conjugate **8** was studied over 14 days

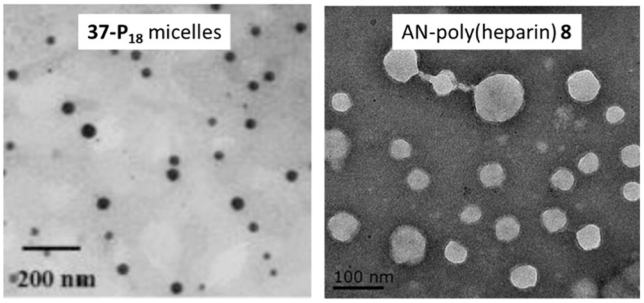

Fig. 29. TEM images of **37-P_{18}** micelles (on the left) and AN-poly(heparin) conjugates **8** (on the right).
(a) (*Reproduced from ref.* 127 and 98 *with permission from Elsevier*).

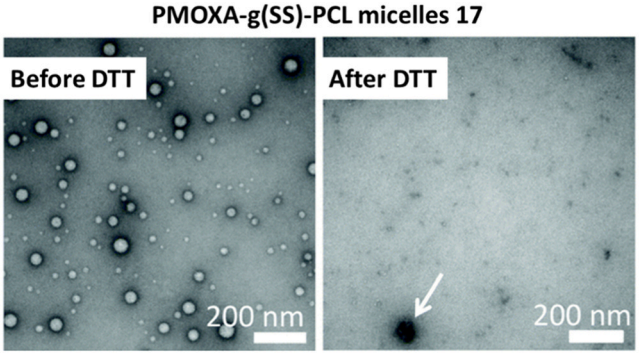

Fig. 30. TEM image showing the degradation of micelles **17** in presence of DTT.
Reproduced from ref. [141] with permission from the Royal Society of Chemistry.

at different time checkpoints (Fig. 27). No significant variation in particle size was observed, leading to the conclusion that this PDC possessed promising storage stability.[98]

4.2.2. Transmission electron microscopy (TEM) and cryo-TEM

Transmission electron microscopy (TEM) is a standard and indispensable characterization technique for polymer science. [202] This versatile microscopy technique provides a range of valuable information on size, shape, surface morphology, or crystallographic structure. It covers the nanometer size range and resolves microstructure of materials with atomic-scale resolution (up to 1 Å). Agglomeration or aggregation are also visible. TEM uses a high-voltage electron beam transmitted through an ultrathin sample to create an image. The image is formed from the interaction of the electrons with the atoms of the sample. However, while TEM provides high-resolution images, it is hindered by the inherently low contrast and the beam sensitivity of the nanoparticles. Therefore, the sample must be first treated with a contrast

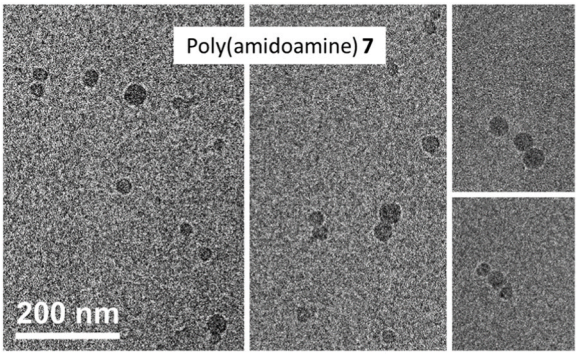

Fig. 31. Cryo-TEM images of the empty PAA **7.**
(*Reproduced from ref.* 95 *with permission from Elsevier*).

agent (staining).

Liposome-like AN-mPEG nanocapsules **36** were stained by cisplatin and analysed by TEM.[193] Cisplatin is extremely lipophilic, giving it a high tropism to be embedded into the hydrophobic region of DDS, thus making it easier to observe. Stained AN-mPEG nanocapsules **36** appeared as dark membranes surrounding less colored cores. This confirmed the vesicular structure of the nanocapsules and indicated an average size of 90 nm (Fig. 28).

On other example, TEM analysis of **37-P$_{18}$** micelles [127] or AN-poly (heparin) conjugate **8**[98] was used to identify the spherical rounded-like structures of these DDS (Fig. 29).

The TEM technique can also be a tool to study polymer stability. Meier and co-workers observed almost full decomposition of their PMOXA-g(SS)-PCL micellar particles **17**[141] upon addition of a reducing agent (DTT), confirming the disassembly of the DDS under this reductive condition (Fig. 30). Note that the TEM technique is usually not appropriate to evaluate the efficiency of a drug encapsulation step. Empty or loaded polymeric systems usually display the same sizes, especially in the dry state. As described above (Section 3.2.1), DLS is a more adapted method to prove a drug encapsulation.

Cryogenic transmission electron microscopy (Cryo-TEM) is another TEM technique based on the same principle of electron beam transmission. However, with Cryo-TEM, the sample is cooled to cryogenic temperatures and embedded in amorphous ice. The rapid cooling with liquid nitrogen allows the sample to be maintained under physiological conditions and thus preserves its morphology and structure in its natural state. [203] In addition to basic size and shape information, this technique provides answers to the behavior of DDS in the physiological environment and/or the involved biological mechanisms.

Xavier Fernàndez-Busquets and co-workers used Cryo-TEM to characterize their poly(amidoamines) conjugates (**5–7**).[95] The images revealed a globular-spherical conformation for the polymer **7** which swelled up to higher diameters of 20–40 nm (in the absence of drug) (Fig. 31).

It is noteworthy that DDS size values can differ depending on the physical technique (DLS, TEM, AFM) used to measure it. Nevertheless, the orders of magnitude within a compared particle series are generally in agreement with those from the different techniques. This is partly due to the mode of preparation of the sample. For instance, size values obtained by TEM from dried samples can be smaller than the values obtained by DLS from samples in solution. The average diameter of the HDLDBC-bGMPA dendrimer **32a** was thus of 13 nm, according to TEM analysis, but 26 nm when determined by DLS.[183]

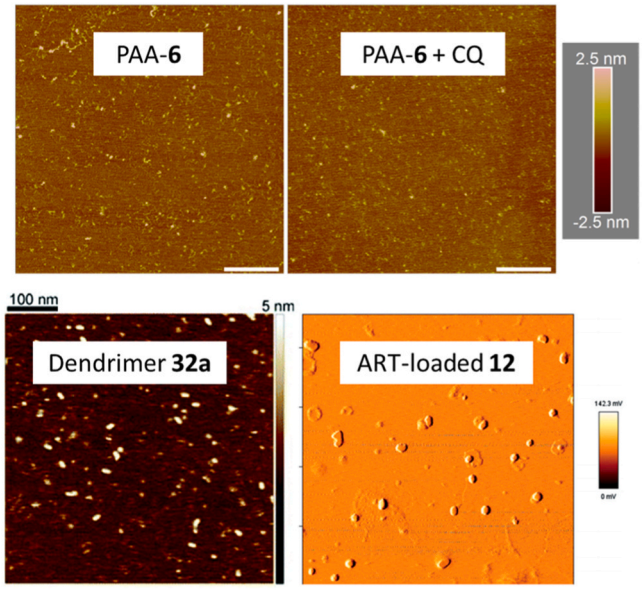

Fig. 32. AFM images of PAA **6,** HDLDBC-bGMPA dendrimer **32a** and ART-loaded PCL-PEG-PCL micelles **12.** (*Reproduced from ref.*96 *with permission from MDPI, from ref.* 183 *with permission from the Royal Society of Chemistry, from ref.*138 *with permission from Taylor & Francis*).

4.2.3. Atomic force microscopy (AFM)

Atomic force microscopy (AFM) gives both qualitative and quantitative information about several physical properties of a polymer, including size homogeneity, morphology, surface texture, topology, volume, and roughness. [204] The AFM technique exploits the interaction (attraction and repulsion) between the atoms of the mobile tip of a mechanical probe and the surface atoms of a fixed sample, to form a 3D image. [205] A wide range of particle sizes from nanometer to micrometer can thus be characterized through very-high resolution images of the three-dimensional shape (topography) of the sample surface. The major difference between AFM and TEM is that AFM does not use beam irradiation. The sample is thus better preserved and does not need to be stained. All the surface variations are associated with distinct morphological aspects.

For instance, the globular conformation of poly(amido-amines) such as **6**[95,96] and their homogeneous size distribution were confirmed by AFM (Fig. 32). In addition, AFM provided evidence that the introduction of CQ into PAAs did not affect DDS size. The AFM technique also confirmed the rounded-structure of HDLDBC-bGMPA dendrimer **32a** [183] with similar height to that of previously measured by TEM (Fig. 32). Similarly, Manjili and co-workers proved by AFM the formation of micellar ART-loaded DDS **12** from the assembly of their PCL–PEG–PCL polymers,[138] with a homogeneous spherical morphology (Fig. 32). The micelle sizes determined by AFM (70 nm) were slightly smaller than that determined by DLS (83 nm). As with TEM methods, the difference can be attributed to the collapse of the micelles upon water evaporation, during AFM sample preparation.

4.2.4. Scanning electron microscopy (SEM) and Energy-Dispersive X-ray microanalysis (EDX)

Scanning electron microscopy (SEM) is another indispensable and versatile technique for imaging the microstructure, topography, and morphology of dried metal-coated materials at nanometer to micrometer scale. [206] The surface of the nanoparticles needs to be coated by a conductive material (such as gold, silver, or platinum) to interact with the electron beam, bombarded by the SEM microscope. [207] SEM has a resolution of 10 nm (100 Å) but advanced instrumental versions can improve resolution to about 2 nm (25 Å). Unlike TEM, SEM hits the sample with a low energy electron beam that reduces irradiation damages onto the surface. Images result from the interaction of this electron beam with atoms at various depths. Variations in signal intensity provides information about the surface topography and composition of the sample. The height differences in the sample give contrast in the image. Other types of detectors are available, and SEM may also be coupled

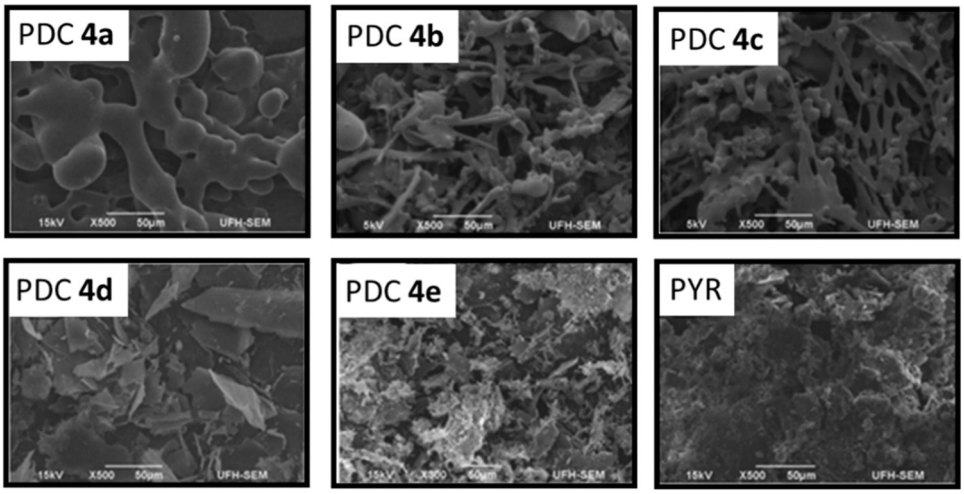

Fig. 33. SEM images of poly (aspartamide) conjugates: PDC **4a** (PYR + 4- aminosalicylic acid), **4b** (PYR + PQ + 4- aminosalicylic acid), **4c** (PYR+ 4-aminoquinoline), **4d** (Aminosalicylic acid), **4e** (A modified DACH Platinum-aminosalicylic acid) and the free pyrimethamine (PYR).
(a) (*Reproduced from ref.* 92 *with permission from Elsevier*).

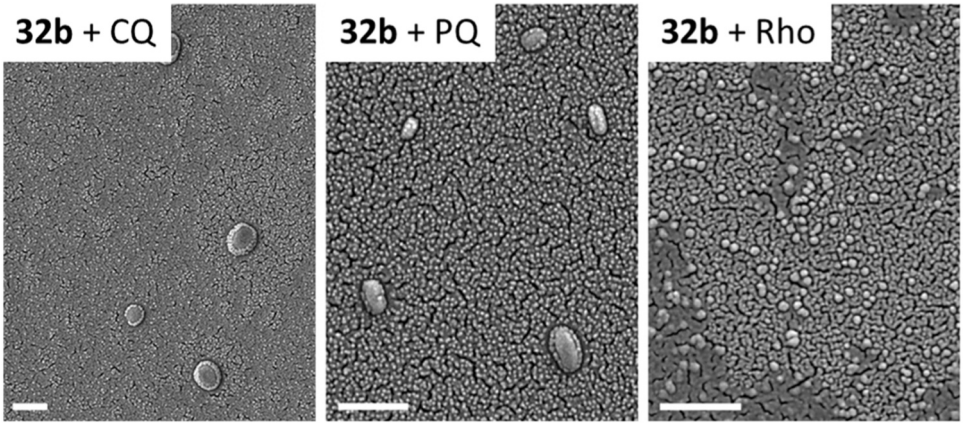

Fig. 34. SEM images of HDLDBC-bMPA **32b** in presence of drugs (CQ and PQ) or fluorescent dye (Rho). (*Reproduced from ref.* 185 *with permission from Elsevier*).

with other devices, including energy-dispersive X-ray microanalysis (EDX) for the determination of the elemental composition or orientation of the sample. SEM is widely used in DDS studies and the technique can generally be applied to determine the appearance of the polymer surface (irregular form, rod-like form, film, etc.) as well as its biodegradability. [208] To define morphological shapes, a formula is used to determine the aspect ratio (AR), which is equal to the length divided by the width. For instance, for $1 < AR \leq 1.2$, nanoparticles are considered spherical, while for $1.2 < AR \leq 3$ they are ovoid and up to 3, they are elongated.

For antimalarial DDS, SEM analysis has for example, provided information about the polymer morphology which can be related to the drug encapsulation process and to its behaviour in physiological medium. Gold-coated poly(aspartamide) PDCs **4**,[92] previously presented in section 2.1.3, were studied by SEM analysis to determine their surface morphologies and compare them with other conjugates. The differences between all these PDCs lie in the nature and number of the drugs conjugated to the polymer (Fig. 33).

Tubular forms with spherically swollen topologies were observed for PDCs **4a** (PYR + 4-aminosalicylic acid), **4b** (PYR + PQ + 4-aminosalicylic acid) and **4c** (PYR+ 4-aminoquinoline) which contain at least two drugs, including pyrimethamine (PYR). While SEM images revealed predominantly flake-shaped morphologies for PDCs **4d** (aminosalicylic acid) and **4e** (a modified 1,2-diaminocyclohexane (DACH) Platinum-aminosalicylic acid without PYR). In order to confirm drug incorporation, the drug-loaded PDC images were compared to drug-free PDC images. No characteristic morphologies were observed for the PYR-free PDC (not shown), unlike the tubular form observed for the PYR-embedded **4a**. This confirmed the successful incorporation of

Table 7
List of methods for DDS biological characterizations.

Methods	Determined parameters	Objectives and information
Cellular biology and cell culture	Parasite viability (fluorescence intensity) Cell viability (absorbance)	*In vitro* activity (IC_{50}) *In vitro* cytotoxicity (CC_{50})
Hemolysis assay (biocompatibility)	Lysis of erythrocytes (absorbance)	Toxicity on RBCs (Percentage of hemolysis)
Flow analysis cell sorting (FACS) Confocal microscopy	Fluorescence of labelled-polymer and stained-cells	Specificity of DDS for pRBCs vs RBCs Selectivity of DDS towards pRBCs stages of the parasite
Confocal microscopy Transmission electron microscopy (TEM) Cryo-TEM	Fluorescence of labelled-polymer and stained-cells	Cell internalization of DDS Entry in pRBCs
In vivo imagery	Fluorescence of labelled-polymer and stained-organs or tissues	Biodistribution of DDS Toxicity and pharmacokinetics

pyrimethamine into the polymer. In addition, the elemental composition of the conjugates was determined by SEM/EDX and percentages of carbon (40–78%), nitrogen (6–26%) and oxygen (13–22%) in PDCs were obtained. For conjugates **4a**, **4b** and **4c**, containing at least two drugs, the percentage composition of nitrogen and oxygen were higher than in those containing only one drug, confirming their successful incorporations into the polymer.

SEM analysis of dendritic micelles such as pluronic derivatives HDLDBC-bMPA **32b**[185] indicated more ovoid shapes for CQ and PQ-loaded dendrimers as underlined by their large diameters ranging from 170 to 500 nm (Fig. 34). On the contrary, the smaller diameter (50 nm) of the rhodamine-loaded polymer **32b** clearly leaned toward spherical aggregates.

To sum up, almost all of the polymeric DDS reported in this review are of size compatible with entry into the new permeability pathways (NPPs) of the pRBCs, ranging from 11 to 143 nm (DLS). Only a few DDS show relatively large particle sizes (up to 360 nm). However, it is important to emphasize here that the choice of analysis method can influence the expected results. Frequently, there is a concordance among the results obtained by DLS, AFM and TEM although those obtained by TEM are often weaker. These differences usually arise from sample preparation (drying for TEM) or behavior in solution (hydration layer for DLS). Both DLS and SEM techniques use polymer solutions to provide the size of the hydrodynamic diameter, which is usually identical to or larger than the size of the dense core provided by SEM. [209]

5. Biological characterizations of DDS and their mechanism of action

The last section of this review will be dedicated to the techniques indispensable for the biological evaluation of polymeric drug-delivery systems and the study of their mechanism of action. As highlighted by their design or their physicochemical characterizations, drug-loaded DDS are engineered nanotechnologies that require specific methods, different from those used in classical therapeutic strategies. In that respect, several biological methods have been developed or adapted to determine the efficiency, selectivity, and specific features of a polymeric vector toward a biological target. From classical cell culture to more specific studies focused on the best *in vitro* candidates, these biological characterizations are essential to assess their contribution in improving the therapeutic index of a drug and to understand their behavior in biological environments Table 7.

5.1. Standard methods for the biological evaluation of DDS

Obviously, the first biological experiments carried out when developing a new polymeric DDS consist in evaluating the *in vitro* cytotoxicity of the system on healthy cells, and its *in vitro* activities on the biological target. Technically, the setting up of the biological assays of a drug-loaded polymeric DDS does not really differ from the classical assay methods used for a free drug. Solutions of drug-loaded DDS are, for instance, prepared at similar concentration ranges and in the same biological-compatible solvents (H_2O, DMSO) as the free drug solutions. Issues of solubility with polymeric DDS can be handled with the same methods used for poorly soluble organic molecules (sonication, temperature-controlled bath, etc). Nevertheless, the particular situation of concentration units deserves to be discussed. For free drugs, biological assay values are typically expressed as molar concentration (C_n, g/mol). However, for polymeric nanovectors, these values are more often expressed in mass concentrations (C_m, g/mL). Indeed, it is important to remember that polymeric vectors are usually not prepared as a single molecular form with a fixed molar mass but are isolated as a population of polymeric backbones with different molar masses. The molar masses of these different molecular sizes are thus expressed as number average

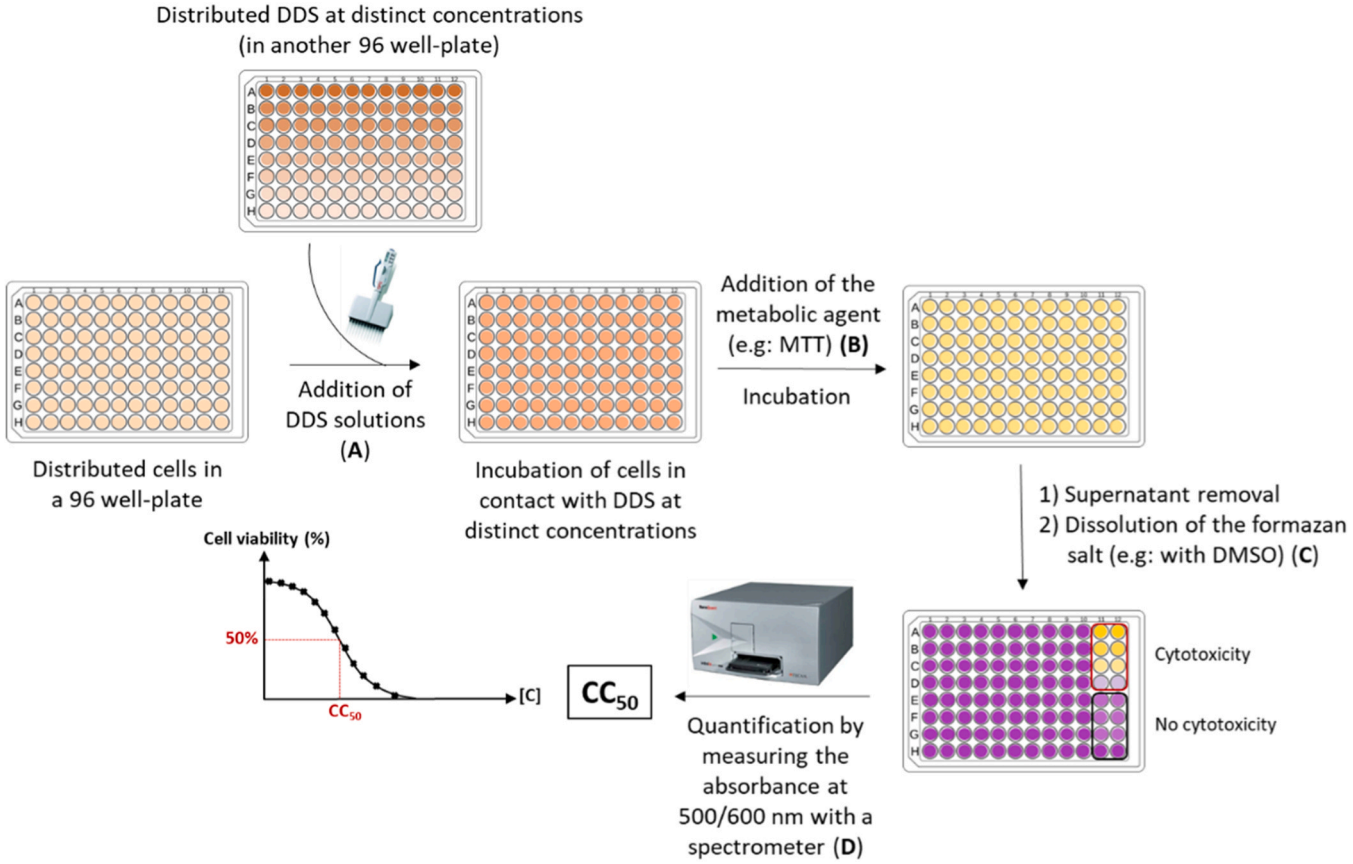

Scheme 21. *In vitro* cytotoxicity assay protocol.

molecular weight (M_n) or weight average molecular weight (M_w) (determined by SEC, Section 3.1.3). The greater the heterogeneity of the polymeric population (dispersity $Đ$), the wider the molecular weight distribution. Moreover, the average molecular weights of a same polymer can also differ according to the choice of SEC conditions (column type, nature of the polymer standards used for the calibration, etc). Hence, it can be difficult to calculate the molar concentration of a nanovector from an imprecise molar weight. In the publications that expressed biological DDS values in molar concentration, it is also unclear which of the values, M_n or M_w, was used by the manipulator, as this is not always specified in the experimental conditions. For all these reasons, we would recommend expressing the biological assays of polymeric vectors in mass concentrations (C_m, g/mL) and comparing them with the values of the free drugs also in mass concentrations. In the case of dendrimers, it could be argued that they are generally made using more controlled synthetic pathways and thus with more accurate molar weights.

A second point worth mentioning is the differences in *in vitro* activities observed between the free drug and its drug-loaded DDS. For instance, in the study case on antimalarial DDS, the *in vitro* activities obtained on *Plasmodium* strains of the evaluated drug-loaded nanocarriers are generally lower than the *in vitro* activities of an equivalent dose of the corresponding free drugs. However, this loss of activity is not necessarily due to a loss of efficiency of the vectorized drug. It can for example be attributed to the gradual release of the drug from the nanocarrier. Moreover, the advantages of drug delivery systems are not measured solely in terms of increased biological activity. The best achievements of DDS are most of the time in terms of decreased toxicities, improved pharmacokinetics, or targeted drug release under specific conditions (pH, enzymes, etc.), all factors that can lead to increase *in vivo* activities and a biological environment that is not reproduced during routine *in vitro* assays.

5.1.1. *In vitro cytotoxicity assay*

Whatever the therapeutic field, this technique is undeniably the one most used in drug-discovery research to screen and detect cytotoxic compounds (Scheme 21). This method provides the cytotoxic concentration (CC_{50}) that reduces the cell viability by 50% (damage or death) when compared to untreated controls. CC_{50} of the evaluated compound is always compared to at least one cytotoxic agent as positive control (e.g.: Doxorubicine), without forgetting the solvent and the cell growth controls. In the case of malaria, several strains of cells, such as HepG2, HeLa, MCF-7 and HUVEC can generally be used to determine the *in vitro* cytotoxicity of new antimalarial DDS. The experimental conditions of cell density, incubation times, temperature or revelation method will depend on the nature of the chosen cellular strain. [210]

Technically, the *in vitro* cytotoxicity assay of a drug-loaded polymeric DDS does not differ from the classical assay of a free drug (Scheme 21). As with small molecules, drug-loaded DDS solutions of different concentrations are distributed into a 96-well plate containing the adherent cell suspension (**A**). After an appropriate incubation time (generally 1–3 days at 37°C), cell viability in each well is revealed through the addition and incubation of metabolic activity-based dyes such as 3-[4,5-dimethylthiazol-2-yl]-2,5-diphenyl tetrazolium bromide (MTT) or 4-[3-(4-iodophenyl)-2-(4-nitrophenyl)-2 H-5-tetrazolio]-1,3-benzene disulfonate (WST-1) (**B**). These metabolic agents react with the mitochondrial succinate-tetrazolium reductase to form the insoluble formazan salt, as purple crystals (**C**). After dissolution of the crystals, quantification of the absorbance of the resulting purple-colored solutions by a multi-well UV/VIS spectrophotometer (500/600 nm) gives the number of viable and metabolically active cells (**D**). As reductases are only present in the living cells, the darker purple the solution, the lower the cytotoxicity of the evaluated compound. As shown in Scheme 21, the CC_{50} value is determined on the curve where the cell viability values re reported according to the different DDS concentrations.

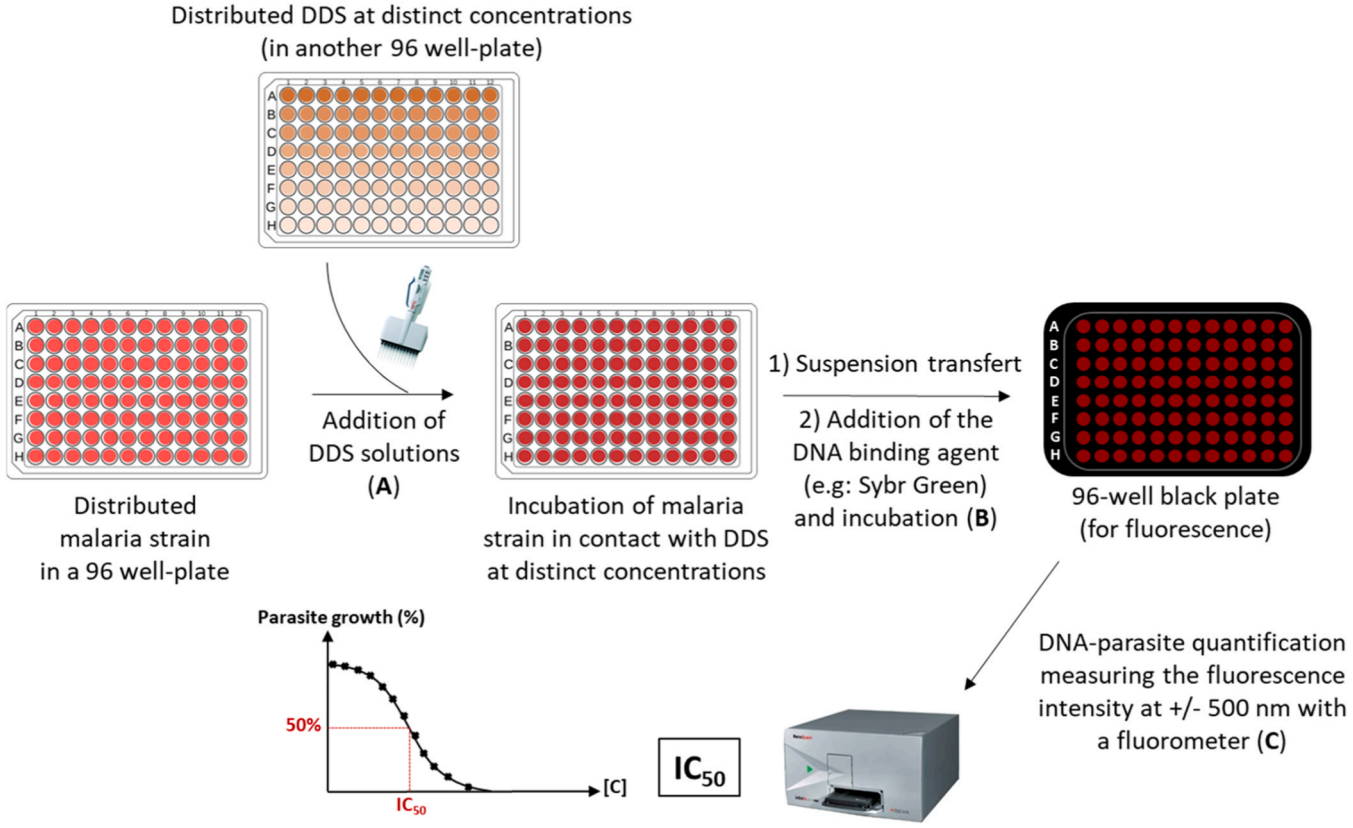

Scheme 22. *In vitro* activity assay protocol.

5.1.2. In vitro activity assay

In vitro activity is the ability for a molecule to inhibit a specific biological or biochemical function. This inhibition can target enzyme, cell, cell receptor or microorganism and can lead, for instance, to the reduction of parasite or bacterial growth. *In vitro* activity assays provide the inhibitory concentration (IC_{50}) that reduces the biological process by 50% compared to untreated controls. IC_{50} of the evaluated compounds is compared to at least one known active drug as active control (e.g.: Chloroquine or Artemisinin derivatives are used as antimalarial active agent), in addition to solvent and the fresh blood controls. To study the growth inhibition of the malaria parasite, several strains of *Plasmodium* with different known mechanisms of resistance to antimalarial drugs are commonly employed in co-culture (mixture of healthy red blood cells and parasite-infected cells) such as *Plasmodium falciparum* 3D7, K1, NF54 or even *Plasmodium berghei* to determine the *in vitro* activity of new antimalarial DDS. The experimental conditions for parasitemia, incubation time, temperature or revelation method will depend on the nature of the *Plasmodium* strain.[210]

Similarly to cytotoxicity assays and as with the small free drugs, the drug-loaded DDS solutions of different concentrations are distributed into a 96-well plate containing the parasite-infected co-culture suspension (RBCs + pRBCs) (Scheme 22, **A**). The hematocrit (the ratio of the volume of fresh red blood cells to the total volume of blood) set during the assay generally ranges between 2% and 3%. The parasitemia (quantitative measure of parasite content in blood) ranges between 1.5% and 4%, although it can be set at a lower level (0.05–1% [211]). In fact, a previous study of Waters and co. has compared several conditions with the SYBR green fluorescence assay and concluded that there was linearity of fluorescence for parasitemia values ranging between 0% and 5%. [212]

Generally, after 48 hours of incubation (to cover the complete life-cycle of the parasite), the incubated suspensions are transferred into a 96-well black-plate to avoid signal background and crosstalk during the reading (**B**). Parasite growth is revealed by adding a fluorescent marker (SYBR Green or Syto-11) that non-covalently binds to the surface of double stranded nucleic acids giving an accurate quantification of DNA chains present in each well. Since the only DNA present in the assay is the parasite DNA (absent in healthy RBCs), the measured fluorescence intensity is proportional to the quantity of living parasites. The fluorescence intensity of each well suspension is measured by the fluorometer and provides the active concentration that reduces the parasite population by 50% (IC_{50}) (Scheme 22). The IC_{50} can also be evaluated by the *Plasmodium* lactate dehydrogenase (pLDH) enzyme-linked immunosorbent (ELISA)-based assay [213], flow cytometric measurement using propidium iodide (PI) staining, antibodies, ^{3}H-hypoxanthine incorporation assay, or indirectly by microscopic evaluation of parasitemia. [214]

Apart from the evaluation of new drugs, parasitaemia quantification methods are also used as diagnostic tools to detect parasitic infections. Gold standard techniques such as blood smears, immunodiagnostics and polymerase chain reactions are reliable for malaria diagnosis. However, they face several technical problems, including low sensitivity and difficult implementation. In this context, the fluorescence-linked immunosorbent assay (FLISA), a more efficient method than the enzyme-linked immunosorbent assay (ELISA), may offer new promise for the high throughput and sensitive analysis of malaria infections.

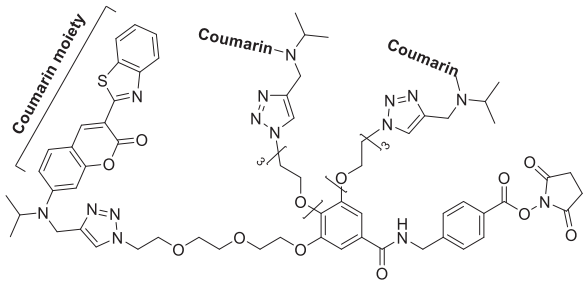

Fig. 35. A Coumarin-conjugated dendrimer **38** for the diagnosis of Plasmodium infection.

While in the ELISA approach, the antigen-antibody interaction is detected by a colorimetric reaction between a substrate and an enzyme, conjugated to an antibody, FLISA uses an antibody coupled to a fluorescent probe. The antigen-antibody interaction is then detected by simply monitoring the fluorescence intensity. To improve this signal, Park and coworkers showed that the triple coumarin-conjugated dendrimer **38** acted as an efficient labelling fluorophore with appropriate spectroscopic properties for the FLISA assay, and thus contributed to increase the detectability of malaria antigens in the early stage of the infection (Fig. 35). [215,216]

5.1.3. Hemolysis assay

Hemolysis is the ability for a molecule to destroy healthy red blood cells. This effect causes metabolic damage and reduces cell lifetime leading to anemia and other serious pathological conditions. The hemolysis assay evaluates hemoglobin release in the plasma and gives a percentage value of hemolysis, related to the concentration of drugs that induces red blood cell lysis compared to untreated controls. [217,218] Independently from cytotoxicity assays, hemolysis assays must be performed to ensure that new polymeric DDS do not display any hemolytic activity. Although the outbreak of the parasite (pRBCs) would be stopped, the destruction of healthy RBCs would cause anaemia. Although it is the only way to identify a lysis effect on healthy RBCs (cytotoxicity assays evaluate disruption of proliferation processes of adherent cells that do not include red blood cells), hemolysis assays are unfortunately not systematically accomplished in the reported DDS studies. [219]

Drug-loaded DDS solutions of different concentrations are added to well-plates or test-tubes containing a suspension of fresh red blood cells (RBCs) in a phosphate buffer saline solution (PBS) (Fig. 36). After the appropriate incubation time, the supernatant containing the potentially released haemoglobin is analyzed by UV/VIS spectrometry (absorption wavelength of the haemoglobin: 540 nm). The hemolysis index corresponds to the measure of the redness of the supernatant: redness is almost exclusively due to the presence of haemoglobin released by the rupture of the red blood cell membrane upon hemolysis. The percentage of hemolysis is calculated following Eq. 7 where A is the absorbance. A sample with a percentage higher than 5% is considered as hemolytic. In the few studies where they have been carried out, the *in vitro* hemolysis assays of the new antimalarial nanocarriers on red blood cells generally indicated low hemolysis effects (<5% *vs* hemolytic control), confirming the good biocompatibility of the DDS.

$$\%of\ hemolysis = \frac{(Asample - Anegative)}{(Apositive - Anegative)} \quad x \quad 100 \tag{7}$$

5.2. Cellular localization and specificity of action towards parasite-infected red blood cells

After (or in parallel to) routine *in vitro* evaluations of drug-delivery systems, more-specific techniques are used to determine important biological parameters and explore the behavior of the drug-loaded DDS in biological environments. Knowledge of the mechanisms of action and the potential target(s) of a new drug-delivery systems is a prerequisite to any marketing. Not only do these studies shed light on the therapeutic effect but they also reveal the possible side effects directly related to the interactions of the DDS with its site of action. For instance, antimalarial mechanistic studies mainly consist in evaluating the specificity of action of antimalarial DDS for parasite-infected red blood cells (pRBCs) compared to non-infected cells. Several techniques can be used to study this specificity that often require fluorescent-labeled polymers.

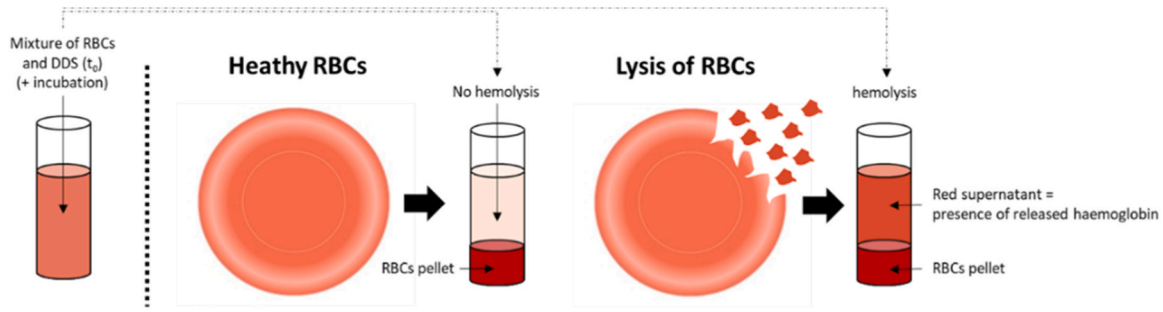

Fig. 36. Hemolysis effect on RBCs.

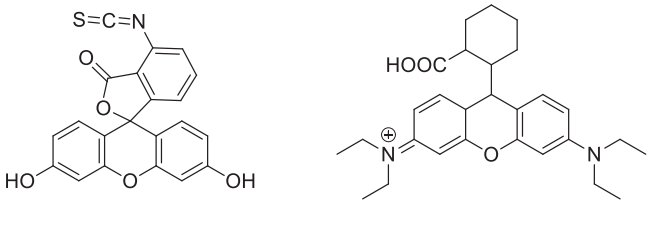

Fig. 37. Common dyes used for the labelling of polymeric DDS.

5.2.1. Fluorescent-labelling methods commonly used to study DDS

The labelling of functional groups on the surface of polymers has been become a very useful tool for biological studies. The most commonly used fluorescent dyes for the detection of polymers by confocal microscopy are fluorescein isothiocyanate (FITC, green-fluorescence, λ_{ex}= 490 and λ_{em}= 525 nm, detection by Argon laser) and the Rhodamine B derivatives (Rho, red-fluorescence, λ_{ex}= 540 and λ_{em}= 625 nm, detection by red diode laser) (Fig. 37).

For DDS with tensioactive behavior, the hydrophobic probe is often encapsulated as a co-drug inside the matrix thanks to electrostatic interactions, or more rarely, conjugated to it. In the case of polymer-drug conjugates (PDC), the probe is generally covalently linked to the polymer backbone. The conjugation of the polymer and the fluorescent dye mainly occurs through 1) the addition of an amino chain-end (-NH_2) or more rarely, an alcohol (-OH) group on the isothiocyanate group (-NCS) of the FITC, or 2) by esterification reaction with a COOH-FITC or Rho dyes. Other methods include azide–alkyne cycloadditions between a polymer containing an azide chain-end (-N_3) and an alkyne group present on the fluorescein (or vice-versa).

In the case of malaria, it is also necessary to label both the red blood cell membranes and the parasite. The red blood cell membranes are generally stained with red-fluorescent germ agglutinin–tetramethylrhodamine conjugate dye (λ_{ex}= 555 and λ_{em}= 580 nm, detection by red diode laser) while the parasitic DNA is generally stained with blue-fluorescent intercalating agents like 4′,6-diamidino-2-phenylindole ((DAPI, λ_{ex}= 350 and λ_{em}= 470 nm) or Hoechst dyes (λ_{ex}= 352 and λ_{em}= 461 nm), detection by UV diode lasers). Other labelling methods consist in the use of naturally fluorescing materials, quantum dots, or isotope labelling. These fluorescent-labelled drug-loaded DDS and materials are then used in the different techniques described below.

5.2.2. Confocal microscopy

Confocal microscopy, also known as confocal laser scanning microscopy (CLSM) or laser confocal scanning microscopy (LCSM), is a fluorescence imaging technique considered as an essential tool in biological research. [220] This technique enables high-speed multidimensional imaging (1 second to generate a 1-megapixel image) such as the three, four or five-dimensional (3D/4D/5D) imaging of labelled-biological samples. A laser beam is focused on a sample where it excites the fluorescent molecules. The fluorescence emitted by the excited labelled-polymers is then collected by the instrument. The technique consists in selectively collecting the fluorescence signals from different planes inside a sample and assembling these planar images to generate the final multidimensional images. Scanning mirrors are used to sweep the laser beam across the sample, generating an image pixel by pixel.

Confocal microscopes offer a more modest resolution than usual epifluorescence microscopes, but generate high-contrast images through optical sectioning. With a high-resolution objective lens, a confocal microscope can generate optical sections thinner than 1 μm without having to physically slice the sample. This allows a very precise quantification of the intensities and investigation of the spatial arrangement of fluorescent labelled-polymers, which is useful for assigning their localizations to specific cellular compartments or assessing the colocalization of different DDS. CLSM is also compatible with living systems (cells and animals) and allows the determination of live imaging (dynamic cellular and molecular processes). [221]

Nevertheless, this powerful technique is limited by the substantial cost of the equipment and the analysis, the poor number of excitation wavelengths available with lasers and the possible damage caused by the high-intensity lasers to living samples. Although lasers commonly used in confocal microscopy produce lines in the ultraviolet, visible, and near-infrared area of the spectrum, the wavelengths of these spectral lines do not always coincide with the maximal absorption wavelength of popular fluorophores.

In the case of malarial infection, confocal microscopy is primary used to localize the *Plasmodium* parasite in infected red blood cells [222] or hepatocytes, [223] as well to characterize its sporozoites forms [224, 225] and the parasite organelles. It has also been used to study host-pathogen interactions. [226,227] For antimalarial DDS biological studies, confocal microscopy has solved issues about the specificity of action of DDS towards pRBCs *versus* RBCs. For instance, FITC-labelled polymeric poly(amido-amines) (FITC-PAAs), such as FITC-**6** and **7** were incubated with a co-culture of living *P. falciparum* 3D7 or blood freshly extracted from *P. yoelii*-infected mice.[96] The fluorescence images obtained by confocal microscopy showed specific interactions of the PAAs with certain pRBCs, depending on the development stages of the parasite (merozoites, rings, trophozoites or schizonts) (Fig. 38). Indeed, the fluorescence of FITC-**7** was only observed inside the advanced pRBCs forms (column C). On the overlay of images (D), it can be observed that FITC-**7** was only present in trophozoite and schizont forms and close to the plasmodium DNA (lines 1 and 2). FITC-**7** was not detected in the ring-pRBCs stages (C:3). In addition, the *in vitro* images of FITC-**6** in *P. yoelii* revealed an interesting binding of the PAA with the merozoite forms (in blue) which are not yet inside the RBCs (D:4). These results opened attractive possibilities for these PAAs as selective drug carriers for malaria therapy.

The fluorescence of FITC-labelled PAAs has also been directly investigated in female mosquitoes (Fig. 39).[96] In order to study DDS distribution and viability on the mosquito body, FITC-**5** was incorporated in their sugar meal at different times. Females were then

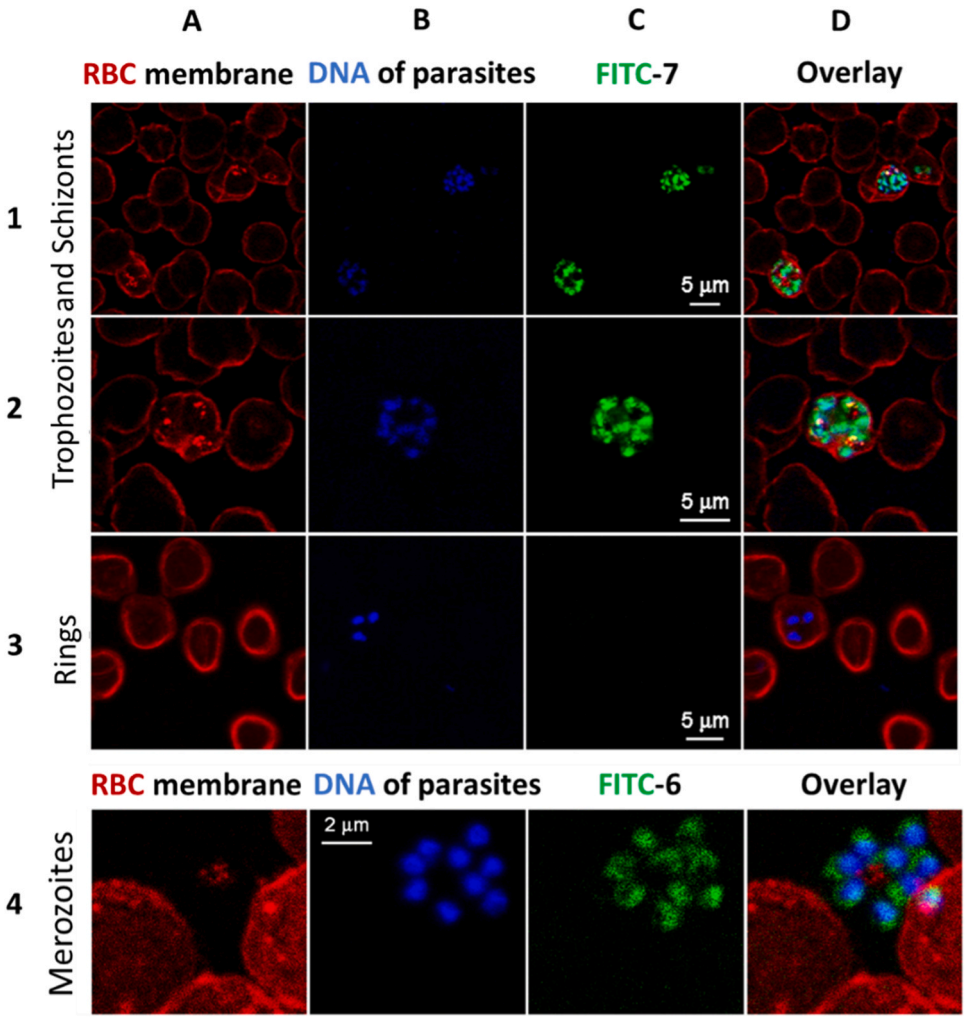

Fig. 38. Confocal microscopy images of FITC-labelled PAAs **6** and **7** in RBs/pRBCs co-culture. A: red fluorescence: RBCs and pRBCs; B: blue fluorescence: parasite DNA; C: green fluorescence: PAAs; D: the overlay represents the superposition of these three images (A-C).
(a) (Reproduced from ref. [95] with permission from Elsevier).

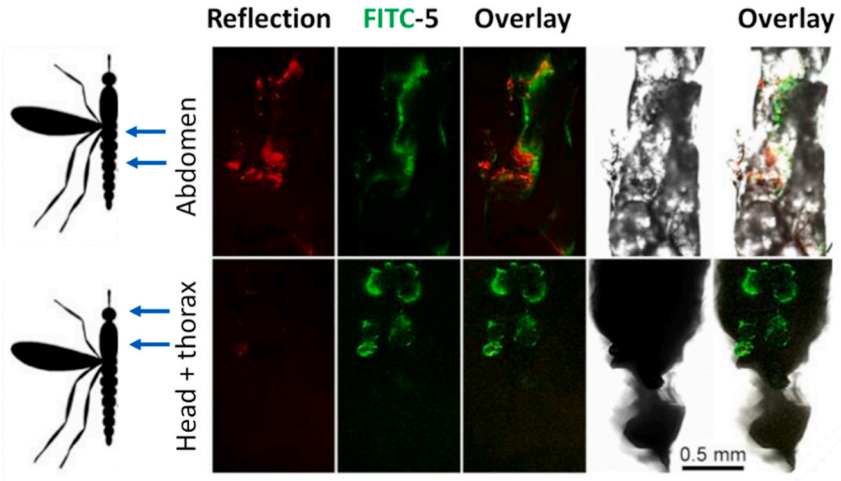

Fig. 39. Living fluorescent microscopy in female mosquito and histological distribution of FITC-labelled PAA **5**.
(Reproduced from ref. [96] with permission from MDPI).

immobilized alive on a microscope slide for confocal analysis. Labelled-polymer fluorescence (green) was detected one day after ingestion in the insect gut (line 1) and three days post-feeding in the thorax, near the head and in the vicinity of the salivary glands (line 2). Preliminary data obtained after feeding indicated that the polymers were non-toxic for the mosquitos, not immediately excreted and had a

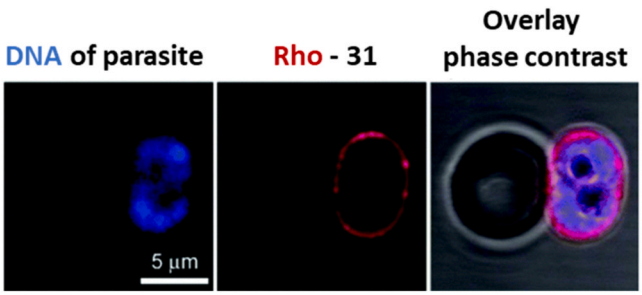

Fig. 40. (a) Confocal microscopy of Rho-DHP-bMPA dendrimer 31. (Reproduced from ref. [183] with permission from the Royal Society of Chemistry).

long residence time in the midgut of both species. These results suggest that encapsulated antimalarial drugs could be delivered directly to anopheles to combat malaria on all fronts.

Finally, confocal fluorescence microscopy for the cellular targeting of the Rho-DHP-bMPA dendrimer **31** [184] revealed interactions between the Rho-dendrimer (in red) and the pRBC plasma membrane (negative contrast), as well as with intraerythrocytic parasites (in blue) (Fig. 40). Given that no polymer fluorescence was detected in the healthy RBCs cytosol and early ring forms, the authors suggested a specific binding of DHP-bMPA to *Plasmodium falciparum* antigens, absent in the early stages of the infection.

5.2.3. Flow cytometry - Fluorescence-activated cell sorting (FACS)

Fluorescence-activated cell sorting (FACS) belongs to the flow cytometry techniques which can be used to detect, count, and rapidly sort a heterogeneous mixture of biological cells into homogeneous subpopulations of interest. [228,229] It can also determine the cycle, the proliferation, the phenotype or even the viability of the analysed cells. FACS allows the purification of individual cells based on their sizes (by the forward-scattered light method) and their internal structure, complexity and granulometry (by the side-scattered light method). This is a technique of choice to obtain a very high purity of cell populations of a specific phenotype. Especially if the targeted cell population expresses a very low level of the identifying marker or when cell populations require separation based on differential marker density. FACS is the only purification method capable to isolate cells based on internal staining or intracellular protein expression. Flow cytometry is also a powerful and versatile tool providing simultaneous multiparametric analysis of the physical, biological, and chemical characteristics of up to thousands of particles per second.

In the examples below (Fig. 41 and Fig. 42), the different cell types are separated according to their fluorescent characteristics. Cell sorting by the flow cytometer is then based on the specific light-scattering and fluorescent characteristics of each stained cell. Negative selection of unstained cells is also possible. The cells, stained with fluorescent antibodies or makers (Section 4.2.1), are placed in a stream of liquid which passes the focus of a laser light beam. The fluorescence detection system can thus detect the specific light emitted and collect the cells according to their fluorescence parameters. In these cases, co-cultures of pRBCs

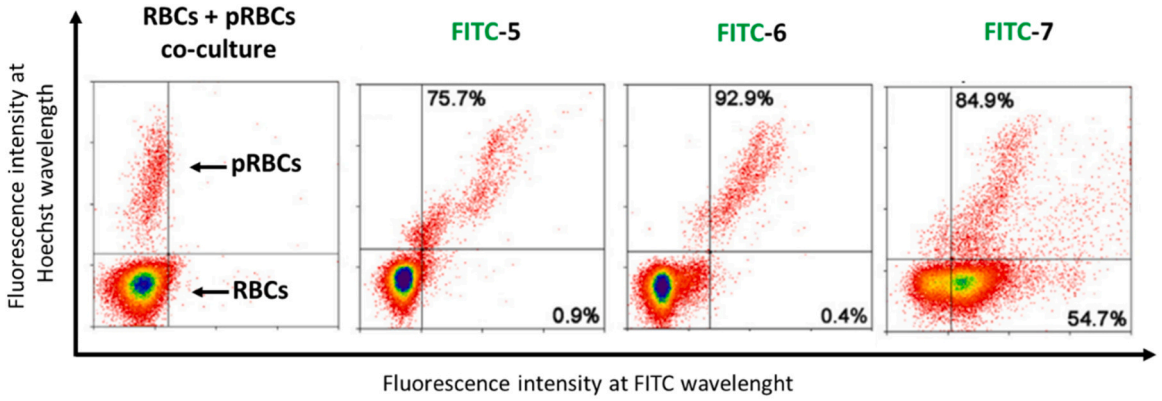

Fig. 41. FACS spectrums of FITC-PAAs with RBCs/pRBCs co-culture. The upper fluorescence is associated to pRBCs and the lower fluorescence to the RBCs populations. (*Reproduced from ref.* 95 *with permission from Elsevier*).

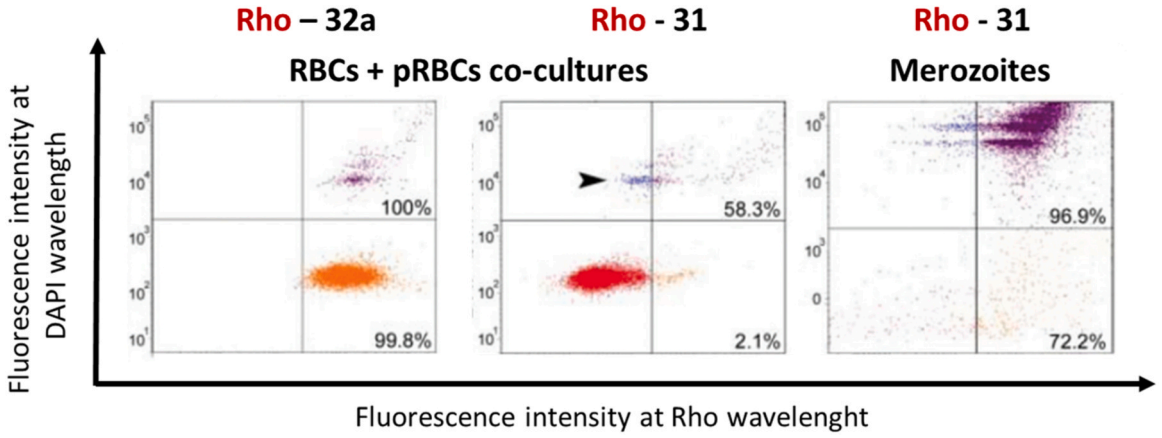

Fig. 42. FACS spectrums of Rho-dendrimers **31** and **32a** with RBCs/pRBCs co-culture and merozoite forms. The upper fluorescence is associated to pRBCs and the lower fluorescence to the RBCs populations.
(a) (Reproduced from ref. [183] with permission from the Royal Society of Chemistry).

and RBCs was subjected to Hoechst or DAPI as fluorescent agents, capable of intercalating within the parasitic DNA (only present in pRBCs). Hence, a high fluorescence intensity (vertical axis) is detected for Hoechst- or DAPI-labelled parasited pRBCs that are shifted to the upper left of the graph (Fig. 41). While no fluorescence intensity is detected for DNA-free healthy RBC that stay in the lower left part. In parallel, the studied DDS were also labelled but with a fluorescent marker of a different wavelength (FITC or Rho), whose intensity is plotted along the horizontal axis. Merging of both fluorescent detections, by multi-angle scattered light methods, allows to identify specific interactions between the fluorescent-labelled nanoparticles and each type of cell (pRBCs and RBCs). Hence, if the labelled nanoparticles interact with RBCs, the spots of these healthy cells will be shifted to higher fluorescence intensities along the x-axis only (detection of only FTIC (or Rho) fluorescence). If the labelled nanoparticles interact with pRBCs, the spots of these parasited cells will be shifted to higher fluorescence intensities along the x- and y-axes (detection of Hoechst (or DAPI) and FITC (or Rho) fluorescence). These graphical shifts are converted into percentage values.

For instance, FITC-labelled PAAs **5** and **6** exhibited a selectivity towards pRBCs (76 or 93% of shift for these cells, respectively) and no significant binding to healthy RBCs (<1% of shift) (Fig. 41).[95] On the other hand, FITC-labelled PAA **7** displayed interactions with both parasited and healthy red blood cells (85 and 55% of shift, respectively). Thanks to their higher affinity for pRBCs and lower cytotoxicity on RBCs, PAAs **5** and **6** thus appeared to be more promising antimalarial DDS than **7**.

In Fig. 42, FACS analysis of dendrimers **31** and **32a** also revealed a better specificity toward pRBCs for Rho-labeled DHP-bMPA pluronic dendrimer **31** (58%) compared to HDLDBC-bGMPA dendrimer **32a**, which highly interacted with both RBCs and pRBCs (≈100% in both case). FACS is also indicated to determine the specificity and the interactions of the DDS with the different stages of parasite forms. For instance, in addition to specificity for pRBCs, DHP-bMPA dendrimer **31** exhibited a specific interaction with the merozoite stage (97%).[183]

5.2.4. *Transmission electron microscopy (TEM) for biological aspects*

The TEM technique previously described (Section 3.2.2) can also be used to study the cellular localization of dye-labelled DDS in pRBCs co-culture, generally *via* immune-staining. Labelled polymers are incubated in presence of pRBCs prior to fixation process and experiment. Fig. 43 represents zoomed TEM images of pRBCs. Both PAAs **6** and **7**, visible as black spots, are localized in the pRBCs cytosol (c) and also inside the area enclosed by the parasitophorous vacuole membrane (PVM). During the cell invasion, the parasite forms this PVM membrane using a portion of the host cell membrane. The PVM surrounds the intracellular parasite, creating a distinct plasma membrane bubble, filled with cytosol (c) inside the host cell.

This newly formed cytosol serves mainly as proteins storage for the parasite before their transport to the parasite's food vacuole for degradation into nutrients. Interestingly, PAA-**6** is more abundant in the pRBCs cytosol than beyond the PVM whereas the opposite is observed for PAA-**7**. These different localizations may imply distinct mechanisms of action for these two DDS. Non-infected RBCs controls showed no intracellular staining thus confirming the selectivity towards pRBCs.

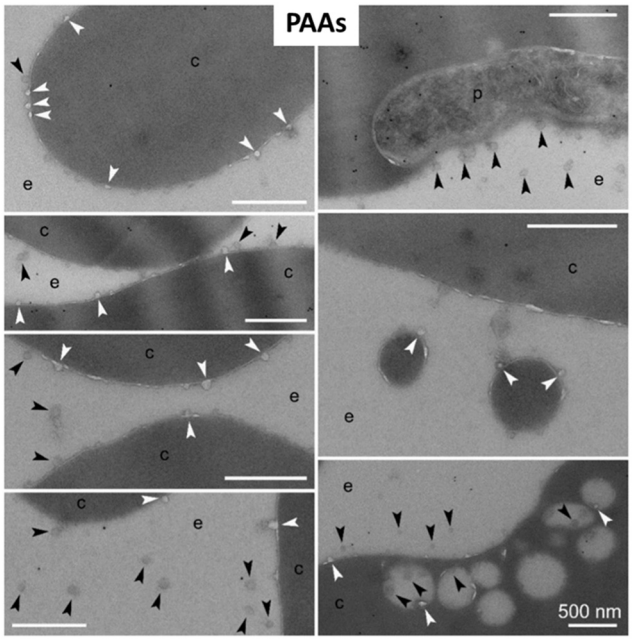

Fig. 44. Immuno-TEM images of RBCs/pRBCs co-culture in presence of PAAs (white arrowheads: PAAs in the process of budding from or merging with RBCs and black arrowheads: vesicles which were not merged to pRBCs membrane). (a) (Reproduced from ref. [96] with permission from MDPI).

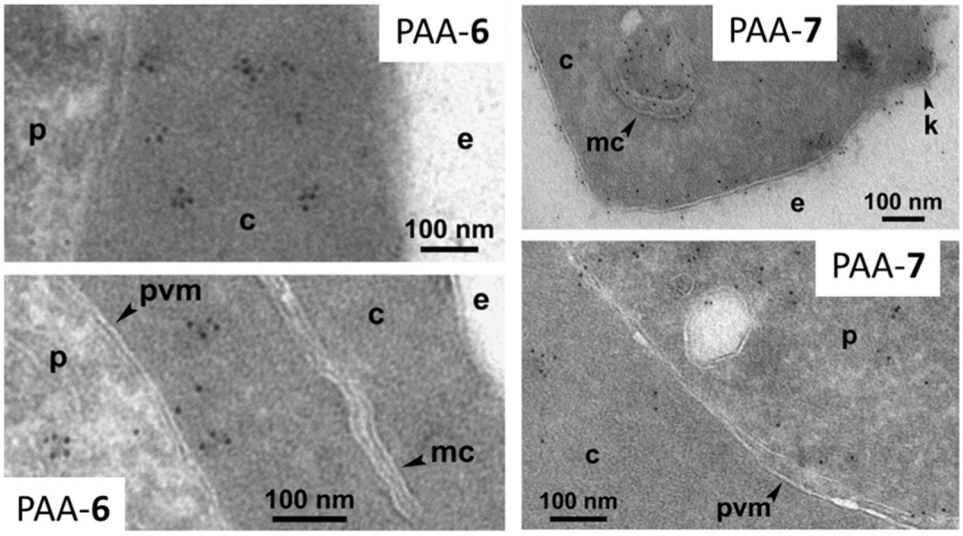

Fig. 43. TEM images of labelled-PAAs **6** and **7** in RBCs/pRBCs co-culture. PAAs are represented by black points. (p: parasite; c: cytosol; e: exracellular domain, mc: mitochondria, pvm: parasitophorous vacuole membrane).
(Reproduced from ref. [95] with permission from Elsevier).

[95]

Xavier Fernàndez-Busquets and co-workers also realized an *in vitro* immuno-TEM experiment using pRBC specific monoclonal antibodies (anti-rabbit IgG coupled to 12-nm colloidal gold particles).[96] White arrowheads point toward particles in the process of budding from or merging with pRBCs, while black arrowheads point at vesicles which were not merged to pRBC membrane (Fig. 44). The fact that PAA polymers penetrated pRBCs and colocalized with the intracellular pathogen raises the possibility of using PAAs for the delivery of drugs directly to the parasite or as transfection vectors for *Plasmodium* genetic engineering. Moreover, immuno-TEM showed that inside the pRBCs, the polymers were not surrounded by a lipid bilayer, suggesting a membrane crossing mechanism not based on the formation of endocytic vesicles. The differences observed in their intracellular distribution also suggest different mechanism of entry for both PAAs (including exomembrane system or cytoadhesion events). Thus, pRBCs have different morphological, physicochemical, and rheological characteristics [71, 230] resulting in widely altered functional properties which allow them higher membrane fluidity and permeability, adhesiveness, and protein trafficking activity. Increased permeability has been established for the low molecular mass solutes[72] (such as with the NPP channels) as well as proteins [231] with which PAAs shares some features, such as a polyelectrolyte zwitterionic nature, which could explain these different input mechanisms observed in immuno-TEM images.

These localization techniques have clearly provided evidence that pRBCs have pores in their membrane favouring the specific entry of nanovectors, since they were found within the parasite. These channels, possible candidates for the new permeability pathways (NPPs) are known to be permeable to charged solutes and have diameters compatible with the entry of most of the reported nanovectors. However, there is still a substantial gap in knowledge of the operation mode of such NPPs. Efforts are underway to elucidate the mechanism and specificity of action of these antimalarial nanovectors.

6. Conclusion

The aim of this review was to provide a detailed how-to guide through the early stages of the discovery of new drug-loaded nanocarriers. Once the lead DDS is identified, the long process of development will obviously continue with pharmacokinetic and *in vivo* studies before any evaluation in clinical trials. The versatility and complexity of engineered polymeric nanotechnologies required the development of specific techniques of synthesis, physicochemical characterizations, or biological evaluations, each of them involving in-depth knowledge of diverse scientific fields. Hence, this review first covered the main synthetic strategies that chemists use to prepare polymeric drug-delivery systems and to conjugate or encapsulate a drug. The synthesis of polymeric backbones usually relies on classical (co-)polymerization reactions such as ring-opening polymerizations, while drug conjugation is mainly realized through simple esterification reactions. However, many of these methodologies still involve using toxic metals such as tin or copper complexes. The therapeutic purposes of these medicinal products call for the development of more sustainable and biocompatible approaches. More controlled synthetic strategies will also be necessary to obtain macromolecular systems with more homogeneous sizes. A clear-cut trend is emerging in the choice of drug encapsulation method: nanoprecipitation and thin film methods are usually preferred for micelles, while the oil-in-water or dialysis methods are used for dendrimers. These methods are well mastered leading to high drug-loadings. The second part of this review presented some fundamental techniques of physicochemical characterization, made possible by the use of state-of-the-art devices. These analytic studies are inescapable to obtain precious information such as the size, shape, and surface morphology of the nanoparticles. Sizes and shapes can greatly vary from one system to the other, obviously depending on the molecular structure, but also on the method of preparation or drug loading. It should be noted that most DDS studied herein presented negative surface charges. Techniques for the analysis of polymeric structures are rapidly evolving and will certainly overcome the last technical barriers to the determination of even more accurate parameters in the foreseeable future. Finally, the most typical assays for the biological evaluation of polymeric vectors and the advanced techniques used to study their mechanism of action were described. Although complex to set up, these techniques are essential to understand the specificity of action and localize the drug-loaded nanocarrier in the biological environment. Through the different sections, the implementation of these various physicochemical and biological strategies was highlighted through concrete examples of antimalarial drug-loaded macromolecular vectors. The advantages of the nanoparticles were not only measured in terms of increased drug activities, but more importantly for in terms of their impact on the high reduction of associated toxicities and on the targeted drug-release. Such improvements were made possible thanks to the specific crossing of permeability pathways, leading to the selective targeting of parasite-infected red blood cells. A still pending question would be on the long-term effect of these nanocarriers on the resistance mechanisms of the parasite against antimalarial treatments. All the DDS vectorized antimalarial drugs on the market are known to cause resistance. The next move might be to adapt these nanocarriers to the vectorization of new drug candidates with ground-breaking mechanism of actions. The mode of administration (oral delivery instead of intravenous) and the cost of production of these nanoformulations, intended for developing countries where malaria is rife are also major obstacles that must be taken into considerations in the future developments.

Declaration of Competing Interest

The authors declare that they have no known competing financial interests or personal relationships that could have appeared to influence the work reported in this paper.

Acknowledgements

The Agence Nationale de la Recherche is gratefully acknowledged for the JCJC ANR grant “iPOD” (17-CE07-000101). Aix-Marseille Université (AMU) and the Centre National de la Recherche Scientifique (CNRS) are acknowledged for financial support. M.C. thanks the College Doctoral of Aix-Marseille University for her inter-doctoral PhD grant. We gratefully acknowledge Dr Anne Rodallec and Dr Marion Rollet for valuable discussions.

References

[1] K.K. Jain, An overview of drug delivery systems, Methods Mol. Biol. 2059 (2020) 1–54, https://doi.org/10.1007/978-1-4939-9798-5_1.
[2] R. Haag, F. Kratz, Polymer therapeutics: concepts and applications, Angew. Chem. Int. Ed. 45 (2006) 1198–1215, https://doi.org/10.1002/anie.200502113.
[3] W.H. De Jong, P.J.A. Borm, Drug delivery and nanoparticles: applications and hazards, Int. J. Nanomed. 3 (2008) 133–149, https://doi.org/10.2147/ijn.s596.
[4] G. Tiwari, R. Tiwari, B. Sriwastawa, L. Bhati, S. Pandey, P. Pandey, S. K. Bannerjee, Drug delivery systems: An updated review, Int. J. Pharm. Investig. 2 (2012) 2–11, https://doi.org/10.4103/2230-973x.96920.
[5] A.M. Vargason, A.C. Anselmo, S. Mitragotri, The evolution of commercial drug delivery technologies, Nat. Biomed. Eng. 5 (2021) 951–967, https://doi.org/10.1038/s41551-021-00698-w.
[6] H. Abdelkader, Z. Fathalla, A. Seyfoddin, M. Farahani, T. Thrimawithana, A. Allahham, A.W.G. Alani, A.A. Al-Kinani, R.G. Alany, Polymeric long-acting drug delivery systems (LADDS) for treatment of chronic diseases: Inserts, patches, wafers, and implants, Adv. Drug Deliv. Rev. 177 (2021) 113957, https://doi.org/10.1016/j.addr.2021.113957.
[7] D. Hwang, J.D. Ramsey, A.V. Kabanov, Polymeric micelles for the delivery of poorly soluble drugs: From nanoformulation to clinical approval, Adv. Drug Deliv. Rev. 156 (2020) 80–118, https://doi.org/10.1016/j.addr.2020.09.009.
[8] A.C. Anselmo, S. Mitragotri, Nanoparticles in the clinic: An update, Bioeng. Transl. Med. 4 (2019) e10143, https://doi.org/10.1002/btm2.10143.
[9] S. Rajeswari, T. Prasanthi, N. Sudha, R. Prasad Swain, S. Panda, V. Goka, Natural polymers: a recent review, World J. Pharm. Pharm. Sci. 6 (2017) 472–494, https://doi.org/10.20959/wjpps20178-9762.

[10] A.C.Q. Silva, A.J.D. Silvestre, C. Vilela, C.S.R. Freire, Natural Polymers-Based Materials: A Contribution to a Greener Future, Molecules 27 (2022) 94–118, https://doi.org/10.3390/molecules27010094.
[11] A. Haider, S. Khan, D. Najaf Iqbal, M. Shrahili, S. Haider, K. Mohammad, A. Mohammad, M. Rizwan, Q. Kanwal, G. Mustafa, Advances in chitosan-based drug delivery systems: A comprehensive review for therapeutic applications, Eur. Polym. J. 210 (2024) 112983, https://doi.org/10.1016/j.eurpolymj.2024.112983.
[12] M. Rial-Hermida, A. Rey-Rico, B. Blanco-Fernandez, N. Carballo-Pedrares, E. M. Byrne, J.F. Mano, Recent progress on polysaccharide-based hydrogels for controlled delivery of therapeutic biomolecules, ACS Biomater. Sci. Eng. 7 (2021) 4102–4127, https://doi.org/10.1021/acsbiomaterials.0c01784.
[13] K. Jung, N. Corrigan, E.H.H. Wong, C. Boyer, Bioactive Synthetic Polymers, Adv. Mater. 34 (2022) 2105063, https://doi.org/10.1002/adma.202105063.
[14] M. Sai Bhargava Reddy, D. Ponnamma, R. Choudhary, K. Kumar Sadasivuni, A comparative review of natural and synthetic biopolymer composite scaffolds, Polymers 13 (2021) 1105–1156, https://doi.org/10.3390/polym13071105.
[15] Y.K. Sung, S.W. Kim, Recent advances in polymeric drug delivery systems, Biomater. Res. 24 (2020) 12, https://doi.org/10.1186/s40824-020-00190-7.
[16] X. Yang, Y. Xie, Recent advances in polymeric core-shell nanocarriers for targeted delivery of chemotherapeutic drugs, Int. J. Pharm. 608 (2021) 121094, https://doi.org/10.1016/j.ijpharm.2021.121094.
[17] L. Xu, X. Wang, Y. Liu, G. Yang, R.J. Falconer, C.X. Zhao, Lipid Nanoparticles for Drug Delivery, Adv. NanoBiomed. Res. 2 (2022) 2100109, https://doi.org/10.1002/anbr.202100109.
[18] J. Vikas, K. Hitesh, C. Pallavi, J. Sourabh, S. Preethi, Lipid-based nanocarriers as drug delivery system and its applications, in: D. Vivek, G. Nikita, S. Srija (Eds.), Introduction to the fundamentals, Nanopharmaceutical Advanced Delivery Systems, Scrivener Publishing LLC, Beverly, 2021, pp. 3–30, https://doi.org/10.1002/9781119711698.ch1.
[19] A.H.A. Zubair, S.M. Sheshe, M.R. Bashir, S.M. Sade, Lipid based drug delivery system: a review, J. Appl. Life Sci. Int. 24 (2021) 33–46, https://doi.org/10.9734/jalsi/2021/v24i330228.
[20] K. HarishKumar, N. Venkatesh, H. Bhowmik, A. Kuila, Metallic Nanoparticle: A Review, Biomed. J. Sci. Tech. Res. 4 (2018) 3765–3775, https://doi.org/10.26717/BJSTR.2018.04.0001011.
[21] V. Chandrakala, V. Aruna, G. Angajala, Review on metal nanoparticles as nanocarriers: current challenges and perspectives in drug delivery systems, Emergent Mater. 5 (2022) 1593–1615, https://doi.org/10.1007/s42247-021-00335-x.
[22] S. Haque, S. Tripathy, C. Ranjan Patra, Manganese-based advanced nanoparticles for biomedical applications: future opportunity and challenges, Nanoscale 13 (2021) 16405–16426, https://doi.org/10.1039/d1nr04964j.
[23] S. Anjum, M. Hashim, S.Asad Malik, M. Khan, J.M. Lorenzo, B.Haider Abbasi, C. Hano, Recent Advances in Zinc Oxide Nanoparticles (ZnO NPs) for Cancer Diagnosis, Target Drug Delivery, and Treatment, Cancers (Basel) 13 (2021) 4570–4601, https://doi.org/10.3390/cancers13184570.
[24] I. Vroman, L. Tighzert, Biodegradable polymers, Materials 2 (2009) 307–344, https://doi.org/10.3390/ma2020307.
[25] U. Arif, S. Haider, A. Haider, N. Khan, A.A. Alghyamah, N. Jamila, M.Imran Khan, W.A. Almasry, I.K. Kang, Biocompatible polymers and their potential biomedical applications: a review, Curr. Pharm. Des. 25 (2019) 3608–3619, https://doi.org/10.2174/1381612825999191011105148.
[26] S. Mura, J. Nicolas, P. Couvreur, Stimuli-responsive nanocarriers for drug delivery, Nat. Mater. 12 (2013) 991–1003, https://doi.org/10.1038/nmat3776.
[27] H.Yu Yang, Y. Li, D. Sung Lee, Multifunctional and Stimuli-Responsive Magnetic Nanoparticle-Based Delivery Systems for Biomedical Applications, Adv. Ther. 1 (2018) 1800011, https://doi.org/10.1002/adtp.201800011.
[28] Y. Sun, E. Davis, Nanoplatforms for targeted stimuli-responsive drug delivery: a review of platform materials and stimuli-responsive release and targeting mechanisms, Nanomaterials 11 (2021) 746–846, https://doi.org/10.3390/nano11030746.
[29] X. Pang, Y. Jiang, Q. Xiao, A.W. Leung, H. Hua, C. Xu, pH-responsive polymer-drug conjugates: Design and progress, J. Control. Release 222 (2016) 116–129, https://doi.org/10.1016/j.jconrel.2015.12.024.
[30] M.T. Manzari, Y. Shamay, H. Kiguchi, N. Rosen, M. Scaltriti, D.A. Heller, Targeted drug delivery strategies for precision medicines, Nat. Rev. Mater. 6 (2021) 351–370, https://doi.org/10.1038/s41578-020-00269-6.
[31] K. Paunovska, D. Loughrey, J.E. Dahlman, Drug delivery systems for RNA therapeutics, Nat. Rev. Genet. 23 (2022) 265–280, https://doi.org/10.1038/s41576-021-00439-4.
[32] S. Kandula, P. Kumar Singh, G. Anit Kaur, A. Tiwari, Trends in smart drug delivery systems for targeting cancer cells, J. Mater. Sci. Eng., B. 297 (2023) 116816, https://doi.org/10.1016/j.mseb.2023.116816.
[33] Y. Sun, D. Chen, Y. Pan, W. Qu, H. Hao, X. Wang, Z. Liu, S. Xie, Nanoparticles for antiparasitic drug delivery, Drug Deliv. 26 (2019) 1206–1221, https://doi.org/10.1080/10717544.2019.1692968.
[34] T. Nakamura, N. Isoda, Y. Sakoda, H. Harashima, Strategies for fighting pandemic virus infections: Integration of virology and drug delivery, J. Control. Release 343 (2022) 361–378, https://doi.org/10.1016/j.jconrel.2022.01.046.
[35] W.Y. Jeong, M. Kwon, H.E. Choi, K.S. Kim, Recent advances in transdermal drug delivery systems: a review, Biomater. Res 25 (2021) 24–39, https://doi.org/10.1186/s40824-021-00226-6.
[36] J. Kaur, G. Singh Gill, K. Bedi, Applications of carbon nanotubes in drug delivery: A comprehensive review, in: P. Scrimin, L. Baltzer (Eds.), Model systems, Current Opinion in Chemical Biology, Elsevier B.V., London, 2019, pp. 674–679, https://doi.org/10.1016/B978-0-12-814031-4.00005-2.
[37] A. Corey, A. Stevens, K. Kaur, H.A. Klok, Self-assembly of protein-polymer conjugates for drug delivery, Adv. Drug Deliv. Rev. 174 (2021) 447–460, https://doi.org/10.1016/j.addr.2021.05.002.
[38] G. Liu, L. Yang, G. Chen, F. Xu, F. Yang, H. Yu, L. Li, X. Dong, J. Han, C. Cao, J. Qi, J. Su, X. Xu, X. Li, B. Li, A Review on drug delivery system for tumor therapy, Front. Pharmacol. 12 (2021) 735446, https://doi.org/10.3389/fphar.2021.735446.
[39] Y. Yao, Y. Zhou, L. Liu, Y. Xu, Q. Chen, Y. Wang, S. Wu, Y. Deng, J. Zhang, A. Shao, Nanoparticle-Based Drug Delivery in cancer therapy and its role in overcoming drug resistance, Front. Mol. Biosci. 7 (2020) 193, https://doi.org/10.3389/fmolb.2020.00193.
[40] A. Aghebati-Maleki, S. Dolati, M. Ahmadi, A. Baghbanzhadeh, M. Asadi, A. Fotouhi, M. Yousefi, L. Aghebati-Maleki, Nanoparticles and cancer therapy: Perspectives for application of nanoparticles in the treatment of cancers, J. Cell. Physiol. 235 (2020) 1962–1972, https://doi.org/10.1002/jcp.29126.
[41] A.R. Kirtane, M. Verma, P. Karandikar, J. Furin, R. Langer, G. Traverso, Nanotechnology approaches for global infectious diseases, Nat. Nanotechnol. 16 (2021) 369–384, https://doi.org/10.1038/s41565-021-00866-8.
[42] B. Loretz, Y.K. Oh, S. Hudson, Z. Gu, C.M. Lehr, Drug delivery for fighting infectious diseases: a global perspective, Drug Deliv. Transl. Res. 11 (2021) 1316–1322, https://doi.org/10.1007/s13346-021-01009-1.
[43] B.A. Aderibigbe, Polymeric therapeutic delivery systems for the treatment of infectious diseases, Ther. Deliv. 8 (2017) 557–576, https://doi.org/10.4155/tde-2017-0008.
[44] M. Salouti, A. Ahangari, Nanoparticle based drug delivery systems for treatment of infectious diseases, in: A. Demir Sezer (Ed.), Application of nanotechnology in drug delivery, InTech, London, 2014, pp. 155–192, https://doi.org/10.5772/58423.
[45] H. Rashidzadeh, S.J. Tabatabaei Rezaei, S. Masih Adyani, M. Abazari, S. Rahamooz Haghighi, H. Abdollahi, A. Ramazani, Recent advances in targeting malaria with nanotechnology-based drug carriers, Pharm. Dev. Technol. 26 (2021) 807–823, https://doi.org/10.1080/10837450.2021.1948568.
[46] L.N. Borgheti-Cardoso, M. San Anselmo, E. Lantero, A. Lancelot, J.L. Serrano, S. Hernández-Ainsa, X. Fernàndez-Busquets, T. Sierra, Promising nanomaterials in the fight against malaria, J. Mater. Chem. B. 8 (2020) 9428–9448, https://doi.org/10.1039/d0tb01398f.
[47] Z. Mhlwatika, B.Atim Aderibigbe, Polymeric Nanocarriers for the Delivery of Antimalarials, Molecules 23 (2018) 2527–2532, https://doi.org/10.3390%2Fmolecules23102527.
[48] S. Mvango, W.M.R. Matshe, A.O. Balogun, L.A. Pilcher, M.O. Balogun, Nanomedicines for Malaria Chemotherapy: Encapsulation vs. Polymer Therapeutics, Pharm. Res. 35 (2018) 237–264, https://doi.org/10.1007/s11095-018-2517-z.
[49] P. Urbán, X. Fernàndez-Busquets, Nanomedicine against malaria, Curr. Med. Chem. 21 (2014) 605–629, https://doi.org/10.2174/09298673113206660292.
[50] N.S. Santos-Magalhães, V.C. Furtado Mosqueira, Nanotechnology applied to the treatment of malaria, Adv. Drug Deliv. Rev. 62 (2010) 560–575, https://doi.org/10.1016/j.addr.2009.11.024.
[51] World Health Organization, Geneva, 2024. Licence: CC BY-NC-SA 3.0 IGO. ⟨https://www.who.int/publications/i/item/9789240090149⟩, 2024 (accessed 23 April 2024).
[52] World malaria report 2023. Geneva: World Health Organization; 2023. Licence: CC BY-NC-SA 3.0 IGO. ⟨https://www.who.int/publications/i/item/9789240086173⟩, 2023 (accessed 30 November 2023).
[53] World malaria report 2005, ⟨https://www.who.int/publications/i/item/9241593199⟩. 2005 (accessed 18 November 2005).
[54] L. Tilley, M.W.A. Dixon, K. Kirk, The Plasmodium falciparum-infected red blood cell, Int. J. Biochem. Cell. Biol. 43 (2011) 839–842, https://doi.org/10.1016/j.biocel.2011.03.012.
[55] World Health Organization, Guidelines for the Treatment of Malaria, 3rd edition, WHO Press, Geneva, Switzerland, 2015. ⟨https://iris.who.int/handle/10665/162441⟩ (accessed April 2015).
[56] M. Chinappi, A. Via, P. Marcatili, A. Tramontano, On the mechanism of chloroquine resistance in Plasmodium falciparum, PLOS One 19 (2010) 14064, https://doi.org/10.1371/journal.pone.0014064.
[57] E. Guantai, K. Chibale, Chloroquine resistance: proposed mechanisms and countermeasures, Curr. Drug Deliv. 7 (2010) 312–323, https://doi.org/10.2174/156720110793360577.
[58] C. Coban, The host targeting effect of chloroquine in malaria, Curr. Opin. Immunol. 66 (2020) 98–107, https://doi.org/10.1016/j.coi.2020.07.005.
[59] K.N. Olafson, M.A. Ketchum, J.D. Rimer, P.G. Vekilov, Mechanisms of hematin crystallization and inhibition by the antimalarial drug chloroquine, Proc. Natl. Acad. Sci. U. S. A. 112 (2015) 4946–4951, https://doi.org/10.1073/pnas.1501023112.
[60] K. Rishikesh, K. Saravu, Primaquine treatment and relapse in Plasmodium vivax malaria, Pathog. Glob. Health 110 (2016) 1–8, https://doi.org/10.1080/20477724.2015.1133033.
[61] A. Wångdahl, K. Sondén, K. Wyss, C. Stenström, D. Björklund, J. Zhang, H. Hervius Askling, C. Carlander, U. Hellgren, A. Färnert, Relapse of plasmodium vivax and plasmodium ovale malaria with and without primaquine treatment in a nonendemic area, Clin. Infect. Dis. 74 (2022) 1199–1207, https://doi.org/10.1093/cid/ciab610.

[62] A. Nzila, The past, present and future of antifolates in the treatment of Plasmodium falciparum infection, J. Antimicrob. Chemother. 57 (2006) 1043–1054, https://doi.org/10.1093/jac/dkl104.

[63] C. Nsanzabana, Resistance to Artemisinin Combination Therapies (ACTs): Do Not Forget the Partner Drug!, Trop. Med. Infect. Dis. 4 (2019) 26–37, https://doi.org/10.3390/tropicalmed4010026.

[64] L. Cui, X.Z. Su, Discovery, mechanisms of action and combination therapy of artemisinin, Expert Rev. Anti Infect. Ther. 7 (2009) 999–1013, https://doi.org/10.1586/eri.09.68.

[65] J.L. Bridgford, S.C. Xie, S.A. Cobbold, C.Flerida A. Pasaje, S. Herrmann, T. Yang, D.L. Gillett, L.R. Dick, S.A. Ralph, C. Dogovski, N.J. Spillman, L. Tilley, Artemisinin kills malaria parasites by damaging proteins and inhibiting the proteasome, Nat. Commun. 9 (2018) 3801, https://doi.org/10.1038/s41467-018-06221-1.

[66] FDA-Approved Drugs, New Drug Application (NDA): 022268, 2009. ⟨https://www.accessdata.fda.gov/drugsatfda_docs/nda/2009/022268s000TOC.cfm⟩, 2009 (Accessed 8 July 2009).

[67] K.R. Stover, S. Travis King, J. Robinson, Artemether-lumefantrine: an option for malaria, Ann. Pharmacother. 46 (2012) 567–577, https://doi.org/10.1345/aph.1q539.

[68] K. Kümpornsin, D. Loesbanluechai, C. de Cozar, N. Kotanan, K. Chotivanich, N. J. White, P. Wilairat, M.G. Gomez-Lorenzo, F. Javier Gamo, L. Maria Sanz, M.C. S. Lee, T. Chookajorn, Lumefantrine attenuates Plasmodium falciparum artemisinin resistance during the early ring stage, Int. J. Parasitol. Drugs Drug Resist. 17 (2021) 186–190, https://doi.org/10.1016/j.ijpddr.2021.09.005.

[69] M.M. Plucinski, P.R. Dimbu, A.P. Macaia, C.M. Ferreira, C. Samutondo, J. Quivinja, M. Afonso, R. Kiniffo, E. Mbounga, J.S. Kelley, D.S. Patel, Y. He, E. Talundzic, D.O. Garrett, E.S. Halsey, V. Udhayakumar, P. Ringwald, F. Fortes, Efficacy of artemether–lumefantrine, artesunate–amodiaquine, and dihydroartemisinin–piperaquine for treatment of uncomplicated Plasmodium falciparum malaria in Angola, 2015, Malar. J. 16 (2017) 62–72, https://doi.org/10.1186/s12936-017-1712-4.

[70] P.M. Glassman, V.R. Muzykantov, Pharmacokinetic and pharmacodynamic properties of drug delivery systems, J. Pharmacol. Exp. Ther. 370 (2019) 570–580, https://doi.org/10.1124/jpet.119.257113.

[71] K. Kirk, Membrane transport in the malaria-infected erythrocyte, Physiol. Rev. 81 (2001) 495–537, https://doi.org/10.1152/physrev.2001.81.2.495.

[72] I.D. Goodyer, B. Pouvelle, T.G. Schneider, D.P. Trelka, T.F. Taraschi, Characterization of macromolecular transport pathways in malaria-infected erythrocytes, Mol. Biochem. Parasitol. 87 (1997) 13–28, https://doi.org/10.1016/s0166-6851(97)00039-x.

[73] B. Pouvelle, R. Spiegel, L. Hsiao, R.J. Howard, R.L. Morris, A.P. Thomas, T. F. Taraschi, Direct access to serum macromolecules by intraerythrocytic malaria parasites, Nature 353 (1991) 73–78, https://doi.org/10.1038/353073a0.

[74] G.A. Biagini, S.A. Ward, P.G. Bray, Malaria parasite transporters as a drug-delivery strategy, Trends Parasitol. 21 (2005) 299–301, https://doi.org/10.1016/j.pt.2005.05.013.

[75] A. Dadwal, A. Garg, B. Kumar, R.K. Narang, N. Mishra, Polymer-drug conjugates: Origins, progress to date, and future directions, in: S.P. Vyas, U. Agrawal, R. Sharma (Eds.), Concept, Design and Therapeutic Applications, Smart Polymeric Nano-Constructs in Drug Delivery, Elsevier B.V., Amsterdam, 2023, pp. 221–248, https://doi.org/10.1016/B978-0-323-91248-8.00015-5.

[76] H. Ringsdorf, Structure and properties of pharmacologically active polymers, Polym. Sci. Polym. Symp. 51 (2007) 135–153, https://doi.org/10.1002/polc.5070510111.

[77] N. Larson, H. Ghandehari, Polymeric conjugates for drug delivery, Chem. Mater. 24 (2012) 840–853, https://doi.org/10.1021/cm2031569.

[78] J.P. Patil, H.S. Mahajan, R.C. Patel, A review on polymer drug conjugate – what, why and how ? Int. J. Pharm. Sci. Res. 6 (2015) 4611–4621, https://doi.org/10.13040/IJPSR.0975-8232.6(11).4611-21.

[79] M. Chang, F. Zhang, T. Wei, T. Zuo, Y. Guan, G. Lin, W. Shao, Smart linkers in polymer-drug conjugates for tumor-targeted delivery, J. Drug Target. 24 (2016) 475–491, https://doi.org/10.3109/1061186x.2015.1108324.

[80] G. Odian. Principles of polymerization, Principles of Polymerization, Fourth Edition, John Wiley & Sons, Inc., Toronto, 2004, pp. 544–618, https://doi.org/10.1002/047147875X.

[81] O. Nuyken, S.D. Pask, Ring-Opening Polymerization—An Introductory Review, Polymers 5 (2013) 361–403, https://doi.org/10.3390/polym5020361.

[82] D. Sharma, L. Lipp, S. Arora, J. Singh, Diblock and triblock copolymers of polylactide and polyglycolide, in: V. Grumezescu, A. Mihai Grumezescu (Eds.), Thermoset and Thermoplastic Polymers, Materials for Biomedical Engineering, Elsevier, Amsterdam, 2019, pp. 449–477, https://doi.org/10.1016/B978-0-12-816874-5.00013-X.

[83] K. Knop, R. Hoogenboom, D. Fischer, U.S. Schubert, Poly(ethylene glycol) in drug delivery: pros and cons as well as potential alternatives, Ang. Chem. Int. Ed. 49 (2010) 6288–6308, https://doi.org/10.1002/anie.200902672.

[84] T. Kopac, Protein corona, understanding the nanoparticle–protein interactions and future perspectives: A critical review, Int. J. Biol. Macomol. 169 (2021) 290–301, https://doi.org/10.1016/j.ijbiomac.2020.12.108.

[85] F. Barbero, L. Russo, M. Vitali, J. Piella, I. Salvo, M.L. Borrajo, M. Busquets-Fité, R. Grandori, N.G. Bastús, E. Casals, V. Puntes, Formation of the protein corona: the interface between nanoparticles and the immune System, Semin. Immunol. 34 (2017) 52–60, https://doi.org/10.1016/j.smim.2017.10.001.

[86] G. Caracciolo, O.C. Farokhzad, M. Mahmoudi, Biological identity of nanoparticles in vivo: clinical implications of the protein corona, Trends Biotechnol. 35 (2017) 257–264, https://doi.org/10.1016/j.tibtech.2016.08.011.

[87] A. Jain, S.K. Jain, PEGylation: an approach for drug delivery. A review, Crit. Rev. Ther. Drug Carr. Syst. 25 (2008) 403–447, https://doi.org/10.1615/critrevtherdrugcarriersyst.v25.i5.10.

[88] J. Soo Suk, Q. Xu, N. Kim, J. Hanes, L.M. Ensign, PEGylation as a strategy for improving nanoparticle-based drug and gene delivery, Adv. Drug Deliv. Rev. 99 (2016) 28–51, https://doi.org/10.1016/j.addr.2015.09.012.

[89] B. Pidhatika, M. Rodenstein, Y. Chen, E. Rakhmatullina, A. Mühlebach, C. Acikgöz, M. Textor, R. Konradi, Comparative Stability Studies of Poly(2-methyl-2-oxazoline) and Poly(ethylene glycol) Brush Coatings, Biointerphases 7 (2012) 1–15, https://doi.org/10.1007/s13758-011-0001-y.

[90] G. Caracciolo, Artificial protein coronas: directing nanoparticles to targets, Trends Pharmacol. Sci. 45 (2024) 602–613, https://doi.org/10.1016/j.tips.2024.05.003.

[91] Z. Zhang, J. Guan, Z. Jiang, Y. Yang, J. Liu, W. Hua, Y. Mao, C. Li, W. Lu, J. Qian, C. Zhan, Brain-targeted drug delivery by manipulating protein corona functions, Nat. Comm. 10 (2019) e3561, https://doi.org/10.1038/s41467-019-11593-z.

[92] B.A. Aderibigbe, Z. Mhlwatika, M. Nwamadi, M.O. Balogun, W.M.R. Matshe, Synthesis, characterization and in vitro analysis of polymer-based conjugates containing dihydrofolate reductase inhibitors, J. Drug Deliv. Sci. Technol. 50 (2019) 388–401, https://doi.org/10.1016/j.jddst.2019.01.038.

[93] Y. Zhang, S. Merali, S.R. Meshnick, p-Aminobenzoic acid transport by normal and Plasmodium falciparum-infected erythrocytes, Mol. Biochem. 52 (1992) 185–194, https://doi.org/10.1016/0166-6851(92)90051-k.

[94] Metal-based compounds such as the 1,2-diaminocyclohexane platinum DACH-Pt, were reported as promising antimalarial drugs and may proceed through interaction with heme and inhibition of the β-hematin formation M. Navarro, W. Castro, M. Madamet, R. Amalvict, N. Benoit, B. Pradines, Metal-chloroquine derivatives as possible anti-malarial drugs: evaluation of anti-malarial activity and mode of action, Malar. J. 13 (2014) 471, https://doi.org/10.1186/1475-2875-13-471.

[95] P. Urbán, J.J. Valle-Delgado, N. Mauro, J. Marques, A. Manfredi, M. Rottmann, E. Ranucci, P. Ferruti, X. Fernàndez-Busquets, Use of poly(amidoamine) drug conjugates for the delivery of antimalarials to Plasmodium, J. Control. Release 177 (2014) 84–95, https://doi.org/10.1016/j.jconrel.2013.12.032.

[96] E. Martí Coma-Cros, A. Biosca, J. Marques, L. Carol, P. Urbán, D. Berenguer, M. C. Riera, M. Delves, R.E. Sinden, J.J. Valle-Delgado, L. Spanos, I. Siden-Kiamos, P. Pérez, K. Paaijmans, M. Rottmann, A. Manfredi, P. Ferruti, E. Ranucci, X. Fernàndez-Busquets, Polyamidoamine Nanoparticles for the Oral Administration of Antimalarial Drugs, Pharmaceutics 10 (2018) 225–245, https://doi.org/10.3390%2Fpharmaceutics10040225.

[97] C. Chauvierre, M.C. Marden, C. Vauthier, D. Labarre, P. Couvreur, L. Leclerc, Heparin coated poly(alkylcyanoacrylate) nanoparticles coupled to hemoglobin: a new oxygen carrier, Biomaterials 25 (2004) 3081–3086, https://doi.org/10.1016/J.BIOMATERIALS.2003.09.097.

[98] M. Ismail, Y. Du, L. Ling, X. Li, Artesunate-heparin conjugate based nanocapsules with improved pharmacokinetics to combat malaria, Int. J. Pharm. 562 (2019) 162–171, https://doi.org/10.1016/j.ijpharm.2019.03.031.

[99] PfEMP1 is the main malarial antigenic ligand synthesized during the erythrocytic stages and is responsible for the cytoadherence of the parasite on RBC and thus for the *P. falciparum* virulence.

[100] V.P. Torchilin, Structure and design of polymeric surfactant-based drug delivery systems, J. Control. Release 73 (2001) 137–172, https://doi.org/10.1016/s0168-3659(01)00299-1.

[101] S.R. Croy, G.S. Kwon, Polymeric micelles for drug delivery, Curr. Pharm. Des. 12 (2006) 4669–4684, https://doi.org/10.2174/138161206779026245.

[102] K. Kataoka, A. Harada, Y. Nagasaki, Block copolymer micelles for drug delivery: Design, characterization and biological significance, Adv. Drug Deliv. Rev. 64 (2012) 37–48, https://doi.org/10.1016/j.addr.2012.09.013.

[103] A.S. Patha, T. Patil, P.K. Pandey, K. Kuche, R. Ghadi, S. Jain, Block copolymer micelles as long-circulating drug vehicles, in: S.P. Vyas, U. Agrawal, R. Sharma (Eds.), Concept, Design and Therapeutic Applications, Smart Polymeric Nano-Constructs in Drug Delivery, Elsevier B.V., Amsterdam, 2023, pp. 187–220, https://doi.org/10.1016/B978-0-323-91248-8.00008-8.

[104] R.H. Müller, M. Lück, S. Harnisch, K. Thode, Intravenously Injected Particles, in: U. Häfeli, W. Schütt, J. Teller, M. Zborowski (Eds.), Colloidal carriers for controlled drug delivery and targeting: modification, characterization, and in vivo distribution, Scientific and Clinical Applications of Magnetic Carriers, Springer, Boston MA, 1997, pp. 135–148, https://doi.org/10.1007/978-1-4757-6482-6_10.

[105] V.M. Martín Giménez, G. Arya, I.A. Zucchi, M.J. Galante, W. Manucha, Photo-responsive polymeric nanocarriers for target-specific and controlled drug delivery, Soft Matter 17 (2021) 8577–8584, https://doi.org/10.1039/D1SM00999K.

[106] H. Danafar, K. Rostamizadeh, S. Davaran, M. Hamidi, Drug-conjugated PLA-PEG-PLA copolymers: a novel approach for controlled delivery of hydrophilic drugs by micelle formation, Pharm. Dev. Technol. 22 (2017) 947–957, https://doi.org/10.3109/10837450.2015.1125920.

[107] G. Gaucher, M.H. Dufresne, V.P. Sant, N. Kang, D. Maysinger, J.C. Leroux, Block copolymer micelles: preparation, characterization and application in drug delivery, J. Control. Release 109 (2005) 169–188, https://doi.org/10.1016/j.jconrel.2005.09.034.

[108] A.X. Gao, L. Liao, J.A. Johnson, Synthesis of Acid-Labile PEG and PEG-Doxorubicin-Conjugate Nanoparticles via Brush-First ROMP, ACS Macro Lett. 3 (2014) 854–857, https://doi.org/10.1021/mz5004097.

[109] M.F.F. Francis, M. Cristea, F.M. Winnik, Polymeric micelles for oral drug delivery: Why and how, Pure Appl. Chem. 76 (2004) 1321–1335, https://doi.org/10.1351/pac200476071321.
[110] H. Cabral, K. Kataok, Progress of drug-loaded polymeric micelles into clinical studies, J. Control. Release 190 (2014) 465–476, https://doi.org/10.1016/j.jconrel.2014.06.042.
[111] S.S. Kulthe, Y.M. Choudhari, N.N. Inamdar, V. Mourya, Polymeric micelles: authoritative aspects for drug delivery, Des. Monomers Polym. 15 (2012) 465–521, https://doi.org/10.1080/1385772X.2012.688328.
[112] N. Scholz, T. Behnke, U. Resch-Genger, Determination of the Critical Micelle Concentration of Neutral and Ionic Surfactants with Fluorometry, Conductometry, and Surface Tension-A Method Comparison, J. Fluoresc. 28 (2018) 465–476, https://doi.org/10.1007/s10895-018-2209-4.
[113] M. Perez-Rodriguez, G. Prieto, C. Rega, L.M. Varela, F. Sarmiento, V. Mosquera, A Comparative Study of the Determination of the Critical Micelle Concentration by Conductivity and Dielectric Constant Measurements, Langmuir 14 (1998) 4422–4426, https://doi.org/10.1021/la980296a.
[114] S. Paillet, B. Grassl, J. Desbrieres, Rapid and quantitative determination of critical micelle concentration by automatic continuous mixing and static light scattering, Anal. Chim. Acta 636 (2009) 236–241, https://doi.org/10.1016/j.aca.2009.02.011.
[115] H. Li, D. Hu, F. Liang, X. Huang, Q. Zhu, Influence factors on the critical micelle concentration determination using pyrene as a probe and a simple method of preparing samples, R. Soc. Open Sci. 7 (2020) 192092, https://doi.org/10.1098/rsos.192092.
[116] A. Dominguez, A. Fernandez, N. Gonzalez, E. Iglesias, L. Montenegro, Determination of Critical Micelle Concentration of Some Surfactants by Three Techniques, J. Chem. Educ. 74 (1997) 1227–1231, https://doi.org/10.1021/ed074p1227.
[117] J. Aguiar, P. Carpena, J.A. Molina-Bolivar, C. Carnero Ruiz, On the determination of the critical micelle concentration by the pyrene 1:3 ratio method, J. Colloid Interface Sci. *258* (2003) 116–122, https://doi.org/10.1016/S0021-9797(02)00082-6.
[118] A. Fluksman, O. Benny, A robust method for critical micelle concentration determination using coumarin-6 as a fluorescent probe, Anal. Methods 11 (2019) 3818, https://doi.org/10.1039/C9AY00577C.
[119] S.C. Owen, D.P. Chan, M.S. Shoichet, Polymeric micelle stability, Nano Today 7 (2012) 53–65, https://doi.org/10.1016/j.nantod.2012.01.002.
[120] A. Judefeind, M.M. de Villiers, Drug Loading into and in vitro release from nanosized drug delivery systems, in: M.M. de Villiers, P. Aramwit, G.S. Kwon (Eds.), Nanotechnology in Drug Delivery. Biotechnology: Pharmaceutical Aspects, Springer, New York, 2009, pp. 129–162, https://doi.org/10.1007/978-0-387-77668-2_5.
[121] X. Ke, V. Wee Lin Ng, R.J. Ono, J.M.W. Chan, S. Krishnamurthy, Y. Wang, J. L. Hedrick, Y.Y. Yang, Role of non-covalent and covalent interactions in cargo loading capacity and stability of polymeric micelles, J. Control. Release 193 (2014) 9–26, https://doi.org/10.1016/j.jconrel.2014.06.061.
[122] R. Thipparaboina, R.B. Chavan, D. Kumar, S. Modugula, N.R. Shastri, Micellar carriers for the delivery of multiple therapeutic agents, Colloids Surf. B. 135 (2015) 291–308, https://doi.org/10.1016/j.colsurfb.2015.07.046.
[123] M. Yokoyama, P. Opanasopit, T. Okan, K. Kawano, Y. Maitani, Polymer design and incorporation methods for polymeric micelle carrier system containing water-insoluble anti-cancer agent camptothecin, J. Drug Target. 12 (2004) 373–384, https://doi.org/10.1080/10611860412331285251.
[124] K. Cholkar, A. Patel, A. Dutt Vadlapudi, A.K. Mitra, Novel Nanomicellar Formulation Approaches for Anterior and Posterior Segment Ocular Drug Delivery, Recent Pat. Nanomed. 2 (2012) 82–95, https://doi.org/10.2174/1877912311202020082.
[125] J.D. Robertson, L. Rizzello, M. Avila-Olias, J. Gaitzsch, C. Contini, M.S. Magon, S. A. Renshaw, G. Battaglia, Purification of Nanoparticles by Size and Shape, Sci. Rep. 6 (2016) 27494, https://doi.org/10.1038/srep27494.
[126] M. Yu, W. Yuan, D. Li, A. Schwendeman, S.P. Schwendeman, Predicting drug release kinetics from nanocarriers inside dialysis bags, J. Control. Release 315 (2019) 23–30, https://doi.org/10.1016/j.jconrel.2019.09.016.
[127] C. Shi, Z. Zhang, J. Shi, F. Wang, Y. Luan, Co-delivery of docetaxel and chloroquine via PEO-PPO-PCL/TPGS micelles for overcoming multidrug resistance, *Int. J. Pharm.* 495 (2015) 932–939, https://doi.org/10.1016/j.ijpharm.2015.10.009.
[128] For an overview of recent strategies to increase drug loadings (>10 wt%), seeY. Liu, G. Yang, S. Jin, L. Xu, C.-X. Zhao (Eds.), Development of High-Drug-Loading Nanoparticles, ChemPlusChem 85 (2020) 2143–2157, ⟨https://doi.org/10.1002/cplu.202000496⟩.
[129] S. Shen, Y. Wu, Y. Liu, D. Wu, High drug-loading nanomedicines: progress, current status, and prospects, Int. J. Nanomed. *12* (2017) 4085–4109, https://doi.org/10.2147/ijn.s132780.
[130] M. Callari, P.L. De Souza, A. Rawal, M.H. Stenzel, The Effect of Drug Loading on Micelle Properties: Solid-State NMR as a Tool to Gain Structural Insight, Angew. Chem. Int. Ed. Engl. 56 (2017) 8441–8445, https://doi.org/10.1002/anie.201701471.
[131] Y. Fu, W.J. Kao, Drug release kinetics and transport mechanisms of non-degradable and degradable polymeric delivery systems, Expert Opin. Drug Deliv. 7 (2010) 429–444, https://doi.org/10.1517/17425241003602259.
[132] S. Trombino, F. Curcio, R. Cassano, Polymersomes as a promising vehicle for controlled drug delivery, in: V. Gajbhiye, K.R. Gajbhiye, S. Hong (Eds.), Recent advances in tailor-made therapeutics, Stimuli-Responsive Nanocarriers, Elsevier B.V, 2022, pp. 351–366, https://doi.org/10.1016/B978-0-12-824456-2.00017-5.
[133] J. Liu, M. Yu, C. Zhou, J. Zheng, Renal clearable inorganic nanoparticles: a new frontier of bionanotechnology, Mater. Today 16 (2013) 477–486, https://doi.org/10.1016/j.mattod.2013.11.003.
[134] B. Du, M. Yu, J. Zheng, Transport and interactions of nanoparticles in the kidneys, Nat. Rev. Mater. 3 (2018) 358–374, https://doi.org/10.1038/s41578-018-0038-3.
[135] H. Kheiri Manjili, H. Malvandi, M.S. Mosavi, H. Danafar, Preparation and physicochemical characterization of biodegradable mPEG-PCL core-shell micelles for delivery of artemisinin, Pharm. Sci. 22 (2016) 234–243, https://doi.org/10.15171/PS.2016.37.
[136] A. Villaverde, Nanoparticles in Translational Science and Medicine, in: A. Villaverde (Ed.), Progress in molecular biology and translational science, Elsevier B.V, Amsterdam, 2011, pp. 1–615. ISBN: 978-0-12-416020-0.
[137] A.G. Maier, B.M. Cooke, A.F. Cowman, L. Tilley, Malaria parasite proteins that remodel the host erythrocyte, Nat. Rev. Microbiol. 7 (2009) 341–354, https://doi.org/10.1038/nrmicro2110.
[138] A. Ramazani, M. Keramati, H. Malvandi, H. Danafar, H. Kheiri Manjili, Preparation and in vivo evaluation of anti-plasmodial properties of artemisinin-loaded PCL–PEG–PCL nanoparticles, Pharm. Dev. Technol. 23 (2017) 911–920, https://doi.org/10.1080/10837450.2017.1372781.
[139] M. Möller, K. Matyjaszewski. Polymer Science: A Comprehensive Reference, 1st Edition, Elsevier, London, 2012. ISBN: 978-0-444-53349-4.
[140] H. Nosrati, P. Barzegari, H. Danafar, H. Kheiri Manjili, Biotin-functionalized copolymeric PEG-PCL micelles for in vivo tumour-targeted delivery of artemisinin, *Artif. Cells Nanomed. Biotechnol.* 47 (2019) 104–114, https://doi.org/10.1080/21691401.2018.1543199.
[141] A. Najer, D. Wu, M.G. Nussbaumer, G. Schwertz, A. Schwab, M.C. Witschel, A. Schäfer, F. Diederich, M. Rottmann, C.G. Palivan, H.P. Beckb, W. Meier, An amphiphilic graft copolymer-based nanoparticle platform for reduction-responsive anticancer and antimalarial drug delivery, Nanoscale 8 (2016) 14858–14869, https://doi.org/10.1039/c6nr04290b.
[142] D. Kasozi, F. Mohring, S. Rahlfs, A.J. Meyer, K. Becker, Real-time imaging of the intracellular glutathione redox potential in the malaria parasite plasmodium falciparum, PLOS Pathog. 9 (2013) 1003782, https://doi.org/10.1371/journal.ppat.1003782.
[143] L. Fortuin, M. Leshabane, R. Pfukwa, D. Coertzen, L.M. Birkholtz, B. Klumperman, Facile Route to Targeted, biodegradable polymeric prodrugs for the delivery of combination therapy for malaria, ACS Biomater. Sci. Eng. 6 (2020) 6217–6227, https://doi.org/10.1021/acsbiomaterials.0c01234.
[144] S. Perrier, 50th Anniversary Perspective: RAFT polymerization—a user guide, Macromolecules 50 (2017) 7433–7447, https://doi.org/10.1021/acs.macromol.7b00767.
[145] D.J. Keddie, G. Moa, E. Rizzardo, S.H. Thang, RAFT Agent design and synthesis, Macromolecules 45 (2012) 5321–5342, https://doi.org/10.1021/ma300410v.
[146] K. Eda, S. Eda, I.W. Sherman, Identification of peptides targeting the surface of Plasmodium falciparum-infected erythrocytes using a phage display peptide library, Am. J. Trop. Med. Hyg. 71 (2004) 190–195, https://doi.org/10.4269/ajtmh.2004.71.190.
[147] D.A. Tomalia, J.M.J. Fréchet, Discovery of dendrimers and dendritic polymers: a brief historical perspective, J. Polym. Sci., Polym. Chem. Ed. 40 (2002) 2719–2728, https://doi.org/10.1002/pola.10301.
[148] F. Vogtle, G. Richardt, N. Werner, Dendrimer Chemistry: Concepts, Synthesis, Properties, Applications, Wiley-VCH Verlag GmbH & Co. KGaA, Weinheim, 2009. ISBN: 978-3-527-62695-3.
[149] D.A. Tomalia, J.B. Christensen, U. Boas, Dendrimers, Dendrons, and Dendritic Polymers: Discovery, Applications, and the Future, Cambridge University Press, Cambridge, 2012, https://doi.org/10.1017/CBO9781139048859.
[150] D.A. Tomalia, A.M. Naylor, W.A. Goddard, Starburst Dendrimers: Molecular-Level Control of Size, Shape, Surface Chemistry, Topology, and Flexibility from Atoms to Macroscopic Matter, Angew. Chem. Int. Ed. 29 (1990) 138–175, https://doi.org/10.1002/anie.199001381.
[151] A.-M. Caminade, C.-O. Turrin, Dendrimers for drug delivery, J. Mater. Chem. B 2 (2014) 4055–4066, https://doi.org/10.1039/C4TB00171K.
[152] J. Pan, S.A. Attia, N. Filipczak, V.P. Torchilin, Dendrimers for drug delivery purposes, in: M. Mozafari (Ed.), Nanoengineered Biomaterials for Advanced Drug Delivery, Elsevier, Amsterdam, 2020, pp. 201–242, https://doi.org/10.1016/B978-0-08-102985-5.00010-3.
[153] A.P. Sherje, M. Jadhav, B.R. Dravyakar, D. Kadam, Dendrimers: a versatile nanocarrier for drug delivery and targeting, Int. J. Pharm. 548 (2018) 707–720, https://doi.org/10.1016/j.ijpharm.2018.07.030.
[154] H. Kobayashi, N.W. Brechbiel, Dendrimer-based macromolecular MRI contrast agents: characteristics and application, Mol. Imaging 2 (2005) 1–10, https://doi.org/10.1162/15353500200303100.
[155] R.J. Sarode, H.S. Mahajan, Dendrimers for drug delivery: an overview of its classes, synthesis, and applications, J. Drug Deliv. Sci. Technol. 98 (2024) 105896, https://doi.org/10.1016/j.jddst.2024.105896.
[156] A.-M. Caminade, Dendrimers, an emerging opportunity in personalized medicine? J. Pers. Med. 12 (2022) 1334, https://doi.org/10.3390/jpm12081334.
[157] S. Svenson, The dendrimer paradox—High medical expectations but poor clinical translation, Chem. Soc. Rev. 44 (2015) 4131–4144, https://doi.org/10.1039/C5CS00288E.
[158] S.M. Grayson, J.M. Frechet, Convergent dendrons and dendrimers: from synthesis to applications, Chem. Rev. 101 (2001) 3819–3868, https://doi.org/10.1021/cr990116h.
[159] J. Sebestik, M. Reinis, J. Jezek, Synthesis of Dendrimers: Convergent and Divergent Approaches. in: Biomedical Applications of Peptide-, Glyco- and

Glycopeptide Dendrimers, and Analogous Dendrimeric Structures, Springer-Verlag, Vienna, 2012, pp. 55–81, https://doi.org/10.1007/978-3-7091-1206-9_6.
[160] F. Najafi, M. Salami-Kalajahi, H. Roghani-Mamaqani, Janus-type dendrimers: synthesis, properties, and applications, J. Mol. Liq. 347 (2022) 118396, https://doi.org/10.1016/j.molliq.2021.118396.
[161] A.M. Caminade, D. Yanc, D.K. Smith, Dendrimers and hyperbranched polymers, Chem. Soc. Rev. 44 (2015) 3870–3873, https://doi.org/10.1039/C5CS90049B.
[162] J. Sebestik, M. Reinis, J. Jezek, Purification and Characterization of Dendrimers. in: Biomedical Applications of Peptide-, Glyco- and Glycopeptide Dendrimers, and Analogous Dendrimeric Structures, Springer-Verlag, Vienna, 2012, pp. 83–92, https://doi.org/10.1007/978-3-7091-1206-9_7.
[163] D.G. Mullen, A. Desai, M.A. van Dongen, M. Barash, J.R. Baker Jr, M.M. Banaszak Holl, Best practices for purification and characterization of PAMAM dendrimer, Macromolecules 45 (2012) 5316–5320, https://doi.org/10.1021/ma300485p.
[164] A. Krupkova, M. Müllerova, R. Petrickovic, T. Strašák, On the edge between organic solvent nanofiltration and ultrafiltration: Characterization of regenerated cellulose membrane with aspect on dendrimer purification and recycling, Sep. Purif. 310 (2023) 123141, https://doi.org/10.1016/j.seppur.2023.123141.
[165] J.T. Rundel, B.K. Paul, V.T. Remcho, Organic solvent nanofiltration for microfluidic purification of poly (amidoamine) dendrimers, J. Chromatogr. A. 1162 (2007) 167–174, https://doi.org/10.1016/j.chroma.2007.06.042.
[166] M.V. Walter, M. Malkoch, Simplifying the synthesis of dendrimers: accelerated approaches, Chem. Soc. Rev. 41 (2012) 4593–4609, https://doi.org/10.1039/c2cs35062a.
[167] K.L. Wooley, C.J. Hawker, J. Frechet, Hyperbranched macromolecules via a novel double-stage convergent growth approach, J. Am. Chem. Soc. 113 (1991) 4252–4261, https://doi.org/10.1021/JA00011A031.
[168] T. Kawaguchi, K.L. Walker, C.L. Wilkins, J.S. Moore, Double exponential dendrimer growth, J. Am. Chem. Soc. 117 (1995) 2159–2165. ⟨https://pubs.acs.org/doi/10.1021/ja00113a005⟩.
[169] M. Arseneault, C. Wafer, J.F. Morin, Recent advances in click chemistry applied to dendrimer synthesis, Molecules 20 (2015) 9263–9294, https://doi.org/10.3390/molecules20059263.
[170] P. Wu, A.K. Feldman, A.K. Nugent, C.J. Hawker, A. Scheel, B. Voit, J. Pyun, J.M. J. Frechet, K.B. Sharpless, V.V. Fokin, Efficiency and fidelity in a click-chemistry route to triazole dendrimers by the copper(i)-catalyzed ligation of azides and alkynes, Angew. Chem. Int. Ed. 43 (2004) 3928–3932, https://doi.org/10.1002/anie.200454078.
[171] Z. Lyu, L. Ding, A.Y.T. Huang, L. Kao, L. Peng, Poly(amidoamine) dendrimers: covalent and supramolecular synthesis, Mater 13 (2019) 34–48, https://doi.org/10.1016/j.mtchem.2019.04.004.
[172] D.A. Tomalia, H. Baker, J. Dewald, M. Hall, G. Kallos, S. Martin, J. Roeck, J. Ryder, P. Smith, A new class of polymers: starburst-dendritic macromolecules, Polym. J. 17 (1985) 117–132, https://doi.org/10.1295/polymj.17.117.
[173] Z. Lyu, L. Ding, A. Tintaru, L. Peng, Self-assembling supramolecular dendrimers for biomedical applications: lessons learned from poly(amidoamine) dendrimers, Acc. Chem. Res 53 (2020) 2936–2949, https://doi.org/10.1021/acs.accounts.0c00589.
[174] J. Wagner, M. Dillenburger, J. Simon, J. Oberländer, K. Landfester, V. Mailänder, D.Y.W. Ng, K. Müllen, T. Weil, Amphiphilic dendrimers control protein binding and corona formation on liposome nanocarriers, *Chem. Commun.* 56 (2020) 8663–8666, https://doi.org/10.1039/D0CC02486D.
[175] Y. Zou, Y. Sun, Y. Wang, D. Zhang, H. Yang, X. Wang, M. Zheng, B. Shi, 2023. Cancer cell-mitochondria hybrid membrane coated Gboxin loaded nanomedicines for glioblastoma treatment, Nat. Commun. 14 (2023) e4557 https://doi.org/10.1038%2Fs41467-023-40280-3.
[176] R. Duncan, L. Izzo, Dendrimer biocompatibility and toxicity, Adv. Drug Deliv. 57 (2005) 2215–2237, https://doi.org/10.1016/j.addr.2005.09.019.
[177] A. Gothwal, S. Malik, U. Gupta, N.K. Jain, Toxicity and biocompatibility aspects of dendrimers, in: A. Chauhan, H. Kulhari (Eds.), Micro and Nano Technologies, Pharmaceutical Applications of Dendrimers, Elsevier B.V., Amsterdam, 2020, pp. 251–274, https://doi.org/10.1016/B978-0-12-814527-2.00011-1.
[178] R. Kharwade, P. Badole, N. Mahajan, S. More, Toxicity and surface modification of dendrimers: a critical review, Curr. Drug Deliv. 19 (2022) 451–465, https://doi.org/10.2174/1567201818666211021160441.
[179] F. Chen, G. Huang, H. Huang, Sugar ligand-mediated drug delivery, Future Med. Chem. 12 (2020) 161–171, https://doi.org/10.4155/fmc-2019-0114.
[180] D. Bhadra, A.K. Yadav, S. Bhadra, N.K. Jain, Glycodendrimeric nanoparticulate carriers of primaquine phosphate for liver targeting, *Int. J. Pharm.* 295 (2005) 221–233, https://doi.org/10.1016/j.ijpharm.2005.01.026.
[181] P. Agrawal, U. Gupta, N.K. Jain, Glycoconjugated peptide dendrimers-based nanoparticulate system for the delivery of chloroquine phosphate, Biomaterials 28 (2007) 3349–3359, https://doi.org/10.1016/j.biomaterials.2007.04.004.
[182] K. Sadler, J.P. Tam, Peptide dendrimers: applications and synthesis, J. *Biotechnol.* 90 (2002) 195–229, https://doi.org/10.1016/s1389-0352(01)00061-7.
[183] E. Martí Coma-Cros, A. Lancelot, M. San Anselmo, L. Neves Borgheti-Cardoso, J. J. Valle-Delgado, J.L. Serrano, X. Fernàndez-Busquets, T. Sierra, Micelle carriers based on dendritic macromolecules containing bis-MPA and glycine for antimalarial drug delivery, Biomater. Sci. 7 (2019) 1661–1674, https://doi.org/10.1039/C8BM01600C.
[184] A. Lancelot, R. González-Pastor, A. Concellón, T. Sierra, P. Martín-Duque, J. L. Serrano, DNA Transfection to Mesenchymal Stem Cells Using a Novel Type of Pseudodendrimer Based on 2,2-Bis(hydroxymethyl)propionic Acid, Bioconjug. Chem. 28 (2017) 1135–1150, https://doi.org/10.1021/acs.bioconjchem.7b00037.
[185] J. Movellan, P. Urbán, E. Moles, J.M. de la Fuente, T. Sierra, J.L. Serrano, X. Fernàndez-Busquets, Amphiphilic dendritic derivatives as nanocarriers for the targeted delivery of antimalarial drugs, Biomaterials 35 (2014) 7940–7950, https://doi.org/10.1016/j.biomaterials.2014.05.061.
[186] T. Fröhlich, F. Hahn, L. Belmudes, M. Leidenberger, O. Friedrich, B. Kappes, Y. Couté, M. Marschall, S.B. Tsogoeva, Synthesis of Artemisinin-Derived Dimers, Trimers and Dendrimers: Investigation of Their Antimalarial and Antiviral Activities Including Putative Mechanisms of Action, Chem. Eur. J. 24 (2018) 8103–8113, https://doi.org/10.1002/chem.201800729.
[187] A. Paquin, C. Reyes-Moreno, G. Bérubé, Recent advances in the use of the dimerization strategy as a means to increase the biological potential of natural or synthetic molecules, Molecules 26 (2021) 2340–2371, https://doi.org/10.3390/molecules26082340.
[188] D. Chaturvedi, A. Goswami, P.P. Saikia, N.C. Barua, P.G. Rao, Artemisinin and its derivatives: a novel class of anti-malarial and anti-cancer agents, Chem. Soc. Rev. 39 (2010) 435–454, https://doi.org/10.1039/b816679j.
[189] T. Frçhlich, A.C. Karagçz, C. Reiter, S.B. Tsogoeva, Artemisinin-derived dimers: potent antimalarial and anticancer agents, J. Med. Chem. 59 (2016) 7360–7388, https://doi.org/10.1021/acs.jmedchem.5b01380.
[190] G.H. Posner, A.J. McRiner, I.H. Paik, S. Sur, K. Borstnik, S. Xie, T.A. Shapiro, A. Alagbala, B. Foster, Anticancer and antimalarial efficacy and safety of artemisinin-derived trioxane dimers in rodents, J. Med. Chem. 47 (2004) 1299–1301, https://doi.org/10.1021/JM0303711.
[191] K. Saalwächter, Applications of NMR in polymer characterization - an introduction, in: R. Zhang, T. Miyoshi, P. Sun (Eds.), NMR Methods for characterization of synthetic and natural polymers, The Royal Society of Chemistry, London, 2019, pp. 1–22, https://doi.org/10.1039/9781788016483-00001.
[192] D. Le, G. Casano, T. Phan, F. Ziarelli, O. Ouari, F. Aussenac, P. Thureau, G. Mollica, D. Gigmes, P. Tordo, S. Viel, Optimizing sample preparation methods for dynamic nuclear polarization solid-state nmr of synthetic polymers, Macromolecules 47 (2014) 3909–3916, https://doi.org/10.1021/MA500788N.
[193] H. Meng, K. Xu, Y. Xu, P. Luo, F. Du, J. Huang, W. Lu, J. Yu, S. Liu, B. Muir, Nanocapsules based on mPEGylated artesunate prodrug and its cytotoxicity, *Colloids Surf.* B. 115 (2014) 164–169, https://doi.org/10.1016/j.colsurfb.2013.11.039.
[194] D. Berek, Size exclusion chromatography–a blessing and a curse of science and technology of synthetic polymers, J. Sep. Sci. 33 (2010) 315–335, https://doi.org/10.1002/jssc.200900709.
[195] P. Groves, Diffusion ordered spectroscopy (DOSY) as applied to polymers, Polym. Chem. 8 (2017) 6700–6708, https://doi.org/10.1039/C7PY01577A.
[196] S. Bhattacharjee, DLS and zeta potential - what they are and what they are not? J. Control. Release 235 (2016) 337–351, https://doi.org/10.1016/j.jconrel.2016.06.017.
[197] S. Samimi, N. Maghsoudnia Reza, B. Eftekhari, F. Dorkoosh, Lipid-Based Nanoparticles for Drug Delivery Systems, in: S.S. Mohapatra, S. Ranjan, N. Dasgupta, R. Kumar Mishra, S. Thomas (Eds.), Micro and Nano Technologies, Nanoscience and Nanotechnology in Drug Delivery, Characterization and biology of nanomaterials for drug delivery, Elsevier B.V., Amsterdam, 2019, pp. 47–76, https://doi.org/10.1016/C2017-0-00272-0.
[198] V. Selvamani, Stability studies on nanomaterials used in drugs, in: S. S. Mohapatra, S. Ranjan, N. Dasgupta, R. Kumar Mishra, S. Thomas (Eds.), Micro and Nano Technologies, Nanoscience and Nanotechnology in Drug Delivery, Characterization and biology of nanomaterials for drug delivery, Elsevier B.V., Amsterdam, 2019, pp. 425–444, https://doi.org/10.1016/B978-0-12-814031-4.00015-5.
[199] E. Fröhlich, The role of surface charge in cellular uptake and cytotoxicity of medical nanoparticles, Int. J. Nanomed. 7 (2012) 5577–5591, https://doi.org/10.2147/ijn.s36111.
[200] S. Honary, F. Zahir, Effect of Zeta Potential on the Properties of Nano-Drug Delivery Systems - A Review (Part 2), Trop. J. Pharm. Res. 12 (2013) 265–273, https://doi.org/10.4314/TJPR.V12I2.19.
[201] X.Y. Zhang, B.B. Tong, T. Wu, Y.D. Wang, Synthesis and characterization of a novel amphiphilic poly (ethylene glycol)–poly (ε-caprolactone) graft copolymers, Des. Monomers Polym. 19 (2016) 661–668, https://doi.org/10.1080/15685551.2016.1198882.
[202] L.E. Franken, E.J. Boekema, M.C.A. Stuart, Transmission Electron Microscopy as a Tool for the Characterization of Soft Materials: Application and Interpretation, Adv. Sci. 4 (2017) 1600476, https://doi.org/10.1002/advs.201600476.
[203] P.L. Stewart, Cryo-electron microscopy and cryo-electron tomography of nanoparticles, Wiley Interdiscip. Rev. Nanomed. Nanobiotechnol. 9 (2017) 1417, https://doi.org/10.1002/wnan.1417.
[204] U. Maver, T. Maver, Z. Persin, M. Mozetic, A. Vesel, M. Gaberscek, K. Stana-Kleinsche, Polymer characterization with the atomic force microscope, in: F. Yılmaz (Ed.), Polymer Science, InTech, London, 2013, pp. 114–132, https://doi.org/10.5772/51060.
[205] P. Nguyen-Tri, P. Ghassemi, P. Carriere, S. Nanda, A.Amine Assadi, D. Duc Nguyen, Recent Applications of Advanced Atomic Force Microscopy in Polymer Science: A Review, Polymers 12 (2020) 1142–1170, https://doi.org/10.3390/polym12051142.
[206] A.E. Vladár, V.D. Hodoroaba, Characterization of nanoparticles by scanning electron microscopy, in: V.D. Hodoroaba, W.E.S. Unger, A.G. Shard (Eds.), Micro and Nano Technologies, Measurement Processes for Nanoparticles, Characterization of Nanoparticles, Elsevier B.V., Amsterdam, 2020, pp. 7–27, https://doi.org/10.1016/B978-0-12-814182-3.00002-X.

[207] S. Moraes Silva, R. Tavallaie, L. Sandiford, R.D. Tilley, J. Justin Gooding, Gold coated magnetic nanoparticles: from preparation to surface modification for analytical and biomedical applications, Chem. Commun. 52 (2016) 7528–7540, https://doi.org/10.1039/c6cc03225g.
[208] A. Zankel, M. Nachtnebel, C. Mayrhofer, K. Wewerka, T. Müllner, Characterisation of Polymers in the Scanning Electron Microscope - From Low-Voltage Surface Imaging to the 3D Reconstruction of Specimens, in: R. Hull, C. Jagadish, Y. Kawazoe, J. Kruzic, J. Parisi, U.W. Pohl, T.Y. Seong, S.I. Uchida, Z. M. Wang (Eds.), Materials Science, Springer Nature Switzerland AG, Cham, 2017, pp. 95–108, https://doi.org/10.1007/978-3-319-41879-7_7.
[209] A. Bootza, V. Vogelb, D. Schubertb, J. Kreuter, Comparison of scanning electron microscopy, dynamic light scattering and analytical ultracentrifugation for the sizing of poly(butyl cyanoacrylate) nanoparticles, Eur. J. Pharm. Biopharm. 57 (2004) 369–375, https://doi.org/10.1016/s0939-6411(03)00193-0.
[210] D.L. Doolan, Malaria Methods and Protocols, Methods in molecular medicine, Springer Nature, Switzerland, 2002, https://doi.org/10.1385/1592592716.
[211] M.G. Vossen, S. Pferschy, P. Chiba, H. Noedl, The SYBR Green I malaria drug sensitivity assay: performance in low parasitemia samples, Am. J. Trop. Med. Hyg. 82 (2010) 398–401, https://doi.org/10.4269/ajtmh.2010.09-0417.
[212] J.D. Johnson, R.A. Dennull, L. Gerena, M. Lopez-Sanchez, N.E. Roncal, N. C. Waters, Assessment and continued validation of the malaria SYBR green I-based fluorescence assay for use in malaria drug screening, Antimicrob. Agents Chemother. 51 (2007) 1926–1933, https://doi.org/10.1128/aac.01607-06.
[213] V. Khare, P. Shukla, A. Ansari, S. Yaqoob, Evaluation of enzyme immunoassay based on detection of pLDH antigen for the diagnosis of malaria, Int. J. Med. Res. Rev. *4* (2016) 1897–1902, https://doi.org/10.17511/IJMRR.2016.I10.28.
[214] 6th Edition of Methods in Malaria Research, ⟨https://www.beiresources.org/Publications/MethodsinMalaria⟩ Research.aspx, 2013.
[215] S.J. Yeo, D.T. Huong, J.H. Han, J.Y. Kim, W.J. Lee, H.J. Shin, E.T. Han, H. Park, Performance of coumarin-derived dendrimer-based fluorescence-linked immunosorbent assay (FLISA) to detect malaria antigen, Malar. J. 13 (2014) 266, https://doi.org/10.1186/1475-2875-13-266.
[216] H.O. Song, B. Lee, R.P. Bhusal, B. Park, K. Yu, C.K. Chong, P. Cho, S.Y. Kim, H. S. Kim, H. Park, Development of a novel fluorophore for real-time biomonitoring system, PLOS One 7 (2012) 48459, https://doi.org/10.1371/journal.pone.0048459.
[217] B.W. Neun, A.N. Ilinskaya, M.A. Dobrovolskaia, Updated method for in vitro analysis of nanoparticle hemolytic properties, Methods Mol. Biol. 1682 (2018) 91–102, https://doi.org/10.1007/978-1-4939-7352-1_9.
[218] B.W. Neun, M.A. Dobrovolskaia, Method for analysis of nanoparticle hemolytic properties in vitro, Methods Mol. Biol. 697 (2010) 215–224, https://doi.org/10.1007/978-1-60327-198-1_23.
[219] I. Greco, N. Molchanova, E. Holmedal, H. Jenssen, B.D. Hummel, J.L. Watts, J. Håkansson, P.R. Hansen, J. Svenson, Correlation between hemolytic activity, cytotoxicity and systemic in vivo toxicity of synthetic antimicrobial peptides, Sci. Rep. *10* (2020) 13206, https://doi.org/10.1038/s41598-020-69995-9
[220] A.D. Elliott, Confocal Microscopy: Principles and Modern Practices, Curr. Protoc. Cytom. 92 (2020) 68, https://doi.org/10.1002/cpcy.68.
[221] J. Jonkman, C.M. Brown, G.D. Wright, K.I. Anderson, A.J. North, Guidance for quantitative confocal microscopy, Nat. Protoc. 15 (2020) 1585–1611, https://doi.org/10.1038/s41596-020-0307-7.
[222] C. Grüring, A. Heiber, F. Kruse, J. Ungefehr, T.W. Gilberger, T. Spielmann, Development and host cell modifications of Plasmodium falciparum blood stages in four dimensions, Nat. Commun. 1169 (2011) 165, https://doi.org/10.1038/NCOMMS1169.
[223] M. Prado, N. Eickel, M. De Niz, A. Heitmann, C. Agop-Nersesian, R. Wacker, J. Schmuckli-Maurer, R. Caldelari, C.J. Janse, S.M. Khan, J. May, C.G. Meyer, V. T. Heussler, Long-term live imaging reveals cytosolic immune responses of host hepatocytes against Plasmodium infection and parasite escape mechanisms, Autophagy 11 (2015) 1561–1579, https://doi.org/10.1080/15548627.2015.1067361.
[224] R. Amino, S. Thiberge, B. Martin, S. Celli, S. Shorte, F. Frischknecht, R. Ménard, Quantitative imaging of Plasmodium transmission from mosquito to mammal, Nat. Med. 12 (2006) 220–224, https://doi.org/10.1038/nm1350.
[225] J. Tavares, P. Formaglio, S. Thiberge, E. Mordelet, N. Van Rooijen, A. Medvinsky, R. Ménard, R. Amino, Role of host cell traversal by the malaria sporozoite during liver infection, J. Exp. Med. 210 (2013) 905–915, https://doi.org/10.1084/jem.20121130.
[226] K. Baer, M. Roosevelt, A.B. Clarkson, Jr, N. Van Rooijen, T. Schnieder, U. Frevert, Kupffer cells are obligatory for Plasmodium yoelii sporozoite infection of the liver, Cell. Microbiol. 9 (2007) 397–412, https://doi.org/10.1111/j.1462-5822.2006.00798.x.
[227] A. Sturm, S. Graewe, B. Franke-Fayard, S. Retzlaff, S. Bolte, B. Hoppenser, M. Aepfelbacher, C. Janse, V. Heussler, Alteration of the Parasite Plasma Membrane and the Parasitophorous Vacuole Membrane during Exo-Erythrocytic Development of Malaria Parasites, Protist *160* (2009) 51–63, https://doi.org/10.1016/j.protis.2008.08.002.
[228] K.W. Johnson, M. Dooner, P.J. Quesenberry, Fluorescence activated cell sorting: a window on the stem cell, Curr. Pharm. Biotechnol. 8 (2007) 133–139, https://doi.org/10.2174/138920107780906487.
[229] M. He, H. Huang, M. Wang, A. Chen, X. Ning, K. Yu, Q. Li, W. Li, L. Ma, Z. Chen, X. Wang, Q. Sun, Fluorescence-activated cell sorting analysis of heterotypic cell-in-cell structures, Sci. Rep. 5 (2015) 9588, https://doi.org/10.1038/srep09588.
[230] G. Pasvol, Receptors on red cells for Plasmodium falciparum and their interaction with merozoites, Philos. Trans. R. Soc. Lond. B Biol. Sci. 307 (1984) 189–200, https://doi.org/10.1098/rstb.1984.0119.
[231] J. Marques, E. Moles, P. Urbán, R. Prohens, M.A. Busquets, C. Sevrin, C. Grandfils, X. Fernàndez-Busquets, Application of heparin as a dual agent with antimalarial and liposome targeting activities toward Plasmodium-infected red blood cells, Nanomed 10 (2014) 1719–1728, https://doi.org/10.1016/j.nano.2014.06.002.